TECHNISCHE UNIVERSITÄT MÜNCHEN

Lehrstuhl 2 für Technische Chemie

Oxidative dehydrogenation of ethane over supported alkali chloride catalysts

Christian Achim Gärtner

Vollständiger Abdruck der von der Fakultät für Chemie der Technischen Universität München zur Erlangung des akademischen Grades eines

Doktors der Ingenieurwissenschaften (Dr.-Ing.)

genehmigten Dissertation.

Vorsitzender: Univ.-Prof. Dr. rer. nat. habil. Klaus Köhler

Prüfer der Dissertation:
1. Univ.-Prof. Dr. techn. Johannes A. Lercher
2. Univ.-Prof. Dr.-Ing. Thomas Sattelmayer

Die Dissertation wurde am 9.1.2014 bei der Technischen Universität München eingereicht und durch die Fakultät fur Chemie am 31.7.2014 angenommen.

Acknowledgements

I would like to thank my advisor, Prof. Johannes Lercher, for guiding me through my PhD work. I want to especially thank him for offering me a very interesting and challenging project, for many vivid scientific discussions, for sharing his broad knowledge with me and for giving me a lot of possibilities, i.e. visiting various conferences.
Special thanks to Prof. André van Veen, who accompanied me in my project during the most important time of my PhD work, for a lot of help and support, many good ideas and for always believing in me and my work. Thank you, André for a lot of diccussions, advice, strategic plans and encouragement. Thank you for critically discussing various tricky theories, thank you for being solution-oriented and thank you for your never giving up. Thank you as well for sharing your broad experience in hydrocarbon activation, reaction kinetics and reactor design. Thank you for not hesitating to establish complex theories, thank you for enduring until we found the right solution.
Prof. Andreas Jentys deserves special thanks for supporting me in the last days of my PhD thesis, for sharing his profound knowledge and experience about kinetics with me and for being willing to think out of the bounds. Andy, you are a really great, talented and honest scientist!
I also want to thank Prof. Klaus Köhler for chairing my PhD defense and for helpful and friendly discussions during my thesis. Furthermore, I want to thank Prof. Thomas Sattelmayer for being my second assessor.
I want to thank SOLVIN SA for funding my project and for the excellent cooperation. I especially want to thank Dr. Michel Strebelle, Dr. Armin Liebens and Dr. Marco Piccinini. Thank you for having always an open ear, for always being interested in my work, for a lot of good ideas and for trusting me. It was a very pleasant and fruitful collaboration in which I learned a lot. I further want to thank Mrs. Anne Vanden Abbeele for a very helpful cooperation when drafting the patent applications. I learned a lot from you as well. Thanks you as well for always clearing my abstracts and papers, even when it was hectic.
I want to thank Prof. James A. Dumesic from the University of Wisconsin for introducing me into the big world of catalysis during my Master studies. You will remain my scientific and personal idol for ever.

I thank Xaver Hecht, most important person of TC2, for a lot valuable help, advice and support at the beginning and during the work on my project. Xaver, thank you very much for helping me to design my reactor setup, for many bug-fixings on it, for many BET measurements and for being able to repair everything!
I want to thank Stefanie Maier for a lot of help, for organizing many things in an excellent way and for a lot of physical and mental support. Without Stefanie, TC2 would not work at all.
Many thanks as well to Bettina Federmann and Karen Schulz for taking care of a lot of financial and organziatorial stuff.
I want to devote special thanks to Helen Brenner for taking care of me in the first days at TC2, for making my start into my PhD thesis smoother and for many nice and pleasant conversations during my whole time at TUM. I will never forget this.
Furthermore, I want to thank the mechanics shop, especially Michael Wanninger, Robert Göring. Roland Schwarz and Reinhold Merz for building my setup, a lot of repairs and manufacturing new parts I needed during my thesis.
I want to thank all my colleagues for a lot of help, many advice, coffee breaks, barbecues in the evening, leisure activities and fun nights. It was a pleasure to work with you, Linus Schulz, Sarah Maier, Daniela Hartmann, Claudia Himmelsbach, Despina Tzoulaki, Sonja Wyrzgol, Robil Kolvenbach, Jennifer Hein, Stefanie Simson, Monica Marcovits, Stefan Schallmoser, Eva Schachtl, Stanislav Kasakov, Sebastian Grundner, Tobias Berto, Sebastian Foraita, Elena Wuttke, Anastasiya Pashigreva, Xianyong Sun, Bo Peng, Hui Shi, Francisco Gonzalez, Maximilian Hahn, Elisabeth Hanrieder, Sebastian Müller, Muthusamy Vishnuvarthan, Navneet Gupta ans Michael Salzinger. Especially I want to thank Linus Schulz, who has been my office mate for almost the whole time at TC2. Thank you, Linus for helpful adivce for all kind of problems, having an open ear all the time and being a loyal, but also critical friend. Furthermore, I especially want to thank Maximilian Hahn for many fun times, being my neighbor in the basement labs and supporting me all the time. Thanks you as well for many fintess sessions, skiing days, dinners, evevnigs at your balcony and other activities. Sebastian Foraita also deserves special thanks for a lot of small talks, coffee breaks and other activities.
My students deserve special respect: Manuel Wagenhofer, Johannes Simböck, Katharina Freitag, Christian Charisius, Michael Eckbauer, Thomas Bartesch, Kai Sanwald, Maximilian Knaus, Julia Brockmeier, Christian Waas, Franziska Betzenbichler, Jura Aponaviciute, Sabine Frischhut, Ruben Weiss, Jesper Köster, Hananah Schreyer, Alaxandra Gerstle and Julia Campello. All of you have done a lot of work and thereby contributed to the success of my PhD thesis.
Last nut not least, I want to thank my parents Peter and Barbara for enabling me to study, always supporting me during my studies and my PhD and for having an open

ear for me all the time, for always believing in me and for their love. Without them, I would not be there where I am now.
Munich, January 7^{th} 2014

Christian

Contents

List of Figures

List of Tables

Abbreviations

AAS	Atomic Absorption Spectrometry
BET	Brunauer Emmet Teller
KIE	Kinetic Isotope Effect
OCM	Oxidaive Coupling of Methane
ODH	Oxidative Dehydrogenation
RO	Reaction order
S	Selectivity
$SSITKA$	Steady State Isotopic Transient Kinetic Analysis
TOS	Time on stream
$TPIE$	Temperature Programmes Isotopic Exchange
$WHSV$	Weight hourly space velocity
X	Conversion
XRD	X-ray diffraction
Y	Yield

1. Introduction

The increasing demand for light olefins and the changing nature of basic feedstock has stimulated substantial research activity into the development of new process routes. Steam cracking remains the most industrially relevant pathway, but other routes for light-olefin production have emerged. Fluid catalytic cracking only produces ethene in minor concentrations. Challenged by marked catalyst deactivation, in contrast, catalytic dehydrogenation ethane up opens a more selective route to ethene. The oxidative dehydrogenation (ODH) of ethane, which couples the endothermic dehydration of ethane with the strongly exothermic oxidation of hydrogen, would potentially be the most attractive alternative route because it avoids the need for excessive internal heat input, but also consumes valuable hydrogen. In this chapter, the current state of the ODH of ethane is compared with other routes for light-olefin production, with a focus on the catalyst and reactor system variants. New catalyst systems and reactor designs have been developed to improve the industrial competitiveness of the ODH reaction of ethane. The current state of the fundamental understanding of the ODH of light alkanes, in particular in terms of catalyst and reactor development, is critically reviewed. The proposed mechanisms and the nature of the active site for the ODH reaction are described and discussed in detail for selected promising catalysts. The reported catalytic performance and the possible limitations of these ODH catalysts will be examined and the performance of the emerging approaches is compared to the currently practiced methods.

1.1. Ethene

Ethene is one of the most important building blocks in the chemical industry. Among organic chemicals ethene ranks first with respect to volume, with an annual worldwide production of 120×10^6 tons in 2008.[1] It is used to synthesize polymers, styrene, ethene oxide, vinyl chloride and vinyl acetate monomers, functionalized hydrocarbons (i.e., dichloroethane, ethylbenzene, acetaldehyde and ethanol) and many other basic and intermediate products. The direct activation and conversion of alkanes to chemicals results in more complicated process schemes than those for the analogous processes employing olefins.[2] Nevertheless, the availability of alkanes as well as increasing demand for olefins [3] and the necessity to minimize negative environmental impacts [4] stimulate research in new directions. Steam cracking, i.e., high temperature pyrolysis in the presence of diluting steam, is the best established industrial process to manufacture ethene. Feedstocks are various naphtha grades and components of natural gas. Different steam cracking processes are known depending on the carbon chain length in the feedstock. While naphtha is the main feedstock for ethene production in Western Europe and Japan, natural gas derived feedstocks are mainly used in the United States and the Middle East. The lighter feedstocks consist either of liquefied petroleum gas (containing propane and different butanes) or ethane, propane and butane originating from natural gas. For naphtha crackers, full-range naphtha (boiling point 30°C -200°C) or C_6-C_8 cuts are typical feedstocks. In the middle east, the feedstock basis was shifted to ethane only in the recent decade, leading to attractive production costs.[1] It should be mentioned in passing that the emerging availability of shale gas will markedly shift the overall scene towards processes using light alkanes. The recurring increases in crude oil prices and especially the availability of ethane in association with shale gas advanced the interest in alternative processes for ethene production, including the dehydration of ethanol (enabling the utilization of biomass-derived feeds) and the (oxidative) dehydrogenation of ethane. The latter offers conceptual advantages and has therefore been subject of substantial research activities. The lack of suitable catalysts combining high activity and selectivity has, however, prevented the industrial realization so far. Excellent reviews addressing ODH broadly exist [3, 4, 5, 6, 7]. Because of the special role of ethane ODH and the associated potential to realize a process, a different approach is taken here. The present chapter therefore summarizes the current status of ethene production as a baseline for the potential and challenges for new processes. This chapter also describes insight into an atomistic and molecular level and ongoing developments in catalytic processes and reactor engineering concepts.

1.2. Current practice - steam cracking, ethane dehydrogenation and ethanol dehydration

1.2.1. Steam Cracking

Steam cracking of hydrocarbons is the industrially most widespread process for manufacture of ethene. Steam diluted alkanes are converted at high temperatures (approximately 800°C) in reactor tubes, leading to homogeneous pyrolysis. A wide variety of feeds up to a boiling point of 600°C can be converted via a radical chain mechanism. Having been practiced for over 50 years, the process is very mature. The feed is preheated together with steam to the initial cracking temperature (500°C - 680°C). Subsequently, the mixed stream is fed into a high temperature-reactor (750°C - 875°C) to complete the steam pyrolysis with residence times of 0.1 to 0.5 seconds. Cracking furnaces are externally fired and the radiant tubes (or coils) have different arrangements (split coil or parallel millisecond pyrolysis)[1]. The feed is cracked into small olefins and di-olefins. Owing to the high reactivity of products, the effluent has to be quenched within 0.02 s - 0.1s to avoid product degradation. Products are separated by a combination of distillation and absorption processes. Steam cracking can be described by complex kinetic models accounting for the progress of the ultra-fast reactions in radical chemistry. Parameters influencing the performance and product distribution are residence time, partial pressures of feedstock and steam as well as the process temperature (profile) in the reactor. Typical hydrocarbon conversion levels reach 70% [1] with olefin yields around 50% using ethane as a feedstock, while single pass conversion yields are lower in naphtha crackers. As the process operates at very high temperatures with high reactant streams, the requirements on the equipment are demanding. Materials have to be heat-resistant, as temperatures up to 1100°C are reached in the reaction tubes. Given the importance of the heat management, the sophistication of detail engineering of heat exchangers is crucial and involves a major effort. Although being the industrial standard for ethene production, steam cracking has disadvantages. It is a highly energy intensive process, its total energy demand of produced ethene is 16 GJ/t in the case of ethane as a feedstock and 23 GJ/t if naphtha is used as a feedstock.[1] A part of the light effluent from the product gas stream has to be combusted to provide heat, leading to CO_2 and NO_x formation. Per ton of ethene, 1-1.6 t CO_2 are produced through this external heating[1]. Additionally, noticeable amounts of coke are formed on the inside reactor walls, which requires periodic reactor shut down for maintenance and coke removal [8] by air and steam gasification, as mechanical coke removal is not possible.

1.2.2. Dehydrogenation of ethane

Catalytic dehydrogenation of alkanes has been industrially applied since the 1930s. The strongly endothermic and equilibrium-limited process (see equation 1) is carried out in fixed-bed reactors.

$$C_2H_6 \rightleftharpoons C_2H_4 + H_2 \qquad \Delta_r H_{298} = 136\ kJ\ mol^{-1} \tag{1}$$

Thermodynamic reasons make the use of high temperatures and low pressures mandatory.[12] For instance, at atmospheric pressure reaction temperatures of 550°C to 700°C are required to reach ethane equilibrium conversions of 10% to 40% respectively. High pressure shifts equilibrium toward ethane. Typical catalysts are based on Cr (i.e., chromia-alumina) or Pt. [9, 10]. Major challenges are the suppression of side reactions and a suitable catalyst pellet shape that ensures efficient feed distribution and minimizes pressure drop. Consecutive side reactions lead to the formation of dienes, polymers and coke.[9] Coke removal from the catalyst during the required frequent regeneration is needed to maintain acceptable catalyst lifetimes. Regular catalyst regeneration occurs by oxidation and the associated heat of combustion, is straightforward to be recovered, especially when several catalyst beds are operated in parallel. One of the first commercial dehydrogenation processes using chromia-alumina, Catadiene^{TM}, was employed for butadiene production, using a parallel fixed bed line-up of reactors, operated in swing mode to alternate dehydrogenation and coke removal. In the late 1980s new processes broadened the application range to the production of propene from propane. The Catofin^{TM} employs dehydrogenation and catalyst regeneration in a swing mode similar to the Catadiene^{TM} process. An adiabatic fixed bed reactor is used as pre-heated propane is fed into the reactor, cooling as the reaction proceeds along the reactor.[11] In the early 1970s, the continuous catalyst regeneration (CCR) concept was introduced by UOP, the associated process using an adiabatic fluidized bed reactor (UOP Oleflex^{TM}).[7, 9] However, ethane dehydrogenation via this route could not compete with steam cracking because of the relatively low activity of the catalysts leading to low single pass yields.

1.2.3. Dehydration of ethanol

The industrial production of ethanol from biomass, particularly in Brazil, made it an available commodity for the introduction as fuel additive or hydrocarbon substitute.[12, 13] Thus ethanol dehydration (equation 2) seems feasible as a niche route to olefins in certain locations.[11] The mildly endothermic dehydration is catalyzed around 300°C by solid acids[1], and selectivities over 99% are possible.

$$C_2H_5OH \rightleftharpoons C_2H_4 + H_2O \qquad \Delta_r H_{298} = 45.6\ kJ\ mol^{-1} \tag{2}$$

While the reaction was carried out for a long time with homogeneous catalysts (sulfuric and phosphoric acid), heterogeneous catalysts such as alumina, silica and other solid acid catalysts have now largely replaced homogeneous catalysts.[14, 15] The process layout is straightforward. Ethanol is heated and fed to the catalytic reactor, followed by a gas-liquid separator, splitting the product stream into a liquid stream containing ethanol and water and a gas stream containing mainly ethene. The ethene stream has to be purified in several stages. Compared to steam cracking, the process consumes less energy and the production of carbon and nitrous oxides is reduced. [1]

1.3. Oxidative dehydrogenation of ethane-mechanistic considerations

In contrast to the above-mentioned processes, oxidative dehydrogenation of ethane (ODH) has not been implemented at large-scale yet. Its conceptual advantage over dehydrogenation, i.e., allowing high ethane conversions, the potentially lower reaction temperature range of around 400°C - 600°C as compared to steam cracking and the fact that the reaction is exothermic, spurs growing interest (equation 3).

$$C_2H_6 + 0.5\ O_2 \rightarrow C_2H_4 + H_2O \qquad \Delta_r H_{298} = -105.5\ kJ\ mol^{-1} \tag{3}$$

Short alkanes, especially ethane extracted from conventional natural gas and shale gas, are cheap and abundant and, thus, suitable as a feedstock for oxidative dehydrogenation.[16] However, major practical differences are introduced compared to the established steam cracking. Firstly, O_2 is added to the feed, imposing additional safety measures to prevent a thermal runaway of the reaction and explosions. Secondly, the development of suitable catalysts is particularly challenging, as the olefin product tends to be more reactive than the reacting alkane. This relatively greater reactivity of olefins is attributed to the enhanced additional directed bonding to most catalytic surfaces, while alkanes interact nearly exclusively via dispersion forces.[17] As ethane is converted to ethene via dehydrogenation, a fraction may undergo total oxidation, forming CO and CO_2 as well as H_2O. This latter reaction path originates from oxygen insertion in the C-H bond during the primary activation or oxygen addition to ethene as depicted in Figure 1.

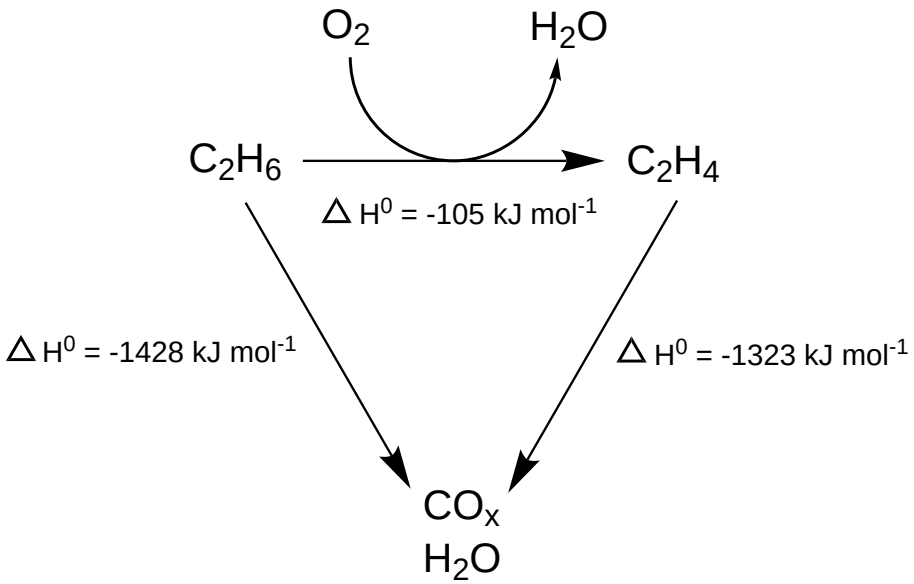

Figure 1.: ODH reaction of ethane with side reactions)

As the latter reaction could involve oxygen anions or electrophilic oxygen, it is important to prevent re-adsorption of ethene and to separate it from O_2. While such oxygenates are intermediates on the route to total oxidation, many of the targeted uses of, e.g., ethene, such as polymerization, require very high olefin purities.[18] Nearly full selectivity towards a single olefin is only feasible with ethane as feedstock, as ethene is the only possible dehydrogenation product and it is sufficiently unreactive towards oxygen addition. The hydrogenolytic C-C bond cleavage of ethane or ethene, resulting in the formation of CH_4, is a highly structure sensitive reaction and hence unlikely under most conditions.[19] By contrast, this does not hold true in the case of propene. The oxidative dehydrogenation of propane is possible nevertheless [20], but propene yields are low, as the allylic structure formed upon further hydrogen abstraction from propene favors a further oxidation,[3] leading to oxygenated by-products and eventually CO_x.[21] The varying reactivities of reactants and products can be better understood when considering their C-H bond energies. Whereas the weakest C-H bond in ethane has a bond energy of 419.5 kJ/mol, its analogue in propane has a value of 401.3 kJ/mol. The weakest C-H bond in ethene, however, has an energy of 444 kJ/mol compared to 360.7 kJ/mol in propene. A more distinct difference can be seen regarding the weakest C-C bond, which has a bond energy of 720 kJ/mol in ethene, as the only C-C bond is a double bond, compared to 413.8 kJ/mol in propene, where the weakest C-C bond is a single bond. Generally, it is mandatory for achieving high selectivities that the weakest C-H or C-C bond in the olefin is less than 30 kJ/mol weaker than the weakest C-H bond in the reacting paraffin.[22] This is true for ethane and ethene, however not for propane and

propene. As a consequence, the ethane ODH is a promising route with potentially high selectivity.[7, 23] The reported exploratory approaches range from catalyst development to combining high activity and selectivity, i.e., to tailor the catalyst in such a way that it favors hydrogen abstraction, while minimizing oxygen insertion [5, 24], to novel reactor concepts.[8, 25, 26] The emerging paradigm is that the development of suitable catalysts requires fundamental insight into the reaction mechanism on a molecular level, including the details of the interactions with the catalytic surfaces and the associated gas phase reactions.[4] As very diverse catalytic materials have been reported, the catalytic chemistry of ethane ODH on these materials will be first described, emphasizing the understanding of the catalytically active site. The mechanism and catalytic performance of selected catalysts are discussed with respect to the overall performance as well as with respect to the applied reaction conditions. The materials explored include transition metal, rare-earth metal, and alkali metal oxides as well as supported alkali chlorides. Optimal reaction conditions for those classes of catalysts differ because of differences in catalytic activity, which for practical reasons are compensated by varying the reaction temperature. As in most cases it is rationalized that the first C-H activation is rate determining, the activation of the first C-H bond will be discussed first.

1.3.1. C-H bond activation and cleavage

Overall, the C-H cleavage steps can occur homolytically or heterolytically, with the homolytic bond cleavage dominating.

1.3.1.1. Single electron processes

The homolytic C-H bond rupture involves unpaired electrons and, hence, in most cases higher energy barriers than elementary steps involving paired electrons. It has to be induced thermally (which can be aided by C-H bond polarization) or by radicals.[27] Figure 2 shows a typical one-electron process, inducing a radical chain mechanism for the oxidative dehydrogenation of ethane. The high energy barriers involved in the single electron process has disadvantages compared to surface catalytic processes. The involvement of free radicals may induce further gas phase reactions, which are complex to control. In ethane conversion, for example, butanes may form by recombination of ethyl radicals. The case of Figure 2 gives a good example, since H_2O_2 formed transiently may decompose to two $OH\bullet$ radicals, which would further enhance the reaction rate by creating new radical cycles.

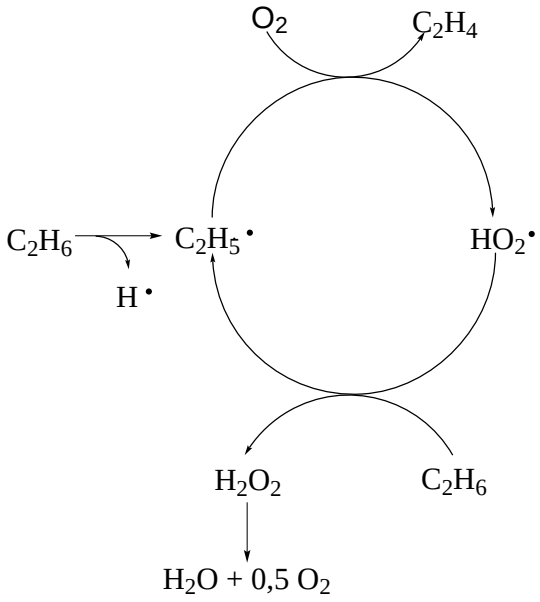

Figure 2.: Single-electron process for C-H bond activation (adapted from [17])

The concentration of alkyl radicals and their reactivity depend on the reaction temperature. Catalytically, one route for alkyl radical generation is formed on the active surface. Especially at elevated temperatures, the radical is released into the gas phase, where it reacts further. A second possibility is that alkyl radicals react close to the catalytic surface, for example in the boundary layer. The third possibility is that the radical reacts quickly, while still adsorbed on the catalyst surface, i.e., conversion to the corresponding olefin by β-elimination or reaction to carbon oxides via attack by adsorbed non-selective oxygen species.[4] Examples of catalysts that generate radicals at the surface, while free radical processes prevail in the gas phase, include rare-earth oxides and alkali oxides.[28, 29, 30] Leveles et al. exemplified this mechanism for the ODH of propane on MgO supported Li_2O.[31, 32] The study showed that alkanes are activated on the catalyst surface in the rate-determining step, producing alkyl radicals. The overall reaction, however, is markedly influenced by gas phase chemistry. Despite a large number of contributions the nature of the active site that abstracts the H-atom is still debated.[33] A likely model suggests that $[Li^+O^-]$ acts as the active site to generate the radicals by abstracting a hydrogen atom and forming an OH^- group [17] (see equation 4).

$$C_2H_6 + [Li^+O^-]_s \rightarrow \bullet C_2H_5 + [Li^+OH^-]_s \tag{4}$$

The alkyl radicals start a chain reaction in the gas phase, leading to the olefin and further radicals. It should be emphasized that in absence of O_2, hydrogen and methyl

radicals are the chain propagators with iso- and n-propyl radicals being the main acting species. In the presence of O_2 the hydroperoxyl radical is the main chain propagator, existing in higher concentrations than radicals formed in the absence of O_2 (equation 5).

$$\bullet C_2H_5 + O_2 \rightarrow C_2H_4 + \bullet HO_2 \tag{5}$$

The hydroperoxyl radical activates hydrocarbons forming H_2O_2 (equation 6):

$$\bullet HO_2 + C_2H_6 \rightarrow H_2O_2 + \bullet C_2H_5 + O_2 \tag{6}$$

The latter decomposes into two hydroxyl radicals acting as the main chain propagators[34],which react with hydrocarbons to form H_2O (equations 7 and 8).

$$H_2O_2 \ \rightarrow 2 \bullet HO \tag{7}$$

$$\bullet HO + C_2H_6 \rightarrow H_2O + \bullet C_2H_5 \tag{8}$$

O_2 regenerates the surface OH^- species (equations 9 and 10):

$$[Li^+OH^-]_s + O_2 \rightarrow [Li^+O^-]_s + \bullet HO_2 \tag{9}$$

$$[Li^+OH^-]_s + \bullet HO_2 \rightarrow [Li^+O^-]_s + H_2O_2 \tag{10}$$

Alternatively regeneration occurs via elimination of H_2O from the surface readily at elevated reaction temperatures. The surface hydroxyl groups, however, are only part of the cycle and do not have catalytic properties.[31, 35] While in the prior example the radical formed at the surface initiated a gas phase process, the homolytic C-H bond cleavage on the catalyst surface may also be followed by propagation on the catalyst surface.[36] Hence, oxidation reactions in microporous materials such as zeolites or redox active oxides may be controlled by surface free radical reactions. Examples of catalysts following this pathway are vanadium or cobalt species in zeolites[17] or on oxide surfaces.[36] The catalyst initiates the reaction by the activation of the first C-H bond via the generation of an ethyl radical. This species reacts quickly on the surface, acting as a chain propagator. Sauer et al. showed that the formation of transient radicals on an oxide surface is energetically favored over gas phase reactions.[37] However, indications exist that this way of activating the first C-H bond via a single electron process is unique

for V containing catalysts.[38] The absence of radical processes propagating into the gas phase, i.e., the fact that the reaction is confined to the catalytic surface, leads to a better control of the reaction and results in enhanced olefin selectivity. Note that also V and Ni containing catalysts undergo one-electron transfer processes, but this will be addressed later.

1.3.1.2. Processes involving paired electrons

In contrast to single electron processes for the ODH of ethane, several catalytic mechanisms invoke involving the simultaneous transfer of two electrons. In this case, the first C-H bond is cleaved heterolytically and a redox pair of one or more metal oxides is involved. In general, a heterolytic cleavage of a C-H bond requires strong basic sites on the catalyst surface to facilitate proton abstraction. A nucleophilic lattice oxygen of a basic oxide can serve as such site.[5] It is disputed if the heterolytic splitting can be facilitated by electrophilic metal cations.[24] Figure 3 represents a typical catalytic cycle involving the transfer of an electron pair, using an example involving a molybdenum oxide. Vanadium based catalysts can follow the same type of paired-electron mechanism.

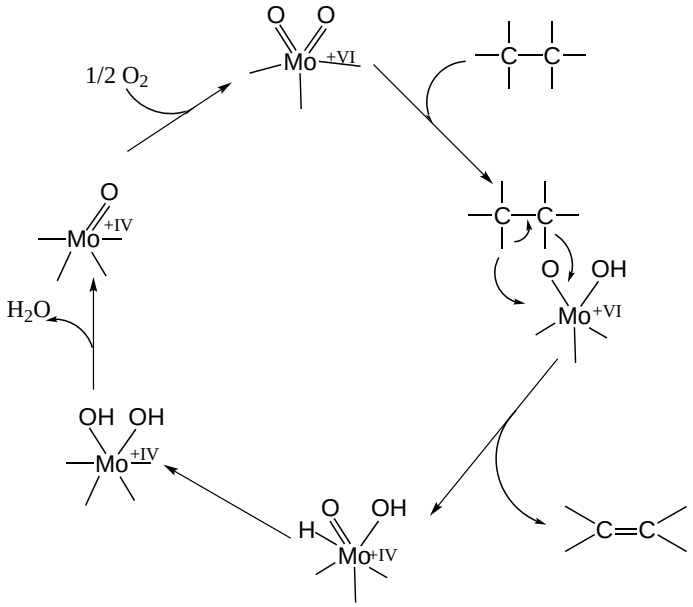

Figure 3.: Redox cycle over Mo involving a paired electron transfer (adapted from [39])

1.3.2. Active sites for ethane ODH

Having shown that sites with single or paired electrons may be involved in the oxidative hydrogen abstraction, the catalytically active sites will be discussed below. Sites for

ODH of alkanes can be grouped into those containing redox active metal cations and those involving anions in the redox cycle.

1.3.2.1. Redox active metal oxides

Most of the catalysts that are reported active for ethane ODH fall into this category. ODH of ethane on such materials follows a Mars-van Krevelen [40] mechanism. Along a polar route, ethane reacts with a metal-oxide-species and forming an ethoxy-hydroxy pair (Figure 3). After the activation of the β-H, ethene is formed and desorbs from the catalyst, leaving a dihydroxy species behind. Water is eliminated from the dihydroxy species, thereby reducing the metal oxide.[39] The reduced metal oxide is subsequently re-oxidized by gas-phase O_2.[41] The cleavage of the first C-H bond may occur homolytically or heterolytically. The most prominent catalysts are based on vanadium oxide [6, 36, 42] with $\gamma - Al_2O_3$ or SiO_2 as typical supports.[43, 44] The oxidic support is not involved in the redox cycle, however, it influences the activity and lability of the oxygen associated with V.[45] Three types of available metal-oxide bonds can be distinguished, i.e., the terminal vanadyl oxygen, oxygen bridging between two V cations, and O bridging between the V cation and the support. The isolated VO_4 species in Figure 4 shows terminal V=O bonds and bridging oxygen bonds between V and the support. The polymeric VO_4 species show additional V-O bonds that bridge between two V atoms. The questions, which of the oxygens participates in the critical first C-H bond activation, and what is the structure of the active site, have been vividly debated, without reaching an unequivocal conclusion.[17]

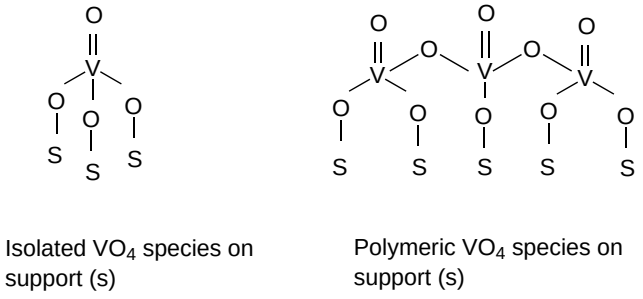

Figure 4.: Different surface vanadium species ([17])

Ethane can be activated at redox active metal centers, involving either one or two centers. The first possibility is that ethane interacts with the oxygen atoms coordinated to one metal cation as depicted in Figure 3. In this case, two terminal M=O bonds are involved in ethane ODH via the transfer of paired electrons. V_2O_5 based catalysts with higher V_2O_5 loadings forming polyvanadate species (e.g., 2 wt% V_2O_5 on Al_2O_3

[46]) are believed to operate via a mechanism in which paired metal centers undergo a one-electron reduction (in this case from V^{5+} to V^{4+}).[46] Two neighboring metal sites actively cooperate in the ODH reaction, however only one of them performing the first C-H bond cleavage. This mechanism is depicted in Figure 5.

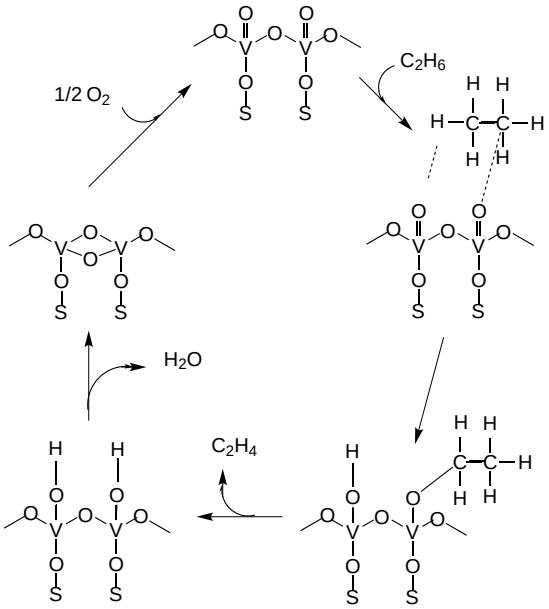

Figure 5.: Mechanism of the ODH reaction over V_2O_5-based catalysts (S=support, adapted from [17])

The other possibility is the cooperation between two neighboring redox sites or materials including two or more different anions. However, the two redox centers must have different oxidation states in this case. This mechanism is mainly known from selective butane oxidation [17, 47], but may also be applied to ethane ODH. For ethane ODH, it is known that neighboring surface vanadia species lead to an enhanced reducibility and thereby also to an increased reactivity. Figure 6 depicts a mechanism using two redox centers with oxidation numbers +4 and +5. In this case, the initial C-H activation occurs via a heterolytic cleavage.

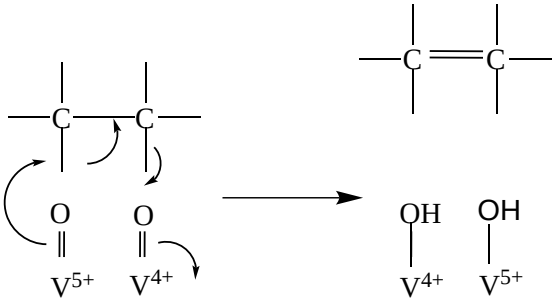

Figure 6.: Cooperation between redox sites (adapted from [17])

1.3.2.2. Catalysts with non-redox active metals

ODH of ethane by homolytic activation of the C-H bonds without a change in the oxidation state of the metal is also possible. In that case the anion, in most cases halogens, assumes the role of redox active element. Depending on the temperature this process may formally involve single or paired electrons. The two possibilities cannot be differentiated, if the bond breaking and forming steps occur without charge separation. The first concept in this chapter is an indirect route of oxidative dehydrogenation, realized by halogenation of CH_4 followed by radical formation or acid catalyzed elimination and subsequently by C-C coupling on catalysts based on $LaCl_3$. Especially HCl and HBr are suitable for such transient halogenations.[17] Of course, ethane can also be directly halogenated and induced to eliminate HX.[48, 49, 50] In this case, formation of vinyl chloride has been observed. Mechanistically, O_2 in the combination with HX leads to the formation of positively charged halogens at the catalyst surface. Subsequently, the hydrogen in the first C-H bond undergoes electrophilic substitution. To complete the catalytic cycle, H_2O is eliminated in the next step, combining one H from the alkane and one from HCl, replenishing the transferred Cl^-. This process involves per se unpaired electrons, but not radical gas phase reactions. The resulting overall chemistry, however, differs only very subtly from free radical reactions. $LaCl_3$ based catalysts are ideally suited to produce chlorinated species, because of a suitable strength of the La-Cl bond. If the strength of the metal-chloride bond is stronger, a similar catalytic chemistry can be realized, but the chloride transfer is drastically reduced and olefins appear as primary products. The second concept comprises a related catalytic route which involves halogen species based on supported alkali chlorides. Ethane activation over these catalysts involves most likely the decomposition of hypochlorite at the surface, forming an $\bullet O^-$ and a $\bullet Cl$ radical (equation 11).[51]

$$[OCl^-] \rightarrow \bullet O^- + \bullet Cl \tag{11}$$

Subsequently, H is homolytically abstracted from adsorbed ethane, resulting in the formation of a hydroxyl group and ethyl radical recombining to ethyl chloride. This can also be interpreted as transient halogenation (equation 12).

$$C_2H_6 + \bullet O^- + \bullet Cl \rightarrow C_2H_5Cl + OH^- \tag{12}$$

The next step can occur via two routes. One possibility is that the ethyl chloride decomposes, forming the olefin and H_2O, while releasing Cl^-. In a later step, Cl^- can undergo a new oxidation step (equation 13).

$$C_2H_5Cl + OH^- \rightarrow C_2H_4 + H_2O + Cl^- \tag{13}$$

The other possibility would be a Cl-C bond formation on the surface, leading to a subsequent homolytic cleavage, releasing an ethyl radical. This route would start a gas-phase radical mechanism.[31, 32] (equation 14).

$$C_2H_5Cl \rightarrow \bullet C_2H_5 + \bullet Cl \tag{14}$$

It is also conceivable that two H atoms are eliminated in a concerted way by hypochlorite anions formed upon reaction of O_2 with LiCl in a concerted fashion.[17] The hydrogen abstraction leads to the reduction of the hypochlorite anion back to chloride, according to the scheme below (equations 15, 16 and 17).

$$LiCl + 0.5\ O_2 \rightarrow LiOCl \tag{15}$$

$$LiOCl + C_2H_6 \rightarrow LiOH \cdot HCl + C_2H_4 \tag{16}$$

$$LiOH + HCl \rightarrow LiCl + H_2O \tag{17}$$

To complete the catalysts following this pathway, also rare earth oxides [28] and LiDyMg mixed oxides [19] have to be addressed here, even if they do not contain halogen atoms, but will be explained in detail later. A third reaction pathway is realized with catalysts able to form peroxo species [52, 53], such as vanadium oxides. V_2O_5 should conceptually allow the formation of such peroxo species.[53] In such a pathway, the vanadium cation itself does not have redox functionality. Figure 7 shows, how the oxidation state of the involved oxygens changes instead.

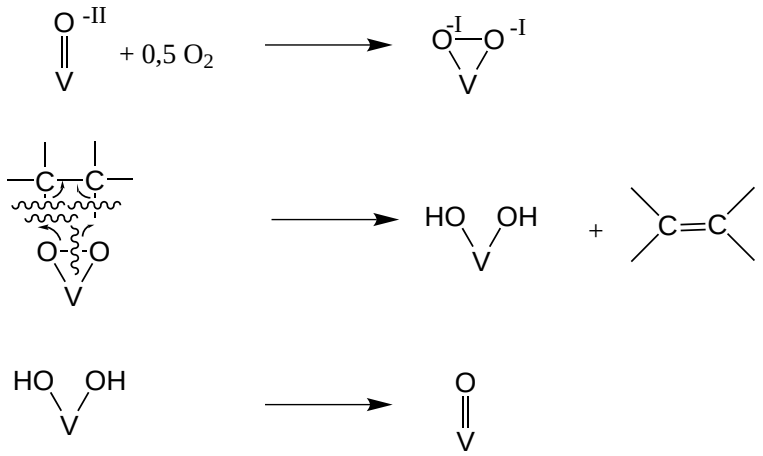

Figure 7.: ODH reactions with pervanadate species

Peroxovanadate species catalyze such a single-site mechanism. C-H bonds at both carbon atoms of ethane are attacked via homolytic cleavage, followed by the formation of ethene and two hydroxyl groups at the V atom. Subsequently, H_2O is eliminated and the V=O bond is formed again. However, V is known to form various metal-oxide bonds in varying structural environments as discussed above.[54] RAMAN and UV-Vis studies have shown that peroxo species may not generally form on certain supports such as silica, but are conceivable in organometallic compounds.[55] Higher concentrations of V-peroxo moieties can furthermore form only at very low temperatures (90 K)[53], which are not realistic for ethane ODH. DFT calculations showed that peroxo species can form at V_2O_5 surfaces. The substitution of O_2 by N_2O as oxidizing agent (described in more detail in section 1.3.3.3), however, disables the formation of peroxovanadates. It is likely that vanadyl species are the active and selective ones for ODH, peroxo forming sites being unselective.[56]

1.3.3. Factors governing activity and selectivity of ODH catalysts

1.3.3.1. Metal-oxygen bond strength

An important parameter especially for redox-active catalysts is the strength of the metal-oxygen bond in the active site, more specifically its strength and its variation with the degree of reduction in a catalytic cycle.[57] As the strength of this bond varies, activity and selectivity of an oxidation catalyst will pass through a maximum in the formation rate of the partial oxidation product, i.e., in the specific case discussed here, the formation rate of olefins. Such a relation is called a volcano relationship. If the metal - oxygen bond is weak, the catalyst is active (for example condensed supported

vanadium oxide clusters) but not very selective, because multiple oxidation steps are facile.[58] As the bond strength increases (smaller clusters of supported vanadia for example) reactivity will gradually decrease, but selectivity will increase.[59] For example, silica is the support leading to the highest selectivity of VO species, as no polymeric vanadia species can be observed.[2] When one site contains more than one oxygen atom in an optimal material, the release of the second oxygen after the initial reduction step is drastically more difficult than the first - for example in a material with a metal site in a high oxidation state combined with a non-reducible oxide site.[60] Even if the support is not directly involved in most redox catalysts for ethane ODH, its acid-base properties may have the role of a mediator of the redox active cluster. A more acidic support increases the metal-oxygen bond strength in the redox active cluster, while a more basic oxide decreases it. This trend can be illustrated with vanadium on a series of different supports, where an increasing acidity is correlated with decreasing activity and increasing olefin selectivity (V_2O_5/MgO < V_2O_5/MgO+Al_2O_3 < V_2O_5/ Al_2O_3).[2]

1.3.3.2. Functionality of active sites and cooperation between phases

ODH is a complex reaction that requires the active sites to provide multiple qualities. It has to be able to adsorb and chemisorb the alkane, to facilitate the abstraction of two hydrogen atoms, to be re-oxidized by oxygen from the gas phase and to desorb the produced olefin.[57] Typical vanadate or molybdate anions are capable of performing multiple reaction steps as depicted in the examples above. However, highly effective catalysts exist that consist of two phases acting concerted, with the two phases being in spatial proximity. The most prominent example for this phenomenon is the combination of V_2O_5 and molybdate sites by depositing V_2O_5 clusters on a polymolybdate surface supported on alumina.[17, 61] While V_2O_5 is still considered to be the active center, Mo seems to decrease the polarity of the metal-oxygen bonds and, hence, increase the acid character of the surface without changing the nature of the active V_2O_5 site. Increasing V_2O_5 content up to one monolayer increased the selectivity for ODH over total oxidation reactions. The ratio between total oxidation and ODH was notably lower compared to V_2O_5 supported on Al_2O_3 without the molybdates. The presence of the molybdate reduces the interactions between V cations and the olefin product, leading to accelerated olefin desorption and, thus, to higher selectivities.[17]

1.3.3.3. Role of O_2 and the density of sites

A comprehensive study comparing O_2 and N_2O as oxidants is reported by Kondratenko et al.[62] This study on vanadia incorporated into MCM-41 also points out nicely the importance of site isolation and the influence of the density of active sites. Using N_2O

instead of O_2 results in lower activity, which is explained by the fact that N_2O has a lower ability to reoxidize the VO_x sites from the reduced state caused hydrogen abstraction and water elimination. As the elementary steps of the reaction are independent of the oxidant and the same oxygen lattice species are formed regardless whether O_2 or N_2O is used, the steady state concentration of lattice oxygen must account for the reactivity difference. Not only is the olefin selectivity markedly higher if N_2O is used as oxidant, but also the decrease in olefin selectivity with increasing activity becomes less notable with N_2O as oxidant compared to O_2. As N_2O tends to re-oxidize the reduced vanadia sites more slowly than O_2, the concentration of those sites is lower, reducing the probability that more than two labile lattice oxygen atoms per site exist. More labile oxygen atoms per site favor non-selective total oxidation reactions. It also eliminates the possibility that adsorbed oxygen species in spatial proximity to the vanadia centers (however not incorporated into the lattice) exist [63] that might enhance total oxidation.

1.3.3.4. Desorption and re-adsorption of ethane

As olefins are more reactive than alkanes, ethene shows a higher affinity as well as a higher reactivity with most surfaces than ethane. Hence, the re-adsorption of the formed olefin on the catalytic surface limits the selectivity. The stepwise oxygen addition is frequently followed by decarbonylation or decarboxylation on acid catalysts. Therefore, oxygen addition leading to products such as acetaldehyde or acetic acid will in turn enhance the selectivity for total oxidation. As re-adsorption of olefins is linked to the presence of accessible metal cations (Lewis acid sites), their presence has to be minimized. Three options exist to realize this. The first option is to use oxides with low specific surface areas, minimizing the concentration of accessible Lewis acid sites. Thus, catalysts with high crystallinity show excellent selectivities in ethane ODH [64, 65] and other oxidation reactions [66], as they expose a limited number of unselective sites. The second concept relies on surfaces that dynamically rearrange to prevent the exposure of cations, such as a supported molten chloride overlayer. The mobility of the melt prevents the formation of defect sites (coordinatively unsaturated metal cations) that are speculated to initiate the reactions leading to deep oxidation. In a melt the surface re-arranges quickly limiting the concentration of these exposed cations by covering the transiently present exposed cations.[51, 67] The fact that mostly anions that are not able to attack the double bond of the olefin are present on the outer surface further enhances the benefits of a molten overlayer. A third concept to improve product desorption is site isolation, which increases the selectivity towards partial oxidation products [68] by restricting the local availability of oxygen. Thus, labile lattice oxygen or ensembles of atoms containing a redox active site need to be spatially isolated. As pointed out above, active sites with more than two labile lattice oxygen facilitate oxygen insertion before

desorption, eventually leading to CO_x.[63] Thus, a good distribution of labile oxygen atoms and the limitation of the number of oxygen atoms per site help to prevent total oxidation.[60] On the other hand, single oxygen atoms on a catalytic surface are inactive or prone to generation of allyl radicals that react further in the gas phase.[57, 68] Therefore, two labile oxygen atoms per site appear to be the optimum for highly selective ODH of alkanes.

1.4. Groups of ODH catalysts

Having discussed the elementary steps, the description of potential catalysts suitable for oxidative dehydrogenation follows now. This should help to relate the discussion of the potential elementary steps of reactions to the specific examples of catalysts. Special attention will be paid to the structure of the active site on different catalysts for ethane ODH and the common properties and differences between the various classes of catalysts.

1.4.1. Transition metal oxides

1.4.1.1. Vanadium oxide based systems

Supported vanadium oxide based catalysts are the most intensively studied ones. The V cations may change their oxidation state between +III, +IV and +V [17, 69] making the catalysts redox-active, but they can also form ODH active peroxo species.[53] In this case, the cation does not change its oxidation state. It is debated whether or not the activation of the first C-H bond occurs via a paired or a single electron transfer with these catalysts. Especially UV/vis and Raman spectroscopy [70, 71] showed vanadium oxide to be present in the form of distinct species. VO_x sites exist in isolated or polymeric form, either as a two-dimensional layer of interconnected tetrahedral vanadate clusters (VO_4^{3-}) connected via corners [36, 72] or as dimeric pyrovanadate clusters ($V_2O_7^{4-}$) connected via an oxygen atom as depicted in Figure 4. [73] To optimize catalytic performance and to explore the mechanism, many parameters including the dispersion of the vanadate centers, the support material (potentially altering the acid/base properties of the catalyst), and the addition of dopants or promoters were systematically varied. The most important parameter proved to be the variation of the dispersion of vanadium oxide on the support. It may markedly influence the reactivity of the catalyst.[43] As consensus has not been reached whether the terminal V=O bond or the bridging V-O-Al bond forms the catalytically active site, let us now introduce the two different leading paradigms, exemplified by different experimental approaches and results, followed by the specific interpretations. Martinez-Huerta[41], studying vanadia catalyst supported on

$\gamma - Al_2O_3$, used temperature programmed reduction, in situ Raman, IR, UV-Vis diffuse reflectance as well as X-ray photoelectron spectroscopy combined with kinetic measurements. By synthesizing isolated and polymeric VO_x species as well as crystalline V_2O_5 nanoparticles the combination of physicochemical and catalytic measurements allowed important conclusions regarding the active site. While at low sub-monolayer vanadia loadings only isolated surface species with three V-O-support bonds and one terminal V=O bond were found, an increase in the vanadia loading resulted in the formation of polymeric vanadia species with only one V-O-support bond, one V=O terminal bond and two V-O bridging bonds. Only after a surface monolayer of vanadia was present, three-dimensional V_2O_5 nanoparticle crystallites formed on top of the surface monolayer.[74] The catalysts with higher vanadia loadings (mostly polymeric surface vanadia species) showed the lowest reduction temperatures, thus being most reducible. The reduction of isolated surface vanadia species was more difficult for V_2O_5 nanoparticles. Interestingly, the V=O bond of vanadia species becomes stronger with increasing coverage (shift from 1010 cm^{-1} to 1023 cm^{-1} for the main peak in Raman spectra), even though the reducibility of the polymeric surface vanadia species is the lowest. Thus, one may conclude that the rate determining reduction step cannot be influenced by the terminal V=O bond, suggesting that the terminal V=O bond is not the primary active site for ethane ODH. Increasing the surface concentration of vanadia species - which results in a higher concentration of bridging V-O-V bonds - did not change the catalytic activity, suggesting that those bonds are not catalytically active for ethane activation.[75, 76] As crystalline V_2O_5 nanoparticles tend to catalyze total oxidation, the lower selectivity at high V loadings has been explained with the presence of such nanoparticles. It should be kept in mind, however, that the V_2O_5 nanoparticles might undergo a solid-state-reaction with the support at higher temperatures, forming $AlVO_4$ as a new phase. This would in turn lower the number of V-free Al_2O_3 sites, thereby reducing the trend to total oxidation reactions.[41] Thus, it was concluded that in supported surface vanadium oxide neither the terminal V=O bond, nor the bridging V-O-V bond nor V_2O_5 nanoparticles are active in ODH. [41] The bridging V-O-Al-bond is according to that rationale the only left option, and is therefore inferred to be the active site in this catalytic system. Other authors have accepted this argument, especially the aspect that the bridging V-O-V site cannot be active for the initial C-H bond cleavage in ethane ODH.[17] DFT calculations using well-defined vanadia clusters with the metal oxidation state +5 have been found to be an excellent approach to obtain a more in-depth insight into the reactivity.[77, 78] Evaluation of the energy barriers leads to the conclusion that a hydrogen atom is abstracted by the cleavage of the V=O terminal bond with formation of transient radicals and subsequently a carbon-V bond.[37, 77, 78] A bridging oxygen atom could abstract the second hydrogen atom in this case, resulting in ethene formation. One drawback of this theoretical experiment is that the V-O-support bond is not present in the model

vanadia cluster. Thus, further DFT calculations were performed using a V substituted silsequioxane cluster with bridging oxygen atoms between V and support cations.[78] DFT calculations showed that even in the presence of V-O-support bonds the terminal V=O (vanadyl) bond is the only active species for the activation and cleavage of the first C-H bond. To summarize, consensus exists in the literature that the bridging V-O-V bond cannot be responsible for the activation of the first C-H bond. However, some discrepancy exists between theory and experiment, whether the terminal V=O bond or the V-O-support bond is the site for the activation of the first C-H bond. The concept of site isolation assumes a special role in this context. Apparently, the spatial proximity of two but not more vanadia centers is essential. This agrees with the hypothesis, that the bridging V-O-V bond does not boost the initial C-H bond activation in ODH, but facilitates the second H abstraction. Thus, an ensemble of two vanadium centers seems to be the active site - regardless whether the V=O terminal bond or the V-O-support bond acts as active site. A study investigating the influence of different V loadings showed that in accordance with expectations an increasing V loading on $\gamma - Al_2O_3$ results in an increase of the activity and ethene selectivity.[41] This can be explained with the fact that V-free Al_2O_3 cation sites exist on this catalyst. Those acid sites are reported to be inactive for ODH, but to catalyze total oxidation of the olefin to mainly CO. Thus, the acid sites of $\gamma - Al_2O_3$ mainly contribute to the acidity of the supported catalyst at low V loading, whereas the vanadate compounds are mainly responsible for the acidity at higher V loadings. However, in this case only the vanadia related acid sites are responsible for product degradation towards carbon oxides.[41] The overall activity increased with the total concentration of acidic sites and with the electronegativity of the dopants.[79] However, there is an upper vanadia loading limit beyond which the ODH yield decreases. While the sites on Al_2O_3 should be covered at those loadings, V_2O_5 particles formed catalyze the total oxidation of ethene to CO.[41] Neither acid-base properties nor the chemical composition show pronounced effects. The presence of vanadia-free Al_2O_3 sites leads to the question whether other supports might be more appropriate. Indeed, the activity of supported vanadia based catalysts strongly depends on the interaction with the oxide support as well as the support structure.[80] The dispersion and the formation of the active sites are influenced by the nature of the support material. A comparison between $\gamma - Al_2O_3$ and SiO_2 nicely illustrates this. $\gamma - Al_2O_3$ is a better support than SiO_2 due to the better dispersion of vanadium oxide and the coordination of the V cations. Its acidic character plays a less important role in this case.[36] As discussed above the active site (two oxygen-bridged V cations in tetrahedral coordination) are preferentially formed on $\gamma - Al_2O_3$. These sites can be more easily reduced by ethane than the vanadate monomers in tetrahedral coordination that are mainly formed on the SiO_2 support and the octahedrally coordinated V species in pure V_2O_5.[36] Another proposed support is hexagonal mesoporous silica (HMS).[81]

The influence of the V loading on the catalytic performance was explored with respect to propane ODH though. Up to 3.2 wt.% V, the ODH activity increased in proportion with the V content. Above 3.2 wt.% V, the reaction selectivity and yield decreased. This can be explained with different vanadium oxide species detected and characterized on the surface employing temperature-programmed reduction with H_2 and UV-Vis spectroscopy, being specifically
(i) monomeric V species in tetrahedral coordination (VO_4) that are active and selective in ODH,
(ii) oligomeric and distorted tetrahedral vanadium oxide species (both up to 3.2 wt% V) that are highly active but less selective, and
(iii) aggregated vanadium oxide clusters in octahedral coordination (VO_6) having low activity and selectivity.
The results confirm that a high V dispersion is crucial for catalytic performance. Also in this case the spatial separation of the vanadate centers (site isolation) was a key feature for activity and selectivity.[57, 68]
Another potential catalyst support for vanadate species is the inexpensive and relatively stable MgO. It was subject of several studies. [76, 79, 82] Klisinska et al. studied catalysts with a formal concentration of 1.5 monolayers of vanadium oxide and compared MgO as a support to SiO_2. Dopants such as K, P, Ni, Cr, Nb and Mo influenced the acid-base and redox properties, but did not markedly impact the structure of the catalysts. MgO supported catalysts formed magnesium orthovanadate ($Mg_3V_2O_8$) [82], as sole V-containing species, present either in an amorphous bulk phase or in a thin layer on the support. Only Lewis acid sites were detected on these materials. Their concentration increased with the electronegativity of the dopant. Although the activities of the catalysts could not be correlated to acid-base properties, selectivity depends on the dopant. The main by-product in the ODH of ethane was CO_2, while CO was only formed in trace amounts. As MgO is known to have basic sites and vanadate species as well as pure V_2O_5 do not show any basic sites [42], the surface acidity and basicity (the acid/base character of the vanadium species) do not seem to have a crucial impact on the reaction. However, acid/base properties of the support may have an impact on the reactivity, which will be explained below. Chao et al. investigated MgO as support by comparing two groups of mixed metal oxides, i.e., meso-structured Mg-V-oxide, and a mixed oxide prepared by a solid state reaction between MgO and V_2O_5. For both systems, activity increased with Mg content, but the selectivity towards ethene decreased. In comparison the mesostructured oxides were more active and selective. This can be explained again by highly dispersed Mg species in the V_2O_3 phase and high surface areas. Mg species are assumed to lower the redox capacities of V containing species, thereby influencing the activation of ethane.[38] The influence of the oxidation state of vanadia species becomes important, if ODH on vanadia based systems is initiated by a transfer of

paired electrons. For this mechanism, two vanadia centers have to cooperate as depicted in Figure 6. While only V^{5+} could be observed in freshly calcined catalysts, also V^{4+} was detected on used catalysts, especially after experiments at high conversion levels. V^{4+} species alone seem to favor deep oxidation and lead in consequence to lower the selectivity towards the olefin. As a note in passing it should be mentioned that a V^{5+}/V^{4+} ratio of one yields the maximum selectivity in O-insertion reactions.[83] Doping of vanadia containing catalysts as means to improve the catalytic performance will now be further discussed. Galli et al. studied the effect of K^+ doping for a Al_2O_3-supported vanadia catalyst.[84] The incorporation of K^+ lowers the reducibility of vanadia catalysts. The olefin selectivity for ethane ODH decreased, but for example increased in n-butane ODH. The concentration of acid sites decreased with increasing K^+ incorporation suggesting that acid sites favor ODH of short alkanes, while basic sites favor ODH of longer paraffins. Other promising catalyst systems include aluminophosphates containing V (also doped with Co and Mg).[85, 86, 87] The active sites, as V and other metals are incorporated into the microporous aluminophosphate framework, as exemplarily shown by Concepcion et al. for AlPO-5 frameworks containing V, Co and Mg. Co-APO-5 has been explored in depth, since it should have the most pronounced redox and acid properties. The catalyst is active and selective and Co-V-APO-5 was even much more active for ethane ODH. This was attributed somewhat vaguely to the cooperation between V and Co sites. A redox couple was assumed to form, but the acid character of this pair was assumed to change during the reaction. A similar catalyst, VCoAPO-18, containing V and Co in an AEI structure leads to two different redox pairs (V^{5+}/V^{4+} and Co^{3+}/Co^{2+}). In both cases, the crystal structure and the presence of the second Co^{3+}/Co^{2+} redox pair changes the redox properties of the V species. The metal cations also serve as Lewis acid sites. The catalyst shows even a higher selectivity than the AFI-material. ODH over these catalyst proceeds via a Mars-van Krevelen mechanism. The presence of acid sites close to the redox center favors fast desorption of olefin intermediates from the catalyst, thus leading to high ethene selectivity.[85] Too high V loadings lead to the formation of extra-framework VO-species favoring total oxidation. Ideal catalysts have a high degree of incorporation of Co and V into the framework. The insertion of Mg into the VAPO-5 framework, known to create acid sites [88], resulted in a noticeable increase in olefin selectivity compared to the Mg-free catalyst (59.7% compared to 32.1% at T=600°C and a conversion of around 28%)[87]. This example shows again that the spatial proximity of acidic sites to the redox center promoted the desorption of olefin intermediates, thus leading to a lower total oxidation rate and higher olefin selectivity at the same conversion level.[87] The identical conversion indicates that the redox sites are active for the paraffin transformation, while the improved selectivity in the presence of acid sites show that acid sites are not directly involved in the redox cycle but facilitate the desorption step.[86, 89, 90, 91, 92] This assumption is corroborated

by the fact that only low olefin selectivities are reported in V-Mg-oxide based catalysts with Mg-O-V pairs, but without the presence of acid sites.[87, 93] Thus, it can be concluded that especially the spatial proximity of acid and redox sites within a molecular sieve framework is positive for ODH reactions. The behavior of acidic sites must not be compared with the influence of acidic sites per se in vanadia species supported on bulk oxides, where acidic centers of the support favor unselective conversion of ethane.
Phosphorus is another known dopant. An example is $(VO)_2P_2O_7$, both as bulk and supported on TiO_2.[94] The supported catalyst contains highly dispersed $(VO)_2P_2O_7$ and yields a performance one order of magnitude higher than the unsupported one. The incorporation of P is another approach to change the reducibility of V. The strong interaction with TiO_2 increases the V reducibility by decreasing the metal-oxygen bond (see section 1.3.3.1) and, thereby, leading to very active catalysts.

1.4.1.2. Mo based systems

Like V oxides also Mo oxides are active for ethane ODH.[95, 96, 97, 98] Similarly to vanadia systems, consensus about the nature of the active site has not been reached. On the one hand the active site was concluded to be a molybdenyl group, which activates the first C-H bond, inducing a homolytic cleavage via a single electron process, as it has been shown that the activity depends on the concentration of Mo=O bonds.[17, 20] On the other hand, different authors have studied molybdenum supported on Al and suggest that the anchoring Mo-O-support bonds are critical for ODH reactivity, thus suggesting that the oxygen between support and molybdenum is responsible for the catalytic activity.[99] Mo can be used on a Si/Ti mixed oxide support.[100, 101, 102] The olefin selectivity is especially increased if Cl^- is added.[103, 104, 105] This increase is explained with the formation of more complex ligand structures formed with Mo=O species on SiO_2, while the formation of those species is hindered on TiO_2. The addition of Cl^- seems to accelerate the olefin desorption by lowering the interaction with ethene, limiting its further oxidation. It also lowers the oxidation potential of the catalyst via lowering the redox potential of Mo^{4+} [104] leading to a lower mobility of lattice oxygen. As a result, Cl^- addition led to strongly bound ethyl species and more weakly bound acetate and formate species, which tend to indicate intermediates on the path to total oxidation.

1.4.1.3. Mixed oxide based systems

Mixed oxide based systems appear to be better suited than single oxides to adjust the redox potential and act cooperatively.[64, 106, 107] One of the most popular mixed oxide system is based Mo/V-oxides. Mo appears to be particularly active together with V on

a mesoporous Al_2O_3 support.[95] However, the main active species is still V. Mo and V do not interact, but the monomeric or polymeric tetrahedral Mo species cover the non-selective support sites, increasing the selectivity. It has been reported that such a catalyst with an orthorhombic Mo_3VO_x structure is very active. The high reactivity has been associated with the formation of pentagonal Mo_6O_{21} units. Arrangement of these units leads to heptagonal channels, constituting micropores. It is speculated that the catalytic reaction proceeds in these pores.[108] More complex systems contain the oxides of V, Mo, Sb and Nb, mainly prepared by hydrothermal synthesis.[109] $MoVNbO_x$ and MoVSbTe are reported to be very active and selective in the ODH of ethane.[39, 110, 111] The catalysts generally consist of two crystalline phases, i.e., the orthorhombic M1-phase $(AO)_{2-2x}(A_2O)_xM_{20}O_{56}$ (A=Te,Sb, M=Mo,V,Nb, 0<x<1) and the distorted orthorhombic M2 phase $A_{2O}M_6O_{19}$ (A=Te,Sb, M=Mo,V,Nb). Further phases have also been found, i.e., $TeMo_5O_{16}/Sb_4Mo_{10}Ox$, $(V,Nb)_xMo_{5-x}O_{14}$ as well as bronze phases.[110] However, the occurrence of a third phase depends on the synthesis method.[112] It is notable that ethene has low reactivity due to a low affinity to the M1 phase, which is rich in Mo-O and V-O pairs that are reported to be the active sites for ethane ODH. For the oxidation of ethene, Mo-Te sites or Mo-Nb sites, however, seem to be required, as they have a higher strength of interactions with olefins.[110] Botella et al. studied $MoVTeNbO_x$ catalysts prepared by different methods.[107, 112] For $MoVTeNbO_x$ mixed oxide catalysts, cooperation between two crystalline phases was suggested to explain the structure of the active site assembled from the multifunctional $Te_2M_{20}O_{57}$ orthorhombic phase and the Mo_5O_{14} phase. The orthorhombic phase contains pentagonal bipyramidic sites and Te-containing hexagonal pores.[107] The catalyst operates at 340°C with around 20% conversion and an ethene selectivity around 97%. The calcination temperature is crucial for the formation of the above mentioned phases. Similarly, for $MoVSbO_x$ catalysts the $(SbO)_2M_{20}O_{56}$ phase is highly active and selective (around 65% conversion and 80% selectivity). Mo-V-based systems have also been reported to be active, if they are promoted with Al, Ga, Bi [113] and Ce [114].

1.4.1.4. Ni and Co based systems

NiO-based catalysts are suitable ODH materials operating at relatively low temperatures (300-400°C). Pure NiO is very reactive towards ethane, however exhibits a low selectivity for ethane ODH. The selectivity drastically improves when supported on an oxide (Al_2O_3 [115], ZrO_2 [116]) or when used as bulk mixed oxide doped with promoters like Nb and Sn.[16, 117, 118, 119, 120] NiO supported on Al_2O_3 interacts strongly with the support forming a non-stoichiometric surface nickel aluminate phase. At higher loadings, capping islands of NiO particles with increasing size begin to form on top of the nickel/alumina interface. The interaction with alumina adjusts the electronic prop-

erties of NiO such that the reduced oxygen mobility leads to highly selective catalysts. Promotion of supported and unsupported NiO based systems by addition of metals cations including Mo, V, Nb, Ta, Co, Li, Mg, Al, Ga, Ti, is possible.[85, 86] The most selective catalysts are based on Ni-Nb-oxides achieving ethene selectivities around 90% remaining almost constant at conversion levels up to 20%. A maximum yield of 46% has been reported at 400°C. Ni cations are speculated to be active sites for the C-H activation, with Nb affecting the oxygen species.[16] Pure NiO predominantly produces the electrophilic O_2^- and O^- species and the nucleophilic O^{2-} species on its surface.[121] The addition of Nb results in elimination of the electrophilic oxygen responsible for the total oxidation of ethane. Thus, the selectivity towards the olefin is improved by Nb acting as electron donor. Other dopants increase or decrease the presence of non-selective electrophilic oxygen species.[118] A systematic study of a series of NiO-based mixed oxides with doping metals varying from low (+1) to high valence (+5) showed that the dissolution of lower/equal to nickel valence cations (Li^+, Mg^{2+}) increases the non-stoichiometric oxygen in NiO, while the higher valence cations (Al^{3+}, Ga^{3+}, Ti^{4+}, Nb^{5+}, Ta^{5+}) act as electron donors and reduce the positive p^+ hole concentration and consequently the electrophilic O^- radicals of the NiO acceptor.[118] Ethane ODH on the Ni-Nb-O catalyst follows a Mars-van Krevelen mechanism. It is important to note that the redox cycle proceeds via a change in the Ni oxidation state, while Nb does not change its oxidation state. Especially at large concentrations of Nb (above 15 wt%), the reoxidation of Ni^{2+} can be retarded by the Nb atoms, reducing in this way the catalytic activity of Ni-Nb-O compared to pure NiO.[115, 122] However, the addition of Nb reduces the concentration of electrophilic oxygen, thereby increasing the olefin selectivity.[123, 124] Notably, an optimum of the reactant partial pressures exists. Low O_2 partial pressure leads to high olefin selectivities, while a minimum O_2 pressure is needed to keep the catalyst in fully oxidized state.[123] If a catalyst contains more than 15% Nb, it was seen to deactivate. This is related to the formation of $NiNb_2O_6$ phase, which is thermodynamically stable at relevant ODH reaction temperatures employed, but is not active for ODH.[124] Nickel oxide can be used in combination with ceria as a mixed oxide catalyst.[119] Low concentrations of Ce (Ni/Ce>6) lead to a marked increase in catalyst activity and selectivity compared to pure NiO. This is related to an increase of the specific surface area and a decrease in reducibility. The addition of higher ceria concentrations (Ni/Ce ratio of 0.2 - 0.3) changes the mechanism. In this case, ceria is responsible for transportation of the oxygen from the bulk to the surface, forming both NiO and $Ce_{1-x}Ni_xO_2$, and leading to a faster reoxidation of Ni. Tungsten is also used to promote NiO.[118] The activity decreases with increasing W content, indicating that active sites are associated with accessible Ni cations. Again, W-rich and Ni-rich systems behave differently. W-rich systems mainly form $NiWO_4$ and WO_3, while Ni-rich systems mainly form NiO and WO_x. W-rich systems favor ethane decom-

position, thus, decreasing the ethane selectivity during ODH. Ni-rich catalysts, however, have a higher ethene selectivity compared to pure Ni-based catalysts, but also a lower activity. The catalysts contain small NiO and WOx particles, the latter being assumed to block unselective sites of NiO. Besides Ni, also Co is an interesting material for ethane ODH. However, Co^{2+} ions cannot be easily reduced, thus ODH of ethane does not follow the typical Mars-van Krevelen mechanism.[40] Redox properties are associated with adsorbed surface oxygen species, Co^{2+} acting as a non-redox active center.[125] These species may be modified by interactions between Co^{2+} as the active phase and a TiO_2 support.[126] Such catalysts containing various Co and P [125] concentrations showed the best performance with 7,6 wt% Co. While the catalyst deactivated forming a Co-Ti species, a maximum steady state yield of 13.3% was achieved at a conversion around 25% and selectivity of around 60%. Detailed characterization showed that the active species is Co^{2+} in octahedral coordination. $Co - BaCO_3$ was explored using CO_2 as the oxidant instead of O_2. At 650°C, ethane conversion reached 48% with 92.2% olefin selectivity.[127] Using CO_2 reduces the flammability of the reactants and eliminates the total oxidation of ethane and ethene, while coke can still be removed from the catalyst via reduction of CO_2 and partial oxidation of C. The active sites are reducible Co^{4+}-O species. BaCO3 on the other hand is assumed to form defect centers and trapped electrons, which activate O_2 for ODH. Cooperation between $BaCO_3$ and $BaCoO_3$ - both a redox active metal and a source of active oxygen species - is assumed to be one reason for the good activity and selectivity of this catalyst, being a good example for cooperation between sites as depicted section 1.3.3.2.

1.4.2. Rare earth metal oxides

These catalysts consist typically of La_2O_3, Sm_2O_3, CeO_2, Pr_6O_{11}.[28, 128, 129, 130, 131] Promotion with Na [28] and CaO [132, 133] has also been investigated. The cleavage of the first C-H bond occurs via a single-electron process and catalysts belong to the group of non-redox active materials. The main catalytic function is the production of ethyl radicals that are released into the gas phase, ethene and CO being the main carbon containing products.[28] Catalysts were operated between 600°C and 900°C and selectivity was around 50%, both conversion and selectivity towards olefins increasing with temperature. This is concluded to be related to the release of ethyl radicals increasingly taking place at elevated temperatures. Enhancing the release rates implies that less ethoxy species (intermediates of the CO_2 production) exist on the surface at steady state.[28] The addition of alkali earth / alkali metals to rare earth oxides improves the catalytic performance.[134] A Sm_2O_3 catalyst doped by 10% of Na^+ cations shows a notably higher selectivity compared to a pure Sm_2O_3 catalyst. For both catalysts, olefin selectivity decreases with increasing oxygen concentration, however, this effect

was not as pronounced for Na^+-doped catalysts than for pure Sm_2O_3. While ethene and CO are the main products with rare earth oxides, CO_2 was observed instead of CO in presence of Na^+ cations. This suggests the formation of lattice oxygen species play a role in the alkane activation and it points to a heterogeneous surface catalyzed mechanism. This trend is even more obvious in the case of La_2O_3.[28] Adding Sr^+ to rare earth oxides leads to a marked increase in activity and selectivity. At 700°C, Sr_2O_3 on neodymium oxide is the best catalyst regarding activity and selectivity, while Sr^+-doped CeO_2 and praseodymium oxides show the poorest performance.[134] Rare earth oxides are either employed as bulk materials or MgO is used as a support, being per se also a potential catalyst for ethane ODH. Comparing the performance of Sm_2O_3-covered MgO with that of pure MgO it is interesting that Sm_2O_3 does not increase the catalytic activity, although it increases the specific surface area. However, covering MgO in the same way with La_2O_3 strongly enhances the catalytic activity. As this cannot be explained with only the surface stabilization by keeping specific surface areas higher, thus the intrinsic activity of the catalyst seems to be drastically improved by La^{3+}.[28] CeO_2 is an exception having two oxidation states in a catalytic cycle. Ceria-based catalysts are unique as CO_2 can be used as oxidant.[132] However, higher temperatures are required for CO_2 activation compared to oxygen.[135] In this case, a combination of a homogeneous and heterogeneous mechanism is assumed. For the heterogeneous catalyst part Ce^{4+} is reduced by ethane to Ce^{3+} supplying oxygen and is re-oxidized via reduction of CO_2. CeO_2 plays a role not only because of its redox properties, but also regarding its oxygen-storage capacities. To further improve the catalytic performance, the addition of Ca^{2+} to Ce^{4+} increases the oxygen-ion mobility of CeO_2. It also contributes to a higher surface basicity, leading to a faster olefin desorption (higher olefin selectivity).[132] Interestingly, olefin desorption is accelerated in the presence of basic sites on this class of catalysts in contrast to redox active catalysts, where acid sites in spatial proximity to redox pairs favor olefin desorption as mentioned before. Improvement of the catalytic performance of rare earth oxides can also be achieved by addition of halides.[136, 137, 138, 139] Au et al. reported that adding 50 mol% $BaCl_2$ to Ho_2O_3 [136] lowers the reactivity of the oxygen species and thus favors the activation of the weaker C-H-bond in ethane (410 kJ mol^{-1}) instead of the C-H-bond in ethene (452 kJ mol^{-1}). Raman spectroscopy showed that the intensity of the bands of O_2 species was higher for the $BaCl_2$-containing catalyst compared to pure Ho_2O_3. Thus, the addition of $BaCl_2$ results in a higher storage capacity and activation activity of O_2 species. Again a higher concentration of basic sites, increased by addition of $BaCl_2$, reduces the ethene adsorption and, thus, the total oxidation of ethane. It can be inferred that intrinsically weaker adsorption and site-isolation is the key concept for avoiding readsorption of ethane on these catalysts, thus, maintaining high selectivities. Cation substitution of Ho^{3+} and Ba^{2+} is assumed to create oxygen defects active for O_2 activation. A similar

phenomenon is observed on Sm_2O_3/LaF_3 catalysts by promotion with BaF_3.[137]

1.4.3. Supported alkali oxides

The simplest and most prominent catalytic system in this class is Li_2O supported on MgO.[140] In general, such oxides belong to the group of non-redox active catalysts. However, it is not known yet whether the first C-H bond is activated via a single electron process or a paired electron process. [17] The active site is concluded to be $[Li^+O^-]$, forming defects on the MgO surface. The fact that $[Li^+O^-]$ sites possess labile O is of special importance, as the ODH activity notably decreases upon catalyst deoxygenation. The O^- species is assumed to abstract the first hydrogen atom. Evidence was found that Li^+ forms clusters on a MgO surface, but it is concluded that Li_2O domains on MgO do not show classical redox properties.[32, 141] It should be emphasized that Li^+ incorporated into a Mg-O matrix is also active and selective and can be prepared by sol-gel synthesis.[142] The reaction is assumed to proceed via radical chain reactions following a homogeneous-heterogeneous reaction pathway. The catalyst serves essentially as element to initiate the radical chain mechanism.[32] In contrast to these conclusions and the assumption that $[Li^+O^-]$ is the active site, Freund concluded that the paramagnetic $[Li^+O^-]$ does not exist under reaction conditions, as the species could not be detected by EPR spectroscopy.[33, 143, 144] Li^+ has been found to introduce oxygen vacancies in the MgO matrix. At higher Li^+ concentrations, Li-Mg oxide islands and Li_xO surface clusters form. However, Li can desorb into the gas phase at elevated temperatures (> 780°C), resulting in the formation of surface defects. Thus, while suggesting that $[Li^+O^-]$ sites may form under non-equilibrium conditions, Myrach et al. raise doubts that these are active for ethane ODH.[33] The addition of halide anions (Cl^-,Br^-) enhances activity and selectivity further.[29, 145, 146] The active sites in the halide promoted materials have not been unequivocally identified. Wang suggests Li_2O to be the catalytically active phase [141] with LiCl forming a thin layer between the support and the catalytically active phase, which modifies the base strength and suppresses Li_2CO_3 formation. Fuchs et al. concluded that the active site consists of a Li^+ cation and nucleophilic oxygen.[19] CO_2 addition to these catalysts markedly decreases the ODH activity, suggesting that carbonate formation indeed blocks active sites. Gaab et al. provided a detailed differentiation between Cl^- - free and Cl^- - containing catalysts.[30] It has been postulated that hypochlorite (OCl^-) anions form in the LiCl melt, providing transiently a highly reactive site in the LiCl melt with dissolved O_2. Alternatively, a surface-gas phase combined mechanism similar to the one for Cl^- - free catalyst has been suggested.[3] However, it cannot explain the increasing selectivity towards ethene with temperature. A third approach invokes a surface catalyzed pathway [30] suggesting the non-selective sites to be covered by or dissolved in the molten overlayer. For Cl^- -

free catalysts, surface ethyl radical formation and a radical reaction pathway in the gas phase was the dominating pathway. The initial activation of ethane to an alkyl radical in the gas phase is considered rate determining. However, at partial pressures above 70 mbar, the reaction order decreases, which is attributed to the saturation of active site.

1.4.4. Supported alkali chlorides

While supported alkali oxide catalysts show certain disadvantages including inhibition by CO_2 and limited selectivity, materials with a molten alkali chloride overlayer and no alkali oxide addition have been reported as catalytically active for ethane ODH.[51, 67] The supported liquid phase catalysts (SLC) are a new catalyst generation for ethane ODH requiring comparatively high reaction temperatures (around 600°C). However, very high selectivities towards ethane (up to 95%) can be achieved. The first C-H bond is cleaved homolytically in a single electron transfer process. Activity and selectivity have been reported for catalysts with overlayers of pure alkali chlorides and several eutecticaCl^-[147] of alkali chlorides, e.g., LiCl, KCl, NaCl, Li-K-Cl, Li-Na-Cl, Li-Sr-Cl and Li-Ba-Cl supported on (Dy_2O_3 promoted) MgO.Cl^-[51, 67] While LiCl leads to the most active catalysts, these are also the least selective ones. The selectivity towards ethene depends inversely on the melting point of the chloride. A linear increase of the selectivity with temperature is observed below the melting point, while it remains essentially constant above the melting point. Metal cations are presumably inactive for the C-H activation, but influence the catalytic behavior of the molten chloride overlayer. The oxygen solubility is the highest for LiCl, Cl^-[51] while larger cations (Na^+, K^+) lead to less dissolved oxygen.[148, 149] Ethane solubilities in the highly polar melt are negligible.[67] It is speculated that O_2 dissolved in the molten chloride reacts to form positively charged Cl atoms.[17] In turn, a transient hypochlorite species (OCl^-) is assumed to catalyze ODH. The hypochlorite anion itself has a high redox potential and is supposed to form at the interface between the chloride melt and the solid support (equation 18.

$$2LiCl(molten) + O_2(dissolved) \rightarrow 2LiOCl(dissolved) \tag{18}$$

Hypochlorite is assumed to be the transient species in low concentrations and diffuses within the melt to the surface, where it activates the C-H bond. As those anions are surrounded by alkali cations, a spatial separation occurs within the melt causing the active sites to be well-dispersed and preventing mutual interaction. However, the exact mechanism is still matter of debate. Cl radicals are not believed to play a role in alkane activation, neither as initiator nor as radical chain propagator. H-Cl bonds are unlikely. A key aspect of the adsorption properties of the melt is the Lewis acid strength of

cations. The addition of, e.g., K^+ lowers the average Lewis acidity compared to pure Li. Thus, the improved olefin selectivity in the presence of alkali/earth alkali chloride to the LiCl-Mg-Dy-O catalyst is speculated to be associated with a decrease in the Lewis acid strength.

1.4.5. Other catalysts

One of the most promising group of catalysts is based on Ni, Cu and Fe metal (cation) loaded Y-zeolites.[150] The first C-H bond is in this case assumed to be cleaved homolytically via a single electron transfer, too. Acidic catalysts were prepared by ion exchange with metal sulfates and a subsequent reduction with hydrogen. For the basic catalysts, an additional ion exchange with KOH was performed. Acidic zeolites were significantly better than the basic zeolites regarding conversion and ethane selectivity. Ni based materials showed the best performance followed by Cu and Fe, the best catalyst (Ni on acidic Y-zeolite) combining ethane conversion of 21% with ethene selectivity of 75% at 600°C. Ethene selectivity increased with increasing temperature. With acidic zeolites, ethane oxidation (leading to ethene) dominates over ethane combustion, while basic zeolites favor ethane combustion. For the ODH reaction of transition-metal supported zeolites, two mechanisms are proposed.[150] One suggests that two surface oxygens react with ethane, forming one surface metal-ethoxide and one surface hydroxyl. The metal ethoxide can undergo two subsequent reactions, α-hydrogen abstraction forming an aldehyde plus a metal hydride or a β-hydrogen abstraction, leading to ethene plus a metal hydroxyl. The second possibility is a formation of an ethyl-metal-complex plus a surface hydroxyl after one ethane molecule reacts with one surface oxide group. Subsequently, a β-hydrogen abstraction takes place, forming ethene plus a metal-hydride site. Various techniques have been applied to address the dominating mechanism[150, 151], yet it could not be clarified whether it takes place via an ethoxy-hydroxy mechanism or an ethyl radical. It was shown, however, that ethoxy groups are not stable at elevated temperatures.[151]
Carbon materials, especially carbon nanotubes, have also been reported to be active. The catalysts appear to be challenging to use, as ethane conversions below 5% at 400°C were reported and the use of higher reaction temperatures is seen problematic, because of the potential oxidation of the catalyst. This problem can be mediated by surface modification by adding B_2O_3 or P_2O_5, having the positive side effect reducing the concentration of electrophilic oxygen, which increases the selectivity. The nature of the active sites is not defined, having a too low concentration to be successfully characterized.[152]

1.4.6. Conclusions

Table 1 provides a synopsis of a selection of active sites presented in this chapter, listing only the basic types of sites. The characteristics of sites and the specific mechanisms are compiled together with typical reaction temperatures and selectivity levels. A complete list of referenced catalysts including their performance is presented in section 1.6. The redox active site is either a cation (such as V^{5+}/V^{4+}) or an anion redox pair (such as OCl^-/Cl^-). High dilution of sites and a higher acid strength appear to promote the desorption of ethyl species and favor the selectivity in this way. The sites with metal redox functionality require lower temperatures than anion redox pairs and yield high selectivities. Especially V or Ni-Nb based oxides are among those with the lowest required reaction temperatures. High reaction temperatures also entail the danger of inducing a radical chain mechanism, which tends to lead to lower selectivity. Thus, the temperature is one of the critical parameters determining whether a mechanism is purely heterogeneous (i.e., redox reactions on catalyst surfaces) or homogeneous (surface induced gas phase radical chain reactions).[4]

Table 1.: Different sites active for ethane ODH

Site	Type of site	Activation of first C-H bond	Mechanism	Operation range [°C]	Selectivity range [%]	Ref.
V-O	Redox	Single electron process, homolytic	Transient radicals on catalyst surface	430 - 650	10-90	[38], [36]
Mo-O	Redox	Single electron process, homolytic	Redox cycle	550 - 580	40-90	[95], [97]
[Ni-Nb-O]	Redox	[a]	[a]	350 - 400	80-90	[16],[153]
Co-O	Non-redox	[a]	[a]	550	45-80	[125]
Sm_2O_3	Non-redox	Single electron process, homolytic	Radical chain	550-700	20-70	[28]
[Li-MgO]	Non-redox	Single electron process, homolytic	Radical chain	570-650	57-75	[140], [154]
$[OCl^-]$	Redox	Single electron process, homolytic		525-600	80-95	[51], [67]

[a]: Not reported or still unclear

1.5. Advanced reactor concepts for ethane ODH

Obviously, activity and selectivity in ODH does not only depend on the properties of the catalyst, but is critically influenced by the reactor as well. As weakly bound oxygen species on catalyst surfaces are concluded to lead to accelerated COx formation, higher O_2 partial pressures lead to lower selectivity, especially with catalysts containing metal redox pairs.[6] Thus, various concepts have been investigated to limit the concentration of this species (such as membranes, cyclic reactors and variations in the oxygen/hydrocarbon feed). In this chapter, focus is given on two important concepts, i.e., membrane reactors and reactors with a millisecond residence time.

1.5.1. Membrane reactors

Two main different types of membrane reactors are known and practically implemented, i.e., the extractor and the distributor reactor.[25] After shortly introducing both concepts, the aim of this section is to rationalize and discuss which reactor type could be promising for ODH reactions. The extractor membrane reactor separates products within the reactor to prevent consecutive reactions. For equilibrium limited reactions it enables higher conversions by selectively extracting the limiting reaction product, such as H_2 from dehydrogenation. However, the H_2 extractor membrane does not provide a solution for coking, a major cause for catalyst deactivation in the dehydrogenation of ethane. The removal of ethene, enhancing the selectivity by avoiding the consecutive reaction, is not feasible for ODH, as membranes with a sufficiently high separation factor between ethane and ethene are not known, thereby limiting the potential of the membrane extractor concept. The distributor membrane reactor disperses a reactant across the catalyst bed avoiding locally high concentrations. This is of special importance to reduce the explosion limits with hydrocarbon - oxygen mixtures so that undiluted feed streams can be used.[4] Furthermore, it has the potential to enhance the product selectivity, if the distributed reactant has a higher reaction order in the undesired reaction path than the desired one, as it is the case for O_2 in ODH.[4] Typically interfacial membrane reactors are used, equipped with catalytic membranes that enable the reaction at the membrane surface. Rodriguez et al. simulated the performance of ethane ODH with a Ni-Nb-O catalyst packed in a tubular porous inorganic membrane reactor dosing oxygen to the shell side across the membrane and ethane to the center compartment [155] and compared the results to a model for a conventional multi-tubular reactor.[156] While the conversion of ethane in a tubular porous inorganic membrane reactor remained about the same compared to a fixed-bed reactor, the selectivity towards the olefin was improved. Higher selectivities were explained by locally lower O_2 partial pressures and smaller temperature gradients achieved with the axial distribution of O_2. The operating conditions have to be fine-tuned especially by O_2 addition to the ethane feed in order to enhance reaction rates. O_2 permeation rates which are higher than O_2 consumption rates lead to an unfavorable concentration profile with oxygen accumulation along the catalyst bed inducing lower selectivity. On the other hand, feeding the majority of oxygen in mixture with ethane would jeopardize the enhancement by the distributor membrane as it leads back to a quasi-conventional reactor with strongly exothermic total oxidation, lowered olefin selectivity and the appearance of hot-spots. Concerning the membrane type, a porous membrane with a weakly temperature dependent trans-membrane oxygen flux is apparently more amenable than dense membrane materials with their temperature related oxygen permeation. Iglesia et al. have studied the staged feed of oxygen for ethane ODH with a well-known V_2O_5 catalyst. Similar

activities have been observed compared to a regular fixed bed reactor despite notable differences in the local oxygen concentration. Kinetics is identical in staged and constant feeds. However, the total oxidation of the produced ethene was lower with a staged oxygen feed. Reaction studies revealed that the homogeneous part of ethene oxidation is dependent on the oxygen concentration, while the heterogeneous part is zero-order in oxygen.[157] As the catalyst-to-volume ratio is high in industrial scale reactors, homogeneous contributions to the whole reaction are almost negligible. Thus, the benefits of a staged oxygen feed become less important in large-scale applications using a V_2O_5 catalyst. Another study compared the performance of a similar catalyst (vanadium oxide supported on gamma-alumina) for ethane ODH, in a fixed-bed or membrane reactor configuration at high space velocities and under oxygen excess.[158] The conversion of ethane was higher in the packed membrane reactor, while the olefin selectivity decreased. This phenomenon is particularly important at oxygen excess, as the total oxidation of ethene is higher in the membrane reactor than in the packed-bed reactor. It is related to the local O_2 concentrations. In the first part of a membrane reactor, ODH is the dominant reaction. However, as this part has the longest contact times, total oxidation of ethane also occurs. In the second part, excess oxygen conditions lead to the total oxidation of ethene, mainly to CO. In the last part, oxygen still being present in excess, leads to the oxidation of ethene and CO. Given those facts, a catalyst does not always perform equally well in fixed-bed and membrane reactors. Kinetics and the influence of contact time are key factors influencing catalyst performance for each reactor type. To use another well-known ODH catalyst in an advanced reactor concept, MgO doped with Li and Sm_2O_3 was used as a packed catalyst in a reactor with oxygen dosing via a porous Al_2O_3 membrane.[159] The Sm_2O_3-doped catalyst showed better performance in the membrane reactor. Limited to low ethane/O_2 ratios in the feed, splitting the O_2 feed gave marked improvements compared to a standard PFR. However, this effect disappeared for higher ethane/O_2 ratios [159], as it is sensitive to contact times. As the O_2 feed rates increased at a low feed ratio, the contact times of oxygen and ethane differed, thus, causing differences in the behavior of the reactor. At higher ethane/O_2 feed ratios, however, the contact times of both reactants became similar to a standard PFR. This example illustrates that staged O_2 admission is beneficial for ethane ODH, with yields for certain conditions to be about three times higher than yields obtained in a fixed-bed reactor. However, the membrane reactor was not performing well at short contact times. As long contact times and a low ethane to O_2 ratio are neither productive nor likely due to flammability issues, this improvement is not realistic for large-scale application due to a very limited parameter window. Some membranes catalyze ODH even without additional catalyst. However, coating those membranes with a catalytically active material enhances the performance of the membrane reactor.[26] Reactions are run at around 1000 K, a temperature at which surface modified dense membranes

allow a constant supply of the catalyst with ionic oxygen extracted from air fed to the other side of the membrane. Perovskite membrane (Ba-Sr-Co-Fe-O) showed outstanding high oxygen permeation, however, the trans-membrane flow of oxygen decreased with time at lower temperatures (< approx. 1000 K).[160] The membrane surface was modified with Pd nanoclusters or V/MgO catalyst on the permeate side surface. A first effect of the modification relates to changes in the oxygen permeability as shown for V-based modification doubling the oxygen flows across the membrane. Ethane conversions increase linearly with temperature up to about 60% at around 800°C for a reactor with bare membrane, while selectivity decreased slightly with rising temperature. The energy of activation was higher for the coated membranes, but selectivities decreased even faster. Nonetheless, the highest ethene yield of about 75% was achieved with a catalyst modified membrane showing a stable performance over at least 23 days. Essential for the operation of those materials was a reasonably high oxygen flux across the membrane that can be controlled with temperature. The membrane transports ionic oxygen converting to the activated species (O^{2-}, O^{-}, O_2^{-}) at the catalyst surface without presence of O_2. Hence, this concept allows fine-tuning for catalytic systems following a Mars-Van-Krevelen mechanism.[25] A staged reactor concept has been introduced that combined the dehydrogenation with the oxidation of the formed H_2.[114] A perovskite-based hollow-fiber membrane made of mixed oxygen-ion electron-conducting dense Ba-Co-Fe-Zr-O, was used to separate O_2 from air. Parts of the membrane were passivated with Au creating different reaction zones, i.e., passivated parts were dehydration zones, where H_2 and ethene were produced, while oxygen was transported into non-passivated parts. Conversions could reach up to 52% with selectivities up to 72%. The membrane is claimed to be coke-resistant and to allow long-term operation. The performance of the reactor concept is supposed to improve upon coating one site of the membrane with a catalyst. However, the reaction is not a classical ODH, because of the intermediate formation of H_2.

1.5.2. Short contact time partial oxidation of ethane

Schmidt and Holmen have utilized monoliths for ethane ODH at very short contact times.[161, 162] Using a very short contact time of the reactant/product mixtures (approx. 10^{-4} s) offers advantages including a small reactor volume and an autothermal operation mode. Typical catalysts are supported Pt and Rh. The extremely short contact times help to minimize ethene re-adsorption to enhance olefin selectivity. The activation of the first C-H bond is homolytic, thermally induced by a single electron transfer. The performance of short contact time reactors can be significantly improved by H_2 added to the feed stream [8], increasing ethene up to 85% for Pt and Pt-Sn catalysts. For very low contact times (around 0.5 ms) the flow rate did not influence the

selectivities. Thus, a homogeneous gas-phase mechanism can be ruled out. It is assumed that H_2 is oxidized, which generates heat and consumes O_2, lowering thereby the concentration of O_2 available for total oxidation, as H_2 is formed by dehydrogenation of ethane. Further studies showed that the metal coating of the monolith directs selectivity. With Pt and Pt-Sn, mainly ethene is formed next to CO, H_2 and water as byproducts. Rh, however, produces mainly synthesis gas. Pd leads to a severe carbon deposition.[161] Three different mechanistic scenarios are discussed, i.e., a completely homogeneous gas-phase mechanism, a completely heterogeneous surface mechanism, and a combination of both, with H_2 oxidation taking place on the surface and the ethane dehydrogenation via radicals in the gas phase. The results cannot be described unequivocally by each of the mechanisms. One prominent way to model the reaction network on Pt-coated monoliths includes the assumption that the catalyst burns a fraction of ethane, generating heat. This heat is used to form radicals that start a homogeneous gas-phase mechanism.[163] The heterogeneous mechanism suggests that ethane is adsorbed dissociatively forming ethene and eventually C and H on the catalyst surface followed by the oxidation of both. However, this model cannot fully explain the catalytic chemistry, when hydrogen is co-fed into the reactor. The combined surface-gas-phase mechanism [164] suggests that ethene is formed in the gas phase (in the case of Pt and Pt-Sn monoliths), while CO, H_2 and H_2O are mainly formed on the surface. Holmen et al. studied the extinction and ignition behavior of short contact time processes.[162] During ignition and extinction, CO and CO_2 were observed as main reaction products together with a noticeable temperature change during these processes. These results also suggest that ODH takes place in the gas phase, while the by-products H_2, CH_4 and CO_x are formed on the Pt surface. Monoliths of rare earth metals and alkaline-earth metal oxides are concluded to follow the same reaction pathway.[105, 165]. The microkinetic aspects of short contact time ethane activation over these materials have been investigated in greater detail by transient kinetic measurements, focusing on the nature of the active oxide species.[166] It has been found that adsorbed monoatomic and diatomic oxygen are active during the ignition of the alkane-oxygen mixture. While the latter was active for ODH, diatomic oxygen was responsible for heterogeneously catalyzed total oxidation. Pt/Al_2O_3 showed a similar behavior, the catalyzed combustion accelerated the ignition of ethane/oxygen mixtures at autothermal conditions, thereby also showing a homogeneous-heterogeneous mechanism.[165] This holds also true for other catalytic materials. Over oxides of non-reducible metals, heterogeneous reaction steps form adsorbed oxide species that are reactive for ethane ODH. Due to the exothermic character of this reaction, the temperature of the catalytic bed rises. This leads to the thermal dehydrogenation of ethane, thus, improving the overall ethene yield. An important improvement for short-time reactor concepts is heat-integration.[105] Reverse-flow operation of a fixed-bed reactor with a coated monolith is possible (about 15s per cycle). While selectivities remain

nearly unchanged, conversion levels can be drastically improved (up to approx. 90

1.6. Summary and outlook on catalytic ODH

Table 2 shows performance data of the catalysts and Table 3 the performance data of the different reactor concepts introduced in this paper. The results are summarized in Figure 8. It should be pointed out that the data represent the best catalytic performance in each of the cited references, but does not consider the space-time yield of the catalytic systems. Interestingly, the concepts with the best performance (>70% ethene yield) are not restricted to one class of catalyst or reactor concept indicating that a multitude of possible solutions to the problem exists.

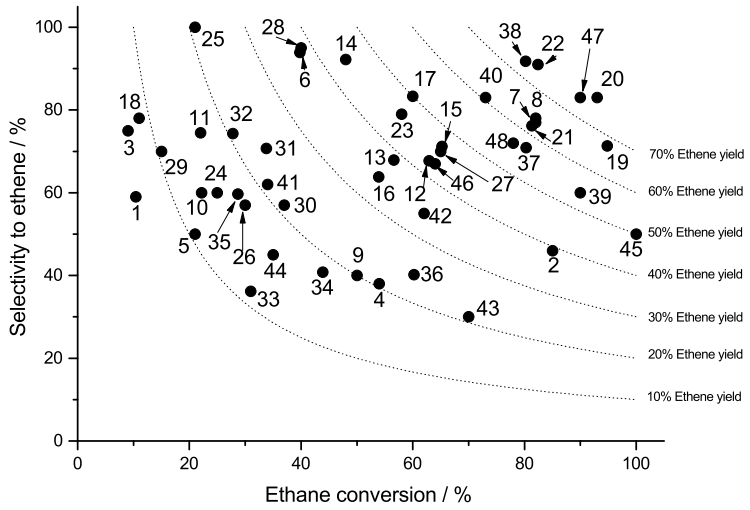

Figure 8.: Performance of catalytic and reactor systems

High selectivities are limited by the high olefin reactivity and the favorable thermodynamics of paraffin and olefins oxidation. In consequence, all catalytic materials show some activity for total oxidation of paraffins and olefins. Rapid ethene desorption by adjusting the acid-base properties, and limiting ethene re-adsorption by minimization of Lewis acid site concentrations as well as coupling surface catalyzed activation of ethane with gas phase radical chain reactions have been found to be the most promising concepts for catalyst and process design. While membrane-based processes show only moderate chance of success, ultra short reactor concepts appear to be closer to the practical realization. Suitable catalysts for ethane ODH are divided into two groups. In the first one, ideal as possible oxide surfaces minimize the concentration of

Table 2.: Performance data for selected catalysts

Nr	Catalyst	T [°C]	X(C_2H_6) [%]	S(C_2H_4) [%]	Ref.
1	Ni12-Ce	275	10,4	59	[119]
2	Pt monolith	450	85	46	[162]
3	MoVNb	400	9	75	[111]
4	NiW0.36	400	54	38	[118]
5	NiW0.45	400	21	50	[118]
6	$MoV_{0.39}Te_{0.16}Nb_{0.17}O$	380	39,8	93,9	[107]
7	LiMgCl/Dy_2O_3	570	81,3	76,2	[167]
8	LiZnOCl	721	82	78	[141]
9	5.2wt%V_2O_5/γ-Al	430	50	40	[36]
10	Co7.6/TiO_2	550	22,2	60	[125]
11	Ni/HY	600	22	74,5	[150]
12	BaF_2/SL1 (Sm_2-LaF_3)	700	62,9	67,7	[137]
13	$BaCl_2/Ho_2O_3$	640	56,6	67,9	[136]
14	7wt%Co-$BaCO_3$	650	48	92,2	[127]
15	SrLaNdO	700	65,2	71,2	[168]
16	3%Li/MgO	625	53,9	63,8	[140]
17	Mg/Dy/Li/O/Cl	600	60	83,3	[169]
18	Li-MgO-Cl	675	11	78	[170]
19	LiCl/ZrON	650	94,8	71,3	[171]
20	NdLi/SZ	650	93	83	[171]
21	Li-MgDy-O-Cl	600	82	77	[67]
22	Li-Na-Mg-Dy-O-Cl	650	82,4	91	[51]
23	Sr-Nd_2O_3	800	58	79	[134]
24	Sm_2O_3	700	25	60	[28]
25	10CaCe	750	21	100	[132]
26	20wt%Vox/Al	550	30	57	[43]
27	$Ni_{0.85}Nb$: 0.15	400	65	70	[16]
28	MoVSbO	400	40	95	[64]
29	VOP/Ti9	550	15	70	[28]
30	10VAl	550	37	57	[41]
31	M10V5	580	33,8	70,7	[95]
32	VCo-2	600	27,8	74,3	[85]
33	ClMoSiTi	600	31	36,2	[104]
34	CoVAPO-5	600	43,9	40,8	[58]
35	MgVAPO-5	600	28,7	59,7	[87]
36	V/Al	600	60,2	40,2	[84]
37	$SrCl_2/Sm_2O_3$	640	80,3	70,9	[138]
38	SmOF	700	80,2	91,8	[172]

Table 3.: Performance data for selected reactor concepts

Nr	Catalyst,Reactor configuration	T [°C]	X(C_2H_6) [%]	S(C_2H_4) [%]	Ref.
39	Pt/alumina, rev. flow reac.	n.r.	90	60	[105]
40	Pt/Sn, H_2 cofeed	n.r.	73	83	[8]
41	Pt/10% Rh gauze	[a]	34	62	[173]
42	Pt foam monolith	875	62	55	[161]
43	PBR, VOx/γ-Alumina	600	70	30	[158]
44	2 wt% V_2O_5/Al_2O_3 staged feed	n.r.	35	45	[157]
45	$BaCo_xFe_yZr_{1-x-y}O$	725	100	50	[174]
46	$BaCo_xFe_yZr_{1-x-y}O$, BCFZ membrane	725	64	67	[175]
47	V/MgO membrane	777	90	83	[26]
48	$Na_{0.009}CaO_x$	[b]	78	72	[166]
[a]: surface: 900°C; gas: 580°C [b] Ignition: 600°C; maximum: 927°C					

accessible Lewis acid metal sites, responsible for ethene re-adsorption. In the second group, molten active components generate dynamically rearranging surfaces that prevent re-adsorption of the olefin by minimizing the concentration of coordinatively unsaturated metal centers. For conventional reactor systems catalysts based on complex vanadia mixed oxides and supported molten chlorides are the best catalysts. Pt-Sn catalysts have been identified to be the best catalysts for ultra-short contact time reactors. Drastic differences in materials emphasize how different energies of activations for the multitude of steps in the complex reaction sequence lead to very different results for optimal catalysts. The complexity of the reaction also makes it nearly impossible to generalize the nature of selective and nonselective sites. The critical catalytic preferences will be influenced by the rates of processes in a complex matrix, influenced by default via the different energies for activations, preexponential factors, and concentrations of the catalyzing sites. Oxygen intermediate species could be, thus, active and selective for ODH on one catalyst, but nonselective on others. The examples shown above illustrate that a detailed understanding of reaction mechanism, the nature of the active sites and kinetics is essential for the designing and optimizing of catalytic properties and the synthesis of new catalysts. The improvement of existing and the realization of new reactor concepts have to occur in a coordinated fashion. The unprecedented increase in insight into the material properties, the strategies to synthesize these materials, the detailed chemistry of the individual reaction steps and last but not least the fluid dynamics of advanced reactor concepts make it appear realistic that ethane ODH will be competitive to steam reforming in the near future.

This chapter is based on the following article: Christian A. Gärtner, Andre C. van Veen, Johannes A. Lercher: Oxidative Dehydrogenation of Ethane: Common Principles and Mechanistic Aspects, *ChemCatChem*, 2013, 11, pp. 3196-3217

2. ODH of ethane via dynamically arranging chloride catalysts supported on redox active supports

Ethane is oxidatively dehydrogenated with selectivity up to 95% on catalysts comprising a mixed molten alkali chloride supported on a mildly redox-active Dy_2O_3 doped MgO. The reactive oxyanionic OCl^- species acting as active sites are catalytically formed by oxidation of Cl^- at the MgO surface. Under reaction conditions O_2 dissolves in the alkali chloride melt, dissociates and replenishes the oxygen vacancies on the MgO surface created by OCl^- formation. The oxyanion oxidatively dehydrogenates ethane at the melt-gas phase interface with nearly ideal selectivity. The reaction is concluded to proceed via two coupled steps following a Mars-van Krevelen mechanism at the solid-liquid and gas-liquid interface. The dissociation of O_2 and/or the oxidation of Cl^- at the melt-solid interface is concluded interface is concluded to have the lowest forward rate constants. The compositions of the oxide core and the molten chloride shell control the catalytic activity via the redox potential of the metal oxide and of the OCl^-. The spatial separation of oxygen and ethane activation sites and the dynamic rearrangement of the surface anions and cations, preventing the exposure of coordinatively unsaturated cations, are concluded to be the origin of the high olefin selectivity.

2.1. Introduction

The oxidative dehydrogenation (ODH) of ethane is conceptually a selective route from ethane to ethene, which replaces the external energy input in the generation of ethene by coupling it to the oxidation of hydrogen. The economic feasibility of the route, however, necessitates very high olefin selectivity, as it competes as a process with ethane steam cracking. To be viable, the process must avoid not only the loss by total oxidation, but also the formation of aromatic by-products.[1] Oxidative dehydrogenation requires the activation of both reactants, O_2 and ethane. It is usually assumed to occur via the formation of the reactive species either by redox [176] or radical [28] chemistry. This is followed by the abstraction of two H atoms and the formation of a C-C double bond upon desorption. As the formed π-bond interacts strongly with coordinatively unsaturated metal cations, it tends to react readily on many redox active catalysts. Total oxidation of ethane and ethene is also more exothermic than ODH, thus, being thermodynamically favored.[177] An ideal catalyst must, therefore, be selective for C-H bond breaking but not for oxygen insertion, the reaction that eventually leads to the total oxidation of the carbon atom to which the oxygen is attached. Such a catalyst should also be able to adsorb the paraffin stronger than the olefin. Ethene desorption must be fast and the re-adsorption of ethene, mainly facilitated by coordinatively unsaturated metal cations on surfaces, should be minimized. A recent review of the main classes of catalysts considered for ethane ODH indicates that for most catalysts the first C-H bond activation either via single electron transfer (i.e., radical) or involving paired electrons (i.e., redox) is rate determining.[177] While in nearly all the cases, the initial CH bond is broken homolytically, catalysts that operate via a Mars - van Krevelen redox mechanism exhibit in general high ethene selectivity, while catalysts supporting free radical pathways yield high selectivity to CO_x. The factors governing activity and selectivity include the metal-oxygen bond strengths in oxide catalysts, the specific atomic arrangement of the active sites, the concentration of these sites as well as the ease of desorption and re-adsorption of ethene.[177] Supported alkali chloride catalysts have been reported to show surprisingly high olefin selectivity in the oxidative dehydrogenation of ethane. The excellent selectivity of such catalysts has been associated with the fact that the catalysts are supported alkali or alkaline earth chlorides that are molten and therefore dynamically rearrange under reaction conditions.[51, 67] Ethene selectivity in the ODH of ethane has been reported to exceed 90%. Especially the low density of sites and the facile desorption of ethene seem to be relevant factors. The density of sites is low, as the active species are concluded to be dissolved in the melt and homogeneously distributed, making it less likely that ethene formed reacts again with such sites. In addition, the molten overlayer provides a dynamically rearranging surface, which is able to minimize the readsorption of ethene, as the chloride termination does not allow a long exposure

of metal cations to the gas phase. Because activity and selectivity critically depend on the nature and concentration of these dynamically forming active sites, this catalytic chemistry is explored mechanistically, and the concentration and dynamic genesis of the active sites under reaction conditions are studied.
For supported alkali chlorides, two different mechanistic hypotheses have been presented. The first proposes the transient formation of OCl^- as catalytically active species, the ODH reaction taking place at the surface of the overlayer.[67] The second suggests the formation of the redox pair Li_2O/Li_2O_2 as active species, which is modified and protected by Cl^- anions.[178] However, both hypotheses have not been substantiated and quantified experimentally. It is reported that alkali chlorides are most effective, if they are used in eutectic compositions, providing faster access to a supported liquid salt. With LiCl as one component, the second can be a different alkali or an alkaline earth chloride.[51, 67] Decreasing the melting point of the eutectic compared to pure LiCl results in an increasing selectivity towards ethene but also decreasing activity. In this study, Li-K-Cl in eutectic composition has been chosen as model system, since it leads to the catalysts with the highest olefin selectivity reported so far.[67] Additionally, the Li-free eutectic system (Na-Cs)Cl was studied to probe the necessity of the presence Li^+ cations for selective catalysis, aiming to develop a comprehensive mechanistic model, which adresses elementary steps and critically distinguishes between the mechanistic hypotheses. This holds especially true for the role of the support, while various overlayer compositions have already been studied.[67] The activation of O_2 and ethane has been addressed using transient kinetic studies. Those are implemented in step experiments, which additionally allow the quantification of the O_2 and ethane uptakes. Temperature programmed isotopic exchange experiments allow to determine and quantify the oxygen dissociation of both support and catalyst, providing important information about the oxygen dissociation step.

2.2. Experimental

Catalyst preparation

Catalysts were prepared by wet impregnation of chlorides. The support material (MgO (Aldrich, >99%), Dy_2O_3 (Aldrich,99,9%) or ZnO (Aldrich, 99.9. %) was added to 100 ml deionized water, followed by the chloride salts forming the overlayer (LiCl (Aldrich,>99,5%) , KCl (Merck,99,5%), NaCl (Merck, puriss.), CsCl (Aldrich, >99,5%)). The slurry was stirred at 80°C for 2 h, followed by the evaporation of water under reduced pressure. The residue was dried at 120°C for 12 h and calcined in synthetic air (100 ml/min) at 650°C for 12 h. Table 4 compiles the chemical compositions of the

catalysts.

Table 4.: Compositions of catalysts

Nr	Support 1	Support 2	Over-layer 1	Over-layer 2	mol support 1	mol support 2	mol over-layer 1	mol over-layer 1	mol% overlayer
1	MgO	Dy_2O_3	LiCl	KCl	0.165	0.0031	0.00129	0.000872	1.27
2	MgO	Dy_2O_3	LiCl	KCl	0.165	0.0031	0.00299	0.00293	3.4
3	MgO	Dy_2O_3	LiCl	KCl	0.165	0.0031	0.0059	0.004	5.57
4	MgO	Dy_2O_3	LiCl	KCl	0.165	0.0031	0.012	0.008	10.67
5	MgO	Dy_2O_3	LiCl	KCl	0.165	0.0031	0.024	0.0159	19.23
6	MgO	Dy_2O_3	LiCl	KCl	0.165	0.0031	0.048	0.0321	32.23
7	MgO	Dy_2O_3	LiCl	KCl	0.165	0.0031	0.072	0.048	41.65
8	MgO	—	LiCl	KCl	0.168	—	0.024	0.0159	19.23
9	ZnO	—	LiCl	KCl	0.168	—	0.024	0.0159	19.23
10	MgO	Dy_2O_3	NaCl	CsCl	0.165	0.0031	0.014	0.026	19.23

To selectively tailor surface properties of MgO, one catalyst (composition according to row 9 in Table 4) was synthesized using MgO sintered at 900°C for 12 h in synthetic air in a muffle furnace.

Physicochemical characterization

BET surface areas and pore size distributions were determined by N_2 adsorption-desorption at 77K using a PMI Automated BET Sorptomatic 1900 Series instrument. Prior to the adsorption, the samples were evacuated at 250°C for 2 h.

HAADF-TEM

HAADF-TEM measurements were performed at a FEI aberration-corrected Titan 80/300 TEM/STEM microscope, equipped with a Gatan Quantum 965 spectrometer for EELS analysis operated at 300 kV.

ICP-OES

ICP-OES was performed with an SpectroFlame Typ FTMOA81A ICP-OES spectrometer from Spectro Analytical Instruments. Samples were suspended in deionized water under ultrasonic treatment. All samples were filtered before analysis.

Reactant gases

For ODH test reactions, the following gases (all supplied from Westfalen AG) were used: He 3.5 , Ethane (99.995%) and oxygen (10.1%, dissolved in He 3.5). For calibrations, ethene 3.5 was used. For the isotopic labeling studies, C_2D_6 and $^{18}O_2$ (97% isotope enrichment) were used.

Catalytic tests

Catalytic tests were carried out in a plug flow reactor consisting of a catalyst fixed-bed in a quartz tube surrounded by heat distributor blocks and heating coils. Most experiments used 300 mg of the catalysts diluted in 700 mg SiC (450-600 μm) to improve the heat transfer and ensure homogeneous temperature over the entire catalyst bed. Layers of SiC and quartz wool encased the catalyst bed to avoid dead volume. Reactant flow rates were individually adjusted by mass flow controllers (Bronkhorst). The effluent stream composition was quantified by a Maxum Edition II Process gas chromatograph (Siemens) equipped with TCD detectors. O_2, CO and CH_4 were separated on a Molesieve 5A column (2 m, 60/80 mesh) and the other hydrocarbons were separated on a HayeSep Q column (2 m, 80/100 mesh) combined with a HayeSep T pre-column (0.5 m, 80/100 mesh). The time resolved product stream analysis in transient experiments and isotopic studies was accomplished with a calibrated Pfeiffer Omni Star^{TM} GSD 320 OC mass spectrometer system connected in parallel.

Steady state kinetic measurements

Standard conditions for steady state experiments were partial pressures of ethane (99.5%) and O_2 (10.1% in He) of 70 mbar each with balance He (99.99%) to atmospheric pressure. A temperature range between 450°C and 650°C was explored, most experiments were performed at a WHSV of 0.8 h^{-1}.

Sequential step transient experiments

The catalyst was heated to the reaction temperature in He and then 10% O_2 in He was subsequently supplied for a variable time (45 min to reach equilibrium, 1 min to establish the kinetics of the intermediate formation in a different experiment) . The probe reaction with ethane (10% C_2H_6 in He) followed a purge with 40 ml/min He of variable duration detecting the ethane consumption and ethene formation by MS analysis. Ethane and ethene were quantified by linear deconvolution of different MS signals m/z = 26,27,28,29,30.

Steady state isotope transient kinetic analysis (SSITKA)

A $LiKCl/MgO + Dy_2O_3$ catalyst was investigated by SSITKA. 300 mg catalyst diluted with 700 mg SiC was used at steady state for 48 hours to achieve steady state. Experiments were performed at 550°C, 600°C and 625°C subsequent to a 20 min. He purge at each temperature. The reaction was run at a WHSV of 0.8 h^{-1} using partial pressures

70 mbar of ethane and O_2 with He balance to atmospheric pressure. Steady state operation was established using a feed containing $^{16}O_2$ for 30 minutes. The influent was switched in a sharp step to a feed containing an identical concentration of $^{18}O_2$ instead of $^{16}O_2$ replacing additionally a small fraction of He by the inert tracer Kr. The isotope transient at steady state was monitored for 40 minutes. A blank experiment at 625°C with inert SiC excluded contributions of gas-phase reactions and back-mixing phenomena. The effluent composition was quantified by MS analysis assigning the following components to the respective mass to charge ratios: $^{16}O_2$ (m/z: 32), $^{16}O^{18}O$ (m/z: 34), $^{18}O_2$ (m/z: 36), $H_2^{16}O$ (m/z: 18), $H_2^{18}O$ (m/z: 20), $C^{16}O_2$ (m/z: 44), $C^{16}O^{18}O$ (m/z: 46), $C^{18}O_2$ (m/z: 48), Kr (m/z: 84).

Isotope scrambling experiments

Temperature programmes isotopic exchange

Temperature programmed isotopic exchange experiments with oxygen isotopes were performed with several catalysts and their respective supports. 300 mg catalyst was diluted with 700 mg of SiC. After pre-heating in He to 450 °C and a short equilibration in the O_2 isotope mixture, the temperature was increased with 5°C/min to 650°C, feeding a gas stream of 10 ml/min with a composition of 2,5% $^{18}O_2$, 2,5% $^{16}O_2$ and 95% He. The temperature was held at 650°C for 15 minutes. $^{18}O_2$ with 97% isotopic enrichment was used. For detection of the different oxygen species, the following m/z signals were used: 32 for $^{16}O_2$, 34 for $^{16}O^{18}O$ and 36 for $^{18}O_2$. For the case of ethane, a gas flow of 9 ml/min He, 0.5 ml/min C_2H_6 and 0.5 ml C_2D_6 was fed. The experiment was started at 450°C with a temperature ramp of 10 K/min up to 650°C. The signals at m/z 30,31,32,33,34,35,36 were recorded.

Isotopic exchange of catalyst bulk oxygen

A $LiKCl/MgO + Dy_2O_3$ catalyst was heated at 625°C for 2 h in He. By switching a valve, 40 ml/min of 10% $^{18}O_2$ (97% isotopic enrichment) in He was fed into the reactor. The outlet stream was analyzed by MS.

2.3. Results and discussion

2.3.1. Role of cations and chloride for the oxidative dehydrogenation of ethane

Figure 9 compiles reaction data for two different eutectic overlayers (Li-K-Cl, mp: 353°C [67], Na-Cs-Cl mp: 486°C [179]) on $MgO+Dy_2O_3$. The rates of ODH reaction markedly exceeded those of total oxidation on both catalysts, i.e., the selectivity to ethene varied between 93% and 100% for Li-K-Cl and between 86% and 94% for Na-Cs-Cl. The preexponential factors for the total oxidation were by far lower than the preexponential factors for ODH indicating only a very small concentration of unselective sites. This difference in the preexponential factors makes the variations in the apparent activation energy less relevant for the activity and selectivity. It is interesting to note that the preexponential factor for CO_2 formation was higher in the case of Na-Cs-Cl indicating that with larger cations (60% Cs^+ in the case of Na-Cs-Cl, 42.5% K^+ in the case of Li-K-Cl) a higher degree of total oxidation was observed.

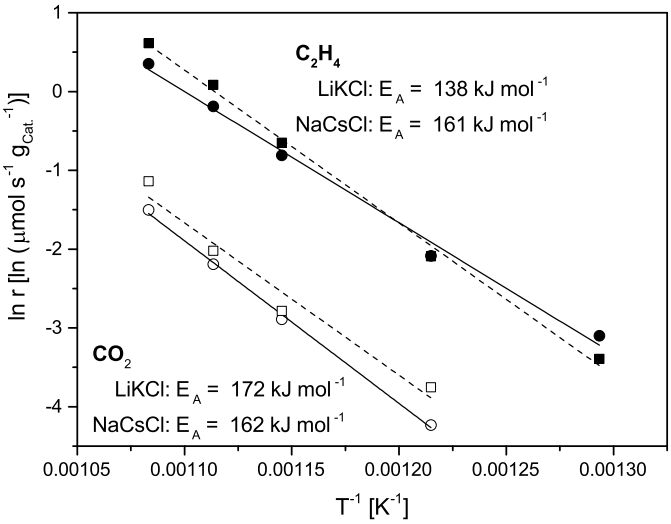

Figure 9.: ODH and side reactions: •, ○:LiKCl/$MgO+Dy_2O_3$ (entry 5, Table 4), ■, □: NaCsCl/ $MgO + Dy_2O_3$ (entry 10, Table 4); 0.3 g catalyst, WHSV = 0.8 h^{-1}- 2.0 h^{-1} ,$p_{O2} = p_{Ethane}$ = 80 mbar, p_{total}=1 bar)

Because both catalysts had similar activities, the conclusion that the redox pair Li_2O/Li_2O_2 is essential for the ODH reaction as proposed e.g. by Landau[178] is rejected. In turn, as chloride is the common component in both catalysts (besides the support, which is concluded not to be exposed to the gas phase), the catalytic activity

is concluded to be related to the chloride anion.

2.3.2. Impact of the nature and thickness of the chloride overlayer

As the chloride anion plays a key role in the ODH of ethane on supported alkali chloride catalysts, the influence of its concentration has been quantitatively explored. A series of catalysts with different molar ratios between chloride overlayer (LiCl/KCl in eutectic composition [51, 67]) and the support (physical mixture of MgO and Dy_2O_3) were tested for their activities and surface properties. The appendix (Figure 51) includes an in situ X-ray diffraction analysis of Li-K-Cl/MgDyO. It is shown that the oxidic support and the chloride overlayer remain in different crystalline phases at ambient temperature and do not form a mixed crystalline phase. Figure 10 reports the surface areas of the catalysts with different molar overlayer fractions ($N_{overlayer}$ / ($N_{overlayer}$ + $N_{support}$)), Table 5 reports the theoretical film thicknesses, for the assumption that the surface area of the support is 69 m^2g^{-1} (fresh support) and for the assumption that the surface area of the support is 33 m^2g^{-1}, i.e., the specific surface area after removal of all chloride (as explained below).

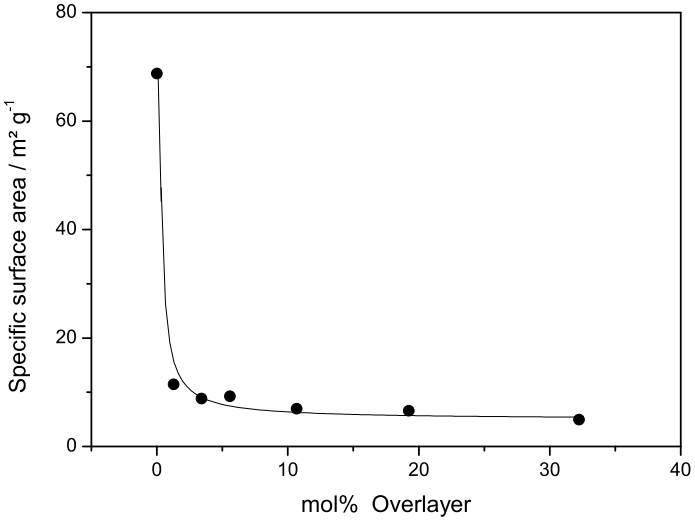

Figure 10.: BET surface areas of catalysts with different chloride loadings

Table 5.: Calculated chloride layer thicknesses (Assumptions: Pores are not filled, densities of LiCl and KCl at 20°C)

Sample Nr	mol% overlayer	Calculated film thickness with assumption of support surface = 68 m^2g^{-1} [nm]	Calculated film thickness with assumption of support surface = 33 m^2g^{-1} [nm]
1	1.27	0.13	0.23
2	3.4	0.26	0.57
3	5.57	0.55	1.15
4	10.67	1.1	2.3
5	19.23	2.2	4.59
6	32.23	4.4	9.18
7	41.65	6.6	13.77

While the pure support had a surface area of 68 m^2g^{-1}, the addition of the minor overlayer of 1.26 mol% alkali chlorides decreased it to only 12 m^2g^{-1}. The addition of more chloride resulted in a further, but slower decrease to 5 m^2g^{-1} at a molar overlayer concentration of 32%. While assuming for these calculations that pore blocking or pore filling did not occur, in reality a fraction of pores will be most likely only partly filled with chloride. Table 18 in the appendix shows the cumulative pore volume of the different samples. Thus, the real film thickness might be larger in average than ideally expected, but also widely varying as clearly shown in Figure 11.

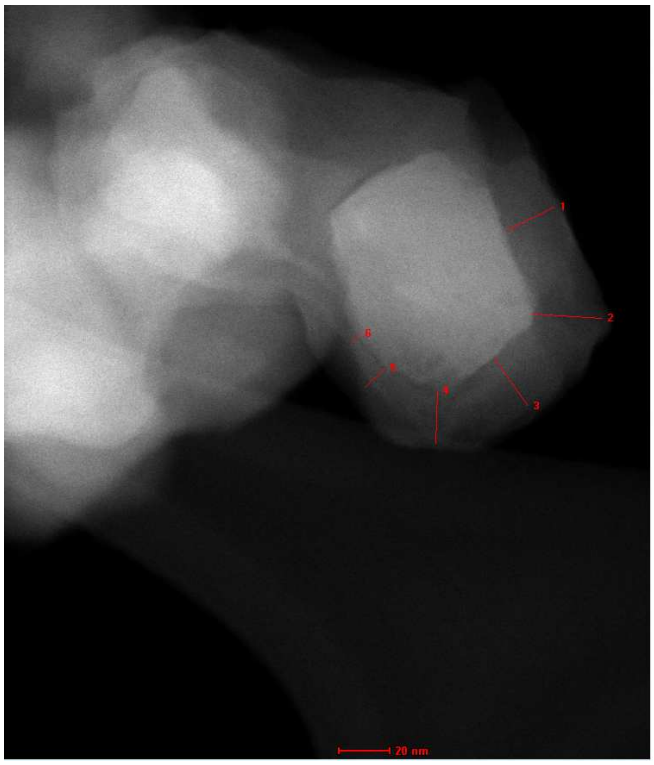

Figure 11.: HAADF-TEM of $LiKCl/MgO + Dy_2O_3$ (Entry 5 in Table 4; measured thicknesses: 1: 22 nm; 2:28 nm; 3: 23 nm; 4: 21 nm; 5: 11 nm; 6: 8 nm)

Obviously, the film thicknesses measured in the example by HAADF-TEM are significantly higher than the calculated film thicknesses compiled in Table 5. In addition to the heterogeneity this suggests that the chloride layer must have induced significant sintering of the support. To test this hypothesis, a catalyst (entry 5 in Table 4) was treated with water in an ultrasonic bath after calcination to wash off the chloride layer. Subsequent BET analysis showed a specific surface area of 33 m^2g^{-1}, indicating chloride induced moderate sintering of the oxide support. However, as about half of the specific surface area and the pore volume were restored, it is concluded that part of the pores were blocked, but not filled. The average nominal overlayer thicknesses of the catalysts (without considering pore blockage) for this specific surface area of the support are also compiled in Table 5. Figure 12 presents the formation rates and selectivities of catalysts with different overlayer molar fractions. The $MgO + Dy_2O_3$ support had modest reactivity and selectivity. This is consistent with the literature reporting moderate olefin selectivities in ODH for oxides of alkaline earth and rare earth metals.[28] Poor selectivity of these oxides resulted from facile formation of alkyl radicals that tend to be easier fully oxidized either at the oxide surface [176] or in the gas phase subsequent to their desorption.[28]

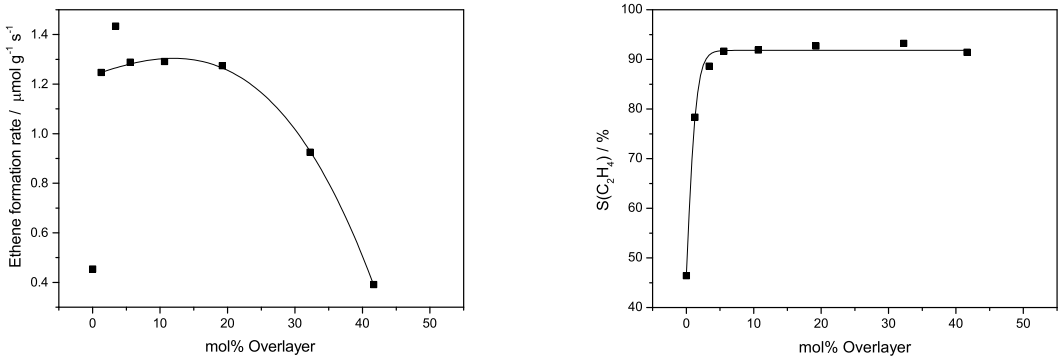

(a) (b)

Figure 12.: Activities (a) and olefin selectivities (b) of catalysts with different support/overlayer molar ratios ($LiKCl/MgO + Dy_2O_3$, T=625°C, WHSV = 0.8 h^{-1}, p_{total} = 1 bar , $p_{Ethane} = p_{O2}$ = 70 mbar)

Addition of the smallest increment of chloride almost doubled the ODH selectivity and increased the rate normalized to the catalyst weight. The addition of more chloride resulted in a further increase in activity and alkene selectivity, reaching an asymptotic value of around 93%. The high activity and selectivity was achieved once an average full layer of the alkali chloride was formed. Ethene formation rates tripled upon the initial addition of chloride suggesting either a boost of activity by chloride or the generation of a new site. A plateau in ethene productivity was observed as the concentration of active sites increased continuously followed by a decrease in catalytic activity at higher chloride loadings. The catalyst with the thickest overlayer (around 40 mol% overlayer) showed only 30 % of the ODH rate compared to the maximum. The addition of increasing concentrations of chloride are concluded to block pores of the support with islands of melt spreading across the surface of the support particles and eventually covering it completely. Apparently, very low concentrations of chloride loaded (see entries 2 and 3 in Table 5) do not prevent the exposure of unselective sites on the supports. Only if a thicker continuous layer is established, the unselective sites are covered and the molten overlayer illustrated by the transmission electron microscopy graph in Figure 11 is formed. The increase and then decrease of the catalytic activity as a function of the loading with chloride is concluded not to be related to restructuring of the catalyst particles, because their specific surface area steadily decreased with chloride loading. Thus, the chloride overlayer is hypothesized to generate a new type of sites, catalyzing the relatively fast and selective formation of ethene from ethane via ODH. The decrease of the activity with higher chloride loading is concluded to be a consequence of the combination of decreasing specific surface area (after the overlayer has been established)

and the complex reaction mechanism shown below. As it will be demonstrated below, the oxidation of Cl^- at the surface of the support has one of the lowest forward rate constants. As the dissolution of O_2 in the molten chloride is quasi equilibrated, and because the outer surface hardly varies with the thickness of the overlayer (Figure 10) the concentration of hypochlorite anions in that layer and, hence, on its surface is concluded to decrease. This decrease together with the lower specific surface area must in turn lead to a lower rate. Table 6 summarizes activation energies and pre-exponential factors of catalysts with different chloride loadings (graphical determination see Figure 52 in appendix). The blank support ($MgO + Dy_2O_3$) showed similar activation energies and pre-exponential factors for ODH and side reactions. The addition of chloride (even in low concentrations) resulted in a drastic increase in the activation energies and pre-exponential factors for both reactions. Activation energies of ODH were in the same range (approx. 140 $kJmol^{-1}$) for all chloride-containing catalysts, slightly decreasing with high loadings. The very high values of the apparent activation energies for the total oxidation (approx. 180-200 $kJmol^{-1}$) together with the high preexponential factors suggest that the main reason for the high selectivity to ethene lies in the energetic blocking off total oxidation. The consistently higher preexponential factor suggests in turn that the transition state for total oxidation is much looser than the transition state for ODH. A recent contribution by Chin et al. suggests that the high apparent energies of activation together with the high preexponential factor point to radical reactions.[180]

Table 6.: Activation energies and pre-exponential factors of ODH and total oxidation reactions of catalysts with different chloride concentrations (WHSV = 1.6 h^{-1}, p_{total} = 1 bar , $p_{Ethane} = p_{O2}$ = 70 mbar)

Overlayer/ mol%	Ethene formation		CO_x formation	
	E_A / $kJmol^{-1}$	A / -	E_A / $kJmol^{-1}$	A / -
0	109	$1.5 \cdot 10^6$	104	$1.7 \cdot 10^6$
5.6	142	$2.1 \cdot 10^8$	201	$3.9 \cdot 10^{10}$
10.7	143	$2.8 \cdot 10^8$	209	$1.2 \cdot 10^{11}$
19.2	142	$1.9 \cdot 10^8$	192	$1.3 \cdot 10^{10}$
32.3	134	$5.2 \cdot 10^7$	186	$2.0 \cdot 10^9$
41.6	135	$2.3 \cdot 10^7$	178	$1.3 \cdot 10^9$

The low solubility of organic molecules in the chloride melt makes it unlikely that ethane diffuses through the chloride layer to the redox active support surface to react, because such low solubility would lead to severe diffusion limitations under practical conditions. Thus, the question arises at this point whether or not a part of the redox active support is dissolved in the chloride melt and acts as distinct redox site at the liquid gas interface. The presence of dissolved support in the melt has been probed by washing the chloride from the catalyst with water and analyzing the removed phase by chemical analysis

(ICP-OES). The results proved the quantitative absence of cations from the support (Mg^{2+}, Dy^{3+}) in the chloride melt and the stoichiometry of chloride anions and alkali cations. In-situ XRD (see Figure 51 in the appendix) furthermore excludes the formation of mixed crystal phases (i.e. $MgCl_2$). Thus, it is concluded that the chloride overlayer does not change in composition during catalysis and that oxidic or chloride species of the support anions do not exist at the surface of the chloride overlayer. Full coverage of the catalyst support can be confirmed by findings of Kumar et al, who showed in-situ RAMAN measurements of $LiKCl/MgO + Dy_2O_3$ at different temperatures. Typical peaks of Dy_2O_3 (382, 471 and 525 cm^{-1}) completely disappeared at a temperature of 500°C, indicating that the whole support is covered by chloride at this temperature.[51] Considering these facts and especially the low solubility of organic reactants in the chloride melt, it is hypothesized at this point that the ODH reaction takes place at the gas-alkali chloride interface and involves only chloride species. At least for the catalysts with higher chloride loading, which show the best performance, the redox active sites of the support are not exposed to the gas phase reactants.

2.3.3. Elementary steps of the oxidation reaction

To follow the C-H bond and O_2 activation, transient step experiments were performed to quantify the uptakes of both reactants by the catalyst. The catalyst was flushed with He for 15 seconds after 45 minutes exposure to an O_2 containing He stream for 45 minutes and prior to reaction with 10% ethane in He. Figure 13 (a) presents the gas concentrations in the effluent.

After equilibrating the catalyst with O_2, ethene formation persisted for approximately 20 minutes (Figure 13 (a)), showing that the ODH active oxidizing species formed by contact with O_2 was retained in the melt. The persistence of the ethene formation without O_2 feed eliminates the possibility that radical gas phase or surface radical reaction are the catalytically active species, because such radical intermediates tend to be quenched rapidly[31] and would not be expected to be stable after 1200 s. Remarkably, CO or CO_2 were not observed in this step experiment, indicating that the reactive intermediate is ideally selective for the ethene formation and does not catalyze total oxidation of ethene or ethane. A similar experiment was performed, feeding the reactants in reverse order (Figure 13 (b)). Ethene was not detected demonstrating that the catalyst did not retain ethane. This can be rationalized by the high polarity of the melt causing a low affinity for non-polar alkanes. It is therefore hypothesized that the conversion of ethane to ethene takes place at the surface of the melt, although the O_2 activation and reaction with Cl^- occurs in the bulk phase of the overlayer or on the interface between melt and the molten overlayer. More information on the O_2 activation was obtained from step

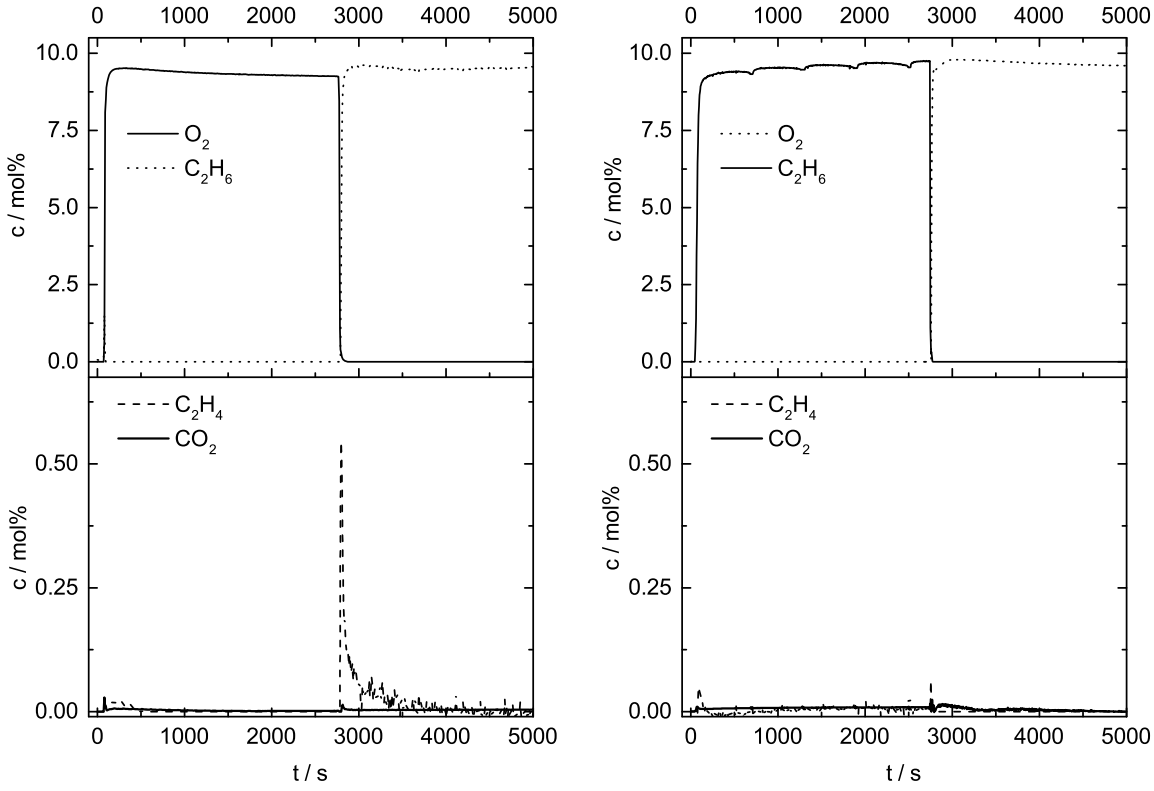

(a) (b)

Figure 13.: Step experiment at 625°C: (a): Step from 10% O_2 to 10% C_2H_6; (b): Step from 10% C_2H_6 to 10% O_2

experiments at various temperatures. The O_2 uptake increased with temperature as shown in Figure 14. The increase of the concentration of O_2, which has reacted to form the oxidizing species, with increasing temperature shows that O_2 uptake is an activated process, likely involving an endothermic step in the reactive dissociation of O_2.

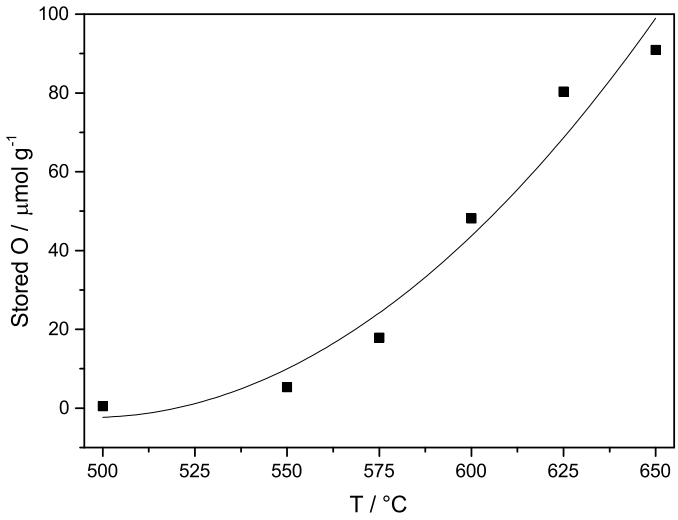

Figure 14.: Dependence of O_2 uptake on temperature (oxygen loading time: 45 min; purge time: 0.25 min)

The values reported in Figure 14 were the maximum capacity of O_2 uptake in the form of the catalytically active intermediate. An experiment starting under steady state conditions, but with an abrupt stop of O_2 feed (see Figure 53 in the appendix) shows that a lower concentration of active intermediate was present in the molten phase under steady state conditions. In order to approximate the rates of the formation of the O-Cl oxidizing intermediate, a step experiment with a short O_2 exposure (1 min) was performed at various temperatures. The results are compiled in Figure 15.

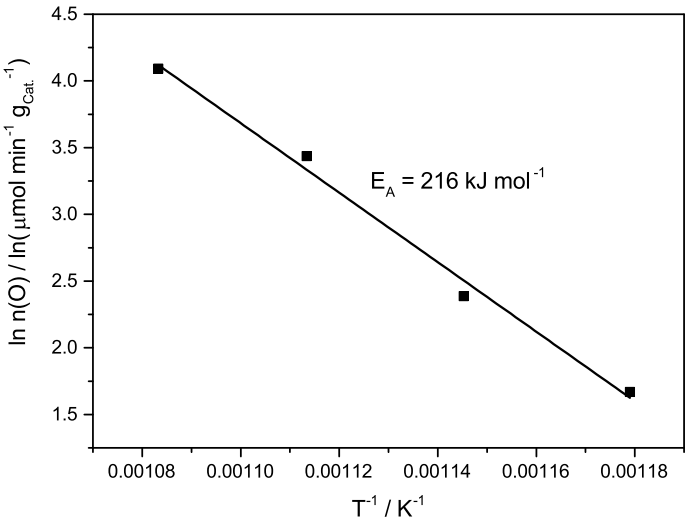

Figure 15.: Dependence of O_2 uptake on temperature (O_2 exposure: 1 min; purge time: 0.25 min)

The activation energy of the O_2 activation step is higher than the activation energy for the overall ODH. It is concluded, therefore, that O_2 is activated in an endothermic step and that the active oxygen oxidizes Cl^- in an exothermic step forming the active oxidizing species for the ODH, i.e., most likely OCl^-. The stability of the O-Cl intermediate was probed by additional step experiments with a variable inert purge period between O_2 and ethane exposures. The results are presented in Figure 16. The concentration of activated oxygen decreased with increasing He purge duration. The decay of the stored oxygen can be described with a second order kinetics. This indicates that the depletion process follows a bimolecular recombination and in turn this suggests that the disproportionation has been the rate determining step, for which the apparent energy of activation of 216 kJ/mol has been determined. O_2 was not be detected via MS during the inert purge period. It is concluded that the release rate was too small to be able to detect the traces of O_2 released.

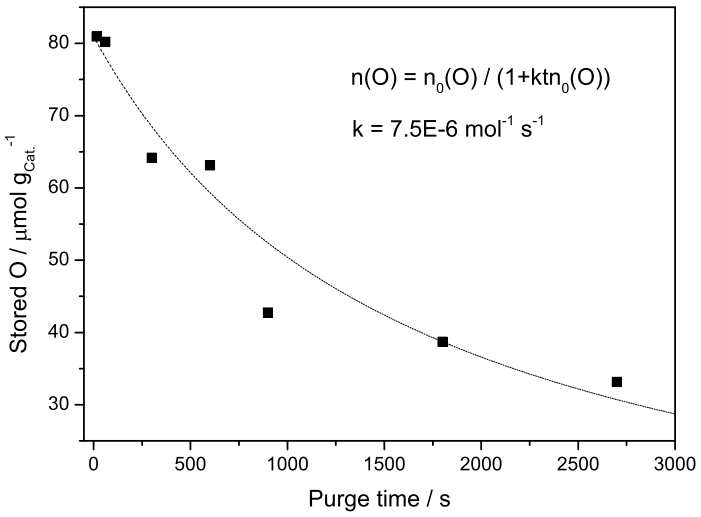

Figure 16.: Dependence of stored oxygen on purge time (T = 625°C)

2.3.4. Reaction pathways of the ODH and side reactions

Having established that it is possible to generate an oxidizing species (the hypochlorite anion) that can be stored and reduced, the changes in the concentration of isotopes of the reactants (steady state transient kinetic analysis (SSTIKA)) were used to estimate the rate constants of the individual steps and the evolution of the products ethene and CO_2. Kr was added as a tracer to monitor the exact signal of the step switch between $^{16}O_2$ and $^{18}O_2$ during steady state ODH reaction with unchanged ethane conversion. Figure 17 shows the responses to the O_2 switch on the product CO_2 and H_2O and on O_2 per se.

By varying the reaction temperature, the overall concentration of the reactive intermediates and conversion rates of oxygen-containing intermediates vary drastically. Expectedly the concentration of O_2 decreased with increasing temperature because of increasing conversion levels, but the concentrations of $^{16}O_2$ and $^{18}O_2$ were nearly identical at steady-state conditions before and after the step. In contrast, the concentrations of H_2O and CO_2 increased with reaction temperature in accordance with the higher reaction rates at higher temperatures. While the formation of ^{16}O containing CO_2 disappeared eventually, $H_2^{16}O$ remained to be significant even after long time on stream, in concentration levels that were proportional to the reaction rates of ODH. Thus, it is concluded that the chloride melt must contain a certain concentration of water under steady state conditions. Its present, it is however not possible to quantify that concentration accurately. After replacing $^{16}O_2$ by $^{18}O_2$ in a step function, unconverted $^{16}O_2$ disappeared quickly,

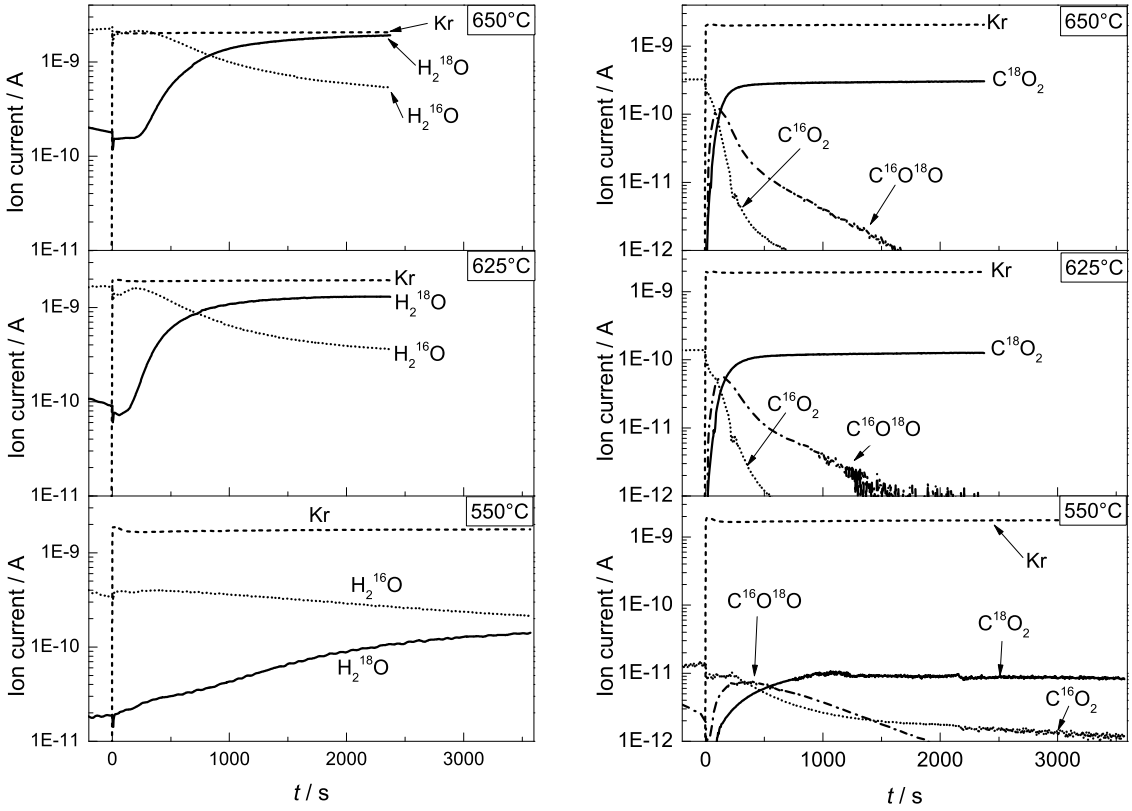

(a) (b)

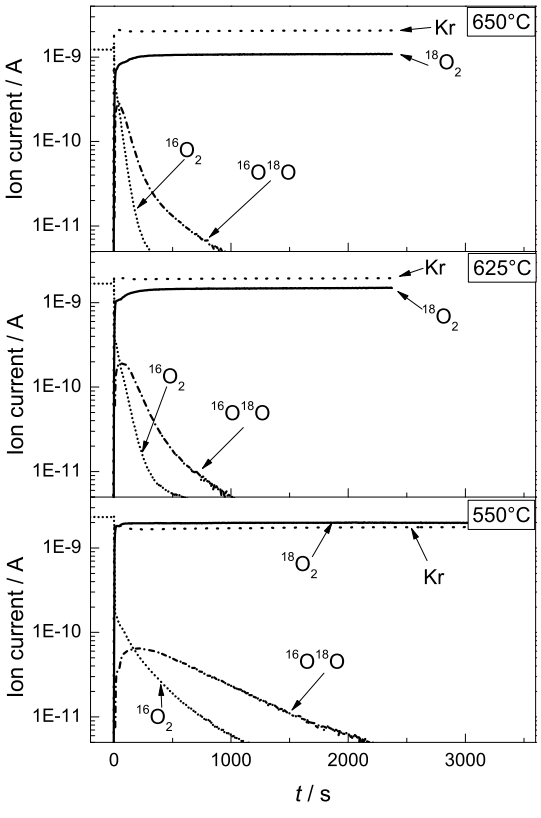

(c)

Figure 17.: SSITKA results at 550°C, 625°C and 650°C

replaced by $^{18}O_2$, which reached the steady-state concentration asymptotically after a time that was shorter for higher temperatures. After the switching, $^{16}O^{18}O$ reached a maximum soon after the step, slowly decreasing thereafter (even at 650°C it took 1000 s until the last trace of ^{16}O had disappeared). As long this species is produced, both oxygen isotopes are present in an exchangeable form at the solid-liquid interface.
Also for CO_2 a similar behavior was observed, including a maximum in the rate of formation of the isotopically mixed product. The time on stream until the last trace of ^{16}O containing CO_2 was detected had been by far longer than the time $^{16}O^{18}O$ was observed. This points to either to a retention of CO_2 on the catalyst or to differences in the reactivities along the pathways to form O_2 and CO_2. The result for water mainly produced by the ODH reaction was different. At the lowest temperature, the exchange between $H_2^{16}O$ and $H_2^{18}O$ was very slow. After 60 min. $H_2^{16}O$ was still the dominating species. At 625°C and 650°C, the transition from unlabeled to labeled H_2O was faster, $H_2^{18}O$ becoming the main product after 15 minutes. There was an induction period about 5 minutes at 650°C during which only $H_2^{16}O$ was formed. This implies that only ^{16}O reactive species were at the surface of the melt and available for reaction with the ethane. This could suggest that the formation of the oxidizing species is slow and competes with O_2 exchange and/or that diffusion of the oxidizing species from the support-liquid interface to the surface of the melt is significant and may influence the overall reaction rate. However, it should be noted that interpreting transient responses of strongly adsorbing H_2O is difficult as its desorption from catalyst and reactor walls can be slow.[117] However, the difference of the induction time at varying the reaction temperature at least excludes the influence of reactor walls.

2.3.5. Experiments to elucidate the critical individual reaction steps

2.3.5.1. Experiments with C_2D_6

The activation of the first ethane C-H bond is the rate determining step for most catalytic oxidations [181] and for most ODH catalysts (e.g., vanadium oxide based catalysts [70])). ODH reaction rates for hydrogenated and perdeuterated ethane have been compared to quantify the kinetic isotope effect (KIE) for $LiKCl/MgO + Dy_2O_3$ (Figure 18 (a)). Ethene formation rates vary in dependence of the feed (reflected in the pre-exponential factors), however, the difference is low compared to other ODH catalysts which show a kinetic isotope effect.[70] Figure 18 (b) presents the experimentally determined ratio of the ethene formation rates of undeuterated and perdeuterated ethane compared to the theoretical rate ratio for a scenario in which the C-H bond activation would be rate determining. The ratio varies with temperature, but remained well below the values for

a KIE in which C-H bond activation is rate determining. Thus, it is concluded that the cleavage of the first C-H bond does not determine the overall rate with the supported chloride catalysts.

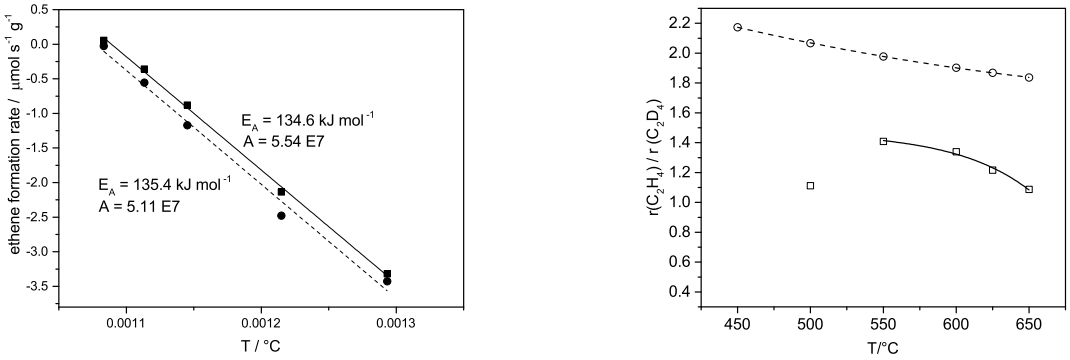

(a) (b)

Figure 18.: Study with deuterated and undeuterated ethane (a): Comparison between ethene productivities for C_2H_6 (■) and C_2D_6 (●) as reactants; (b): Experimental ratio of C_2H_4 and C_2D_4 production rates (□), calculated value for the case of a kinetic isotope effect (○)

Because the reaction rate ratios of the undeuterated and perdeuterated ethane was 1.2, it is concluded that hydrogen is still involved in the rate determining step, for example in the formation of surface hydroxy or alkoxy species as intermediate products, as also observed with other ODH catalysts.[182] Knowing that the O_2 activation is involved in the rate determining step, this is further probed by comparing supports of different O_2 isotope exchange capacity, as it has been concluded that the support is critically participating in the overall reaction.

2.3.5.2. Influence of the support properties on catalyst performance

Having established that the surface of the molten chloride phase is the location of the catalytic activation of ethane and that the concentration of oxidizing species determines the overall rate of reaction, the extent the redox properties of the support influence this catalytic chemistry should be probed. This has been probed by exploring two additional oxides (MgO and ZnO) varying in redox properties, while maintaining identical loadings of LiCl/KCl in eutectic composition as well as constant ratio of the support and the overlayer. To rule out trivial physical effects, the specific surface areas of the supports have been thermally adjusted by sintering MgO (Table 19 in the appendix). Figure 19 shows the activities of catalysts with different supports.

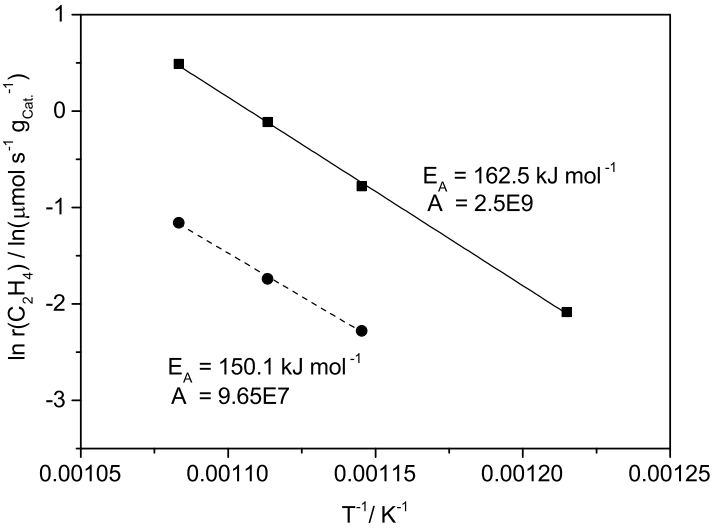

Figure 19.: Activities of catalysts with different supports (□: MgO sintered at 900°C; •: ZnO).

Despite similar chloride loadings MgO showed a much higher reactivity than ZnO. The chemical properties of the supports drastically affected the catalytic activities although the supports are covered with melt and presumably not exposed to the gas phase. This is mostly due to the differences in the pre-exponential factor, while the activation energies were quite similar. Because of the similarity of the apparent energies of activation it is assumed that the differences lie in the steady-state concentration of oxidizing species generated at the support-melt interface. It is hypothesized that a more redox-active support will generate a larger concentration of oxidizing species (OCl^- presumably). As the O_2 dissociation has been concluded to be involved in the rate determining step another side of this reaction is probed by exploring isotope scrambling of $^{16}O_2$ and $^{18}O_2$. A stream containing both O_2 isotopes ($^{16}O_2$ and $^{18}O_2$) was passed over the catalyst while the temperature was increased linearly and the formation of $^{16}O^{18}O$ was followed (temperature programmed isotopic exchange (TPIE) experiments). This allowed to explore the temperature dependence of the O_2 dissociation rates for MgO, MgDyO and ZnO (Figure 20).

As expected the formation rate of $^{16}O^{18}O$ increased exponentially with temperature. The formation of the isotopically mixed O_2 asserts that O_2 was dissociated and recombines. The much higher rate found with the MgO based catalysts and of the higher apparent energy of activation of that process (Figure 19) suggests that for ZnO the concentration of sites is much lower than for the other two oxides.

The activity in the isotope scrambling paralleled the reaction rates in steady state ODH

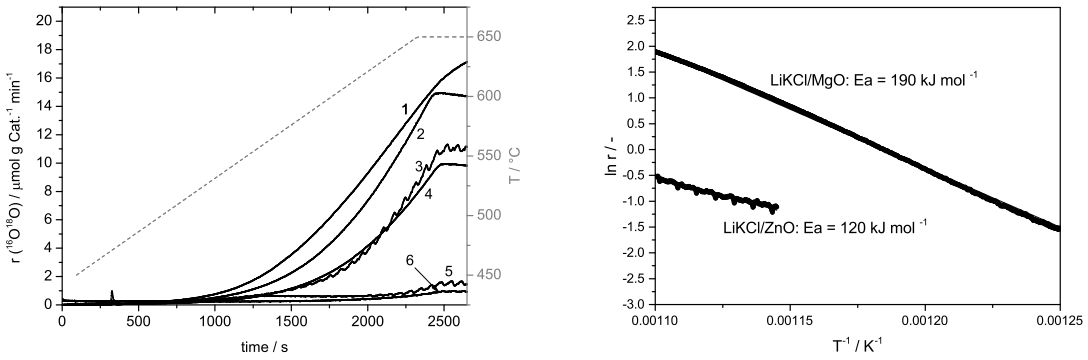

(a) (b)

Figure 20.: TPIE experiments with different supports and the corresponding LiKCl-coated catalysts (1: $MgO + Dy_2O_3$; 2: $LiKCl/MgO + Dy_2O_3$, 3: MgO, 4: LiKCl/MgO, 5:ZnO, 6:LiKCl/ZnO) b: Arrhenius plot of 4 and 6

experiments, for which the ranking of the catalytic activity of the materials was identical to isotope scrambling rates reported here. It is also notable that the rates of formation of the isotopically mixed O_2 on a chloride loaded catalyst and on the corresponding pure support were almost identical, suggesting O_2 dissociation takes place at the interface between support and molten overlayer. The equality of rates of O_2 activation/isotope scrambling rules out that the chloride overlayer influences the exchange sites and shows that transport of O_2 to the solid liquid interface is not diffusion limited. It should be noted in passing that a corresponding experiment with a mixture of C_2H_6+ C_2D_6 did not lead to isotopically mixed ethane, demonstrating that the hydrocarbons do not reversibly dissociate C-H bonds at the catalyst surface generating a concentration of surface bound H or D which would permit kinetically significant scrambling.
An experiment feeding only $^{18}O_2$ to MgO and ZnO based catalysts which were heated to reaction temperature under He without being exposed to $^{16}O_2$ (Figure 21) resulted in the formation of $^{16}O_2$ and $^{16}O^{18}O$ for a short of time in the case of an MgO based catalyst, but only marginally in the case of ZnO.

Lattice oxygen of the support oxide is the only possible source of ^{16}O. Oxygen at the surface of the MgO core is exchanged exposing simultaneously O_2 dissociation sites. ZnO, however, shows almost no oxygen exchange. Thus, the mechanism of O_2 dissociation and exchange depending on the support nature, critically determines the catalytic activity. It is speculated that the differences are related to the fact that MgO forms only labile oxygen vacancies (surface defects)[183], while ZnO is easier to reduce generating more stable oxygen vacancies due to lattice relaxation.[184]

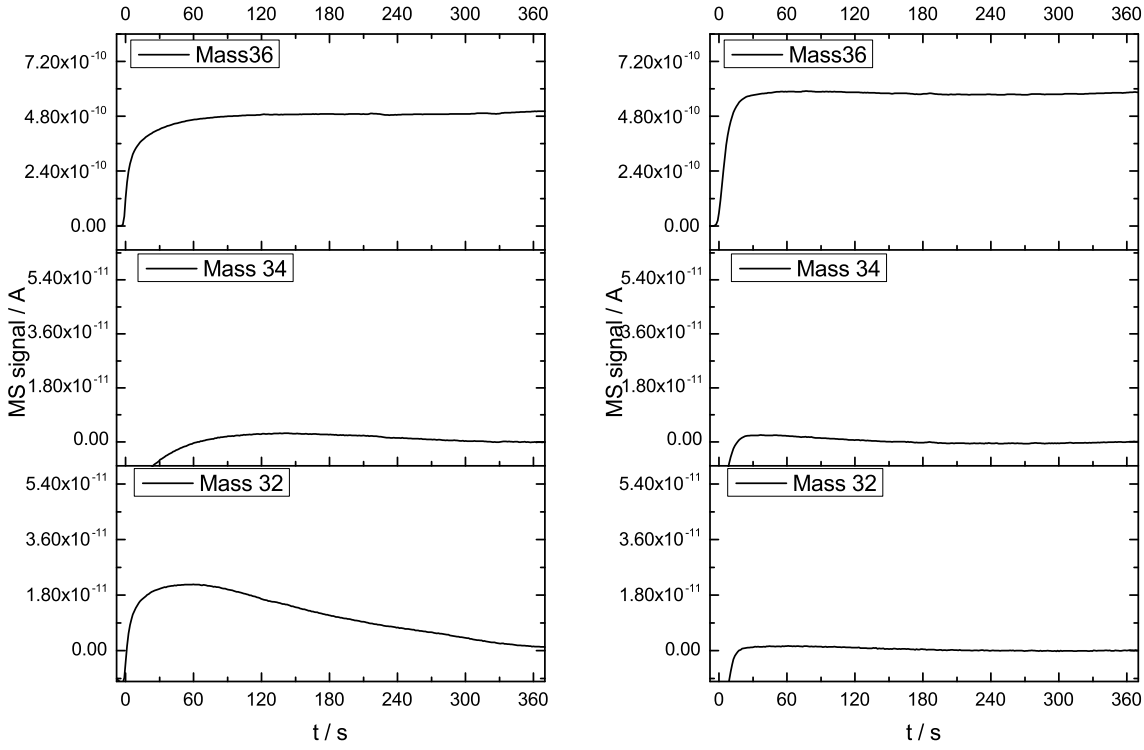

(a) (b)

Figure 21.: Isotope scrambling experiment at 625°C, feeding only $^{18}O_2$: (a): LiKCl/MgO; (b) LiKCl/ZnO

2.4. Formulation of the Reaction Mechanism and Conclusions

The individual experiments are now combined to build a mechanistic hypothesis for the selective catalytic reaction pathway of the oxidative conversion of ethane to ethene considering the proposed sequence of individual reaction steps (Figure 22). Given the complexity of the reaction sequence several conceivable reaction routes have not been considered by excluding them via circumstantial evidence. The presence of a steady state concentration of water in this chloride melt is possible, but its influence on the chloride properties was not considered in this contribution in other than the explicit ways discussed below. The transient formation of Cl• radicals or Cl_2 has been excluded on the basis of the absence of corresponding electron spin resonance spectroscopy signals and of the absence of even traces of chlorinated species from the product mixtures. The formation of ethyl chloride, which eliminates HCl to form ethene has been ruled out, because of the stability of the chloride catalyst, and no retention of HCl when scrubbing the reactor exhaust by a caustic solution. It is also ruled out that significant hydrolysis of the supported chloride by the water formed in the reaction and the formation of HCl through the reaction occurs (eq. 19) because of the position of the thermodynamic equilibrium.

$$NaCl + H_2O \rightleftharpoons NaOH + HCl \tag{19}$$

In consequence, the oxidizing species is most liekly the hypochlorite anion.

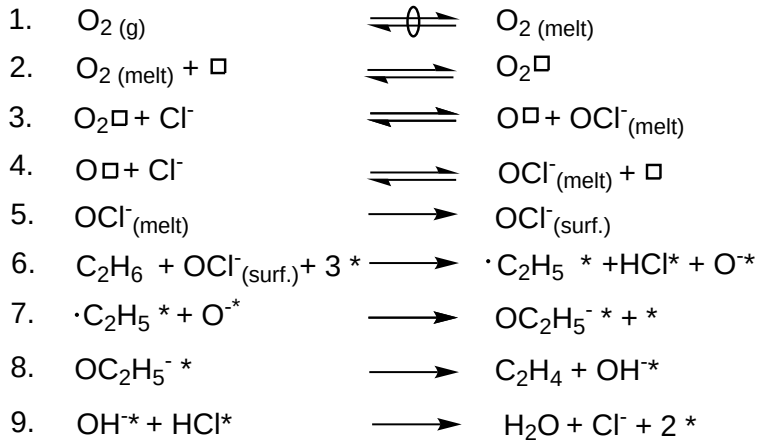

Figure 22.: Suggested elementary steps of the reaction pathway (: active sites on support; *: active sites on surface of melt)

The isotope scrambling experiments show conclusively that the ODH reaction follows

a Mars-van-Krevelen type mechanism with independent, but kinetically coupled steps for the activation of O_2 and ethane. O_2 is molecularly absorbed in the polar chloride melt (Step 1). The temperature programmed exchange between labelled O_2 shows that the exchange takes place at the support surface and is kinetically hardly limited by the presence of the supported chloride. Based on the rapid transient (Figure 13) and the temperature programmed exchange reactions, it is concluded that O_2 is quasi-equilibrated in the melt and that its concentration is low. The reactive dissociation of O_2 (Step 2) takes place at the interface between support and liquid melt (Figure 23).

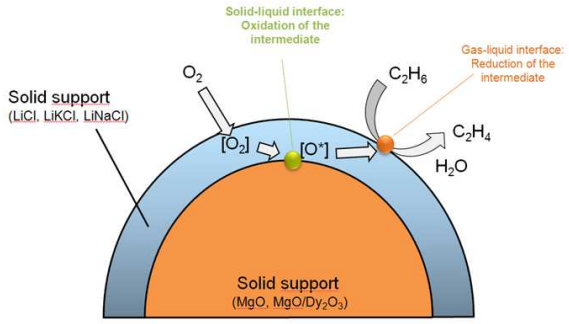

Figure 23.: Mechanistic model of ethane ODH over supported alkali metal chloride catalysts

Dissociated O_2 at the interface forms an oxygen-chlorine intermediate (Steps 3 and 4), which is currently speculated to be hypochlorite. These steps are concluded to be reversible, because the purge period between O_2 loading and ethane exposure decreased the concentration of the active species. It should be noted in passing that the decay followed a second order in the concentration of redox active species and that Cl species have not been detected in the gas phase. The second order kinetics lead to the speculation that the decay is related to a reaction between two hypochlorite anions, but it is unclear whether this occurs in the melt or at the support surface. The reactive intermediate (OCl^-) diffuses throughout the molten chloride, and, hence, establishes a concentration at the surface of the melt proportional to the chemical potential in the bulk and at the two interfaces (Step 5). As shown by the transient between ethene and O_2 exposure (Figure 13 (b)), ethane is not absorbed into the polar melt. Thus, ethane activation is concluded to proceed exclusively at the surface of the melt. Ethane

is hypothesized to adsorb on the surface of the melt on a hypochlorite anion, resulting in the abstraction and the formation of a subsequent C_2H_5 radical species and an $\bullet O^-$ and HCl (Step 6). The $\bullet C_2H_5$ species reacts with the $\bullet O^-$ species and forms a surface complex (Step 7), which is cleaved into ethene and a hydroxyl anion (Step 8). Finally, the hydroxyl anion reacts with HCl forming water (Step 9). As ethane scrambling did not yield isotopically mixed ethane species, those in the latter two steps are concluded to be irreversible. The adsorbed hydrocarbon radical reacts with O^- resulting in the formation of ethene and water via and oxidized intermediate (Steps 6 and 7). Thus, it is concluded that ethane is activated at the gas-melt interface, and O_2 is activated at the melt-support interface. The outstandingly high olefin selectivity is attributed to the separation of alkane and O_2 activation sites.

The nearly ideal selectivity for ODH of the intermediate species stored in the melt does not preclude, however, combustion initiated by gas-phase O_2. This is shown by the step experiments (Figure 13), which demonstrate that the chemically stored oxygen (in the form of an oxidizing species) is active generating ethene, but not CO_2 or CO. The SSITKA experiments additionally showed a slower O_2 isotopic exchange in the ODH pathway compared to the total oxidation pathway. Unlike with many other oxidation catalysts (e.g., supported vanadia [70] or molybdena [182]) the H/D isotope effect strongly suggests that the cleavage of the first C-H bond is not involved in the rate determining over supported alkali chloride. In the present case, the cleavage of the O_2 bond leading to the oxidizing species appears to be the slow step. Only in case ethane collides with this oxidizing species at the surface of the melt, reaction is possible.

At this point the molecular consequences of the spatial separation of oxygen and ethane activation and the fact that ethane has no physical access to the oxygen activation site should be analyzed. O_2 activation on metal oxide surfaces proceeds conventionally by a stepwise electron transfer placing the charge on the oxygen ion.[181] In the present case, the adsorbed surface O_2 becomes ionized. Electrons are provided by redox active sites acquiring partial positive charge, while creating a partially negative charge with the formed oxygen species. A subsequent formation of the ionic oxygen species is hindered by the limited availability of electrons with the redox site being part of an isolating oxide. Low concentrations of such sites and a high barrier (approximately 200kJ/mol) makes this step kinetically slow. The oxygen activation in the supported alkali chloride system is assumed to take place near O vacancies which are likely to form in MgO surfaces.[33] The vacancies are either neutral (with two trapped electrons) or have a single or double positive charge.[185] Over the vacancy on MgO, O_2^- is likely to form while exposed to O_2 [186], known as an unselective oxygen species (Figure 24), which would form on bare metal oxide surfaces.

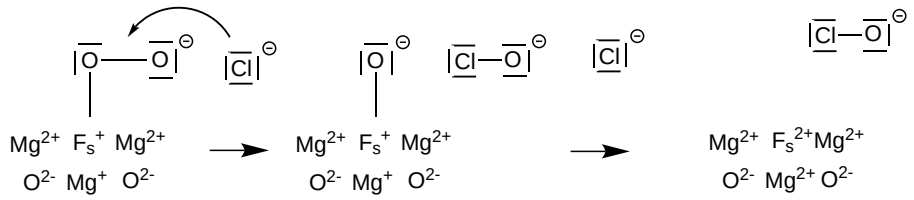

Figure 24.: Possible molecular pathway of chloride-assisted O_2 activation at MgO oxygen vacancies

The chloride layer of the catalysts studied in this work prevents the access of hydrocarbons to such active oxygen. The ubiquitous presence of Cl^- facilitates the formation of an oxidized chlorine species, presumably OCl- (Figure 24, where this process is exemplified for hypochlorite as active species). Its anionic character nature allows the chlorine-oxygen species to desorb readily from the lattice of the support (being formally replaced by Cl^-) and to diffuse in the melt. As the electrophilic oxygen species has reacted with Cl^-, the strongly electrophilic character has been reduced and an anion has been formed. The precise nature of the active oxygen intermediate remains, however, the subject of further investigation. The chlorine containing oxyanion diffuses to the surface of the melt, is stabilized there in low concentrations as isolated species, and reacts eventually with ethane. The formed ethene rapidly desorbs from the melt due to its low affinity to a highly polar and dynamically rearranging surface. Thus, in summary, a (direct and reverse) Mars - van Krevelen mechanism [40] is proposed in which the ethane and the O_2 conversion steps take place at different interfaces, namely the molten overlayer / gas phase and the molten overlayer / solid support interfaces, respectively. The active oxygen species is formed at the oxygen vacancies at the support, e.g., MgO in the present case and diffuses through the chloride melt to the surface. Thus, the active oxygen species is dissolved in a molten phase and exists at the surface only in low concentrations. Because the active hypochlorite anions in the present system are dissolved in a melt with a low viscosity [187], they are mobile and do not agglomerate due to electronic repulsion forces. The species has an anionic character, but it should be emphasized that, e.g., the hypochlorite is able to assume also a radical form. Compared to the highly electrophilic oxygen formed on other typical ODH catalysts[117], the present species react more slowly, but with less tendency to initiate total oxidation. Depending on the overlayer thickness, the concentration of active species varies in different catalysts. Thus, while a continuous cover helps in radically increasing the preexponential factor for the reaction (the apparent energy actually increases), the reactivity of catalysts decreases, as with increasing overlayer thickness the steady state rate of formation of the oxidizing species at the surface of the support leads to a lower density in the chloride volume and on the surface.

The present system of supported chlorides offers an exciting new route towards olefins, which combines high selectivity at high conversions. While the positive effect of chloride for oxidative dehydrogenation had been previously established [30, 141] and has even been observed in molten systems of other halogenides [188], the current contribution shows how the interplay between the support in the chemistry in the supported chloride may direct alkane oxidative dehydrogenation to new levels. Aa further improvement of the molecular understanding of this could lead to step up improvements in the current access to ethene as well as to larger and certainly more complex olefins via oxidative dehydrogenation.

This chapter is based on:
Christian A. Gärtner, Andre C. van Veen, Johannes A. Lercher: Oxidative Dehydrogenation of Ethane on Dynamically Rearranging Supported Chloride Catalysts, *J. Am. Chem. Soc.*, 136(36), 2014, pp. 12691-12701

3. Kinetic investigations of the ODH of ethane over supported alkali chloride catalysts

The oxidative dehydrogenation of ethane is an energetically efficient process to selectively produce ethene. Supported alkali chloride catalysts are a promising class of catalysts, as they show a surprisingly high ethene selectivity. In the previous chapter, the mechanism of ethane ODH over this class of catalysts has been elucidated, proposing a novel Mars-van-Krevelen type mechanism, involving two interfaces being responsible for ethane and oxygen activation. Also, elementary steps for the whole reaction have been suggested. This chapter focuses on kinetic investigations of the ethane ODH and its side reactions over supported alkali chloride catalysts. By combining steady state and transient experiments, kinetic information of the elementary steps could be obtained, finally compiling kinetic data into an overall mathematical model being able to describe ethane ODH and its side reactions. Furthermore, it could be shown that the ODH reaction is not hindered by water and carbon dioxide, both forming as by-products.

3.1. Introduction

Oxidative dehydrogenation of ethane is a mildly exothermic reaction converting ethane into ethene, common building block and intermediate for the production of many products. Even offering many advantages over steam cracking, the industrially state-of-the-art-process, ethane ODH has not yet been exploited for large scale production of ethene. ODH has however the potential to become economically feasible if outstandingly high olefin selectivities can be achieved. Main side reactions are the total oxidation reactions of ethane and ethene -one parallel and one consecutive side reaction. In a kinetic point of view, high selectivities can be achieved if the ODH is much faster than both side reactions. Those side reactions play a different role on various catalysts.
This work focuses on the kinetic description of ODH and its side reactions over supported alkali chloride catalysts, a novel, highly selective catalyst class. Chapter 2 reports the ethane ODH mechanism over this novel type of catalyst, assuming that oxygen can permeate through the alkali chloride overlayer, being activated at the interface between support and melt. The active oxygen-chloride species, forming in low concentrations and being ideally selective towards ethene, diffuses through the salt layer and activates ethane at the interface between melt and gas phase. Objective of this work is a detailed kinetic investigation of the ODH and a quantitative description of the side reactions over supported alkali chloride catalysts. The elementary steps suggested are taken into consideration for this model. To achieve this objective, kinetic information of single elementary steps is determined via transient experiments in combination with steady state experiments. The findings are used to build a model of the overall reaction. Besides ODH, also the parallel and consecutive side reaction (total oxidation of ethane and ethane) are investigated and regarded in the model. Detailed studies are performed with a reference catalyst $LiKCl/MgO + Dy_2O_3$. Finally, a kinetic model will be derived in order to describe all molecular processes occurring during ODH on supported alkali chloride catalysts. Therefore, a rate equation for the ODH reaction on basis on the mechanistic information (oxygen and ethane activation step) will be derived and used in the mathematical fitting procedure. For the side reactions (combustion of ethane and ethene towards carbon oxides), power-law models will be used.

3.2. Experimental

3.2.1. Catalyst preparation

The catalyst used for this study was prepared by wet impregnation as described in Chapter 2.2 (entry 5 in Table 4).

3.2.2. Catalytic tests

Catalytic tests were performed in a plug flow reactor system as described in Chapter 2. Steady state kinetic experiments were performed at atmospheric pressure, using varying partial pressures of ethane (99.5%) or ethene (99.5%) and oxygen (10.1% in He) in balance He (99.99%). Catalysts had been on stream for 2 days before the kinetic measurements to avoid initial overactivity. WHSV was varied between 0.8 h^{-1} and 2.0 h^{-1} in order to keep conversion levels low. Kinetic measurements were recorded at temperatures between 500°C and 650°C, using different combinations of hydrocarbon and oxygen partial pressures (minimum 20 mbar, maximum 100 mbar). For the experiments to investigate product inhibition, part of the balance helium was substituted by carbon dioxide or steam. In this case, the WSHV was 0.8 h^{-1} and reactions were performed in a temperature window between 450°C and 650°C. Step experiments were performed by heating the catalyst in helium, an oxygen loading period (10% O_2 in He, 45 min), an inert purge period with variable time (40 ml/min He) an a reaction in ethane (10% C_2H_6 in He, 45 min) at various temperatures. Gas analysis was performed via MS analysis.

3.2.3. Mathematical modeling

The overall kinetic model was implemented in MATLAB using material balances of a plug flow reactor. The differential equations that describe the changing gas phase compositions down the length of the reactor are solved using the differential equation solver *odt23t* built in MATLAB. Various parameters (activation energies and pre-exponential factors of the different reactions) are optimized to fit the experimental data with the nonlinear optimization function *nlinfit*. The responses being used in the parameter estimation algorithm are the outlet streams of the products ethene and CO_2 in the case of ethane and oxygen in the feed, the outlet streams of the products CO_2 and CO in the case of ethene and oxygen in the feed .

3.3. Results

3.3.1. Kinetics of ODH and its side reactions on various catalysts

In oder to determine the influence of different variables, a reference catalyst system $LiKCl/MgO+Dy_2O_3$ has been studied in detail as it is the reference catalyst used in the mechanistic studies as well. Kinetic measurements have been performed at differential conversion levels, varying the temperature and the reactant partial pressures. In order

to study the ethene total oxidation as well, the same measurements have been performed with ethene as hydrocarbon in the feed. Table 7 compiles the temperature dependent reaction orders regarding both reactants for the case of ethane.

Table 7.: Temperature dependent reaction orders regarding ethane and oxygen of ethane ODH and total oxidation of ethane towards CO_2 ($LiKCl/MgO + Dy_2O_3$)

T / °C	Ethane formation		CO_2 formation	
	RO ethane	RO oxygen	RO ethane	RO oxygen
500	0.44	—	—	—
550	0.39	0.12	—	—
600	0.54	0.14	0.97	0.35
625	0.56	0.15	0.77	0.43
650	0.59	0.21	0.63	0.46

For the catalysts supported on $LiKCl/MgO + Dy_2O_3$, the reactions order in oxygen is around 0.1 up to 0.2 and the one for ethane around 0.5. Those values are similar to the ones obtained for a similar catalyst.[30] It is obvious that the reaction orders increase slightly with temperature for both reactants. For total oxidation towards CO_2, reaction orders regarding ethane are higher than the reaction orders regarding oxygen. Both reaction orders are below 1 for all temperatures.

Steady state operation only allows a determination of apparent reaction orders and activation energies. Reaction orders for both reactants are notably lower than one. As the activation of oxygen is rate determining (see Chapter 2) and thus slow, increasing of the partial pressure of oxygen in the gas phase does not lead to a big increase of the overall rate. The partial pressure of oxygen in the gas phase directly only influences step 1 (molecular absorption of molecular oxygen in the liquid salt melt, see Figure 22). Increasing the concentration of solved molecular oxygen in the melt has apparently only a low effect on the overall reactivity. As the oxygen activation step is slower than the hydrocarbon activation step, an increase of the ethane partial pressure in the gas phase does not correlate linearly with the overall ODH reactivity. Again, the oxygen activation step is slow, thus the concentration of active intermediate species mainly governs activity. The reaction order of ethane is lower than one, as it is present in excess. Reaction orders of both reactants are between zero and one and change with temperature, which can be explained by the fact that the kinetics of the elementary steps of ODH obviously change with temperature. Thus, reaction orders of single steps have to be investigated independently.

Table 8 compiles the temperature dependent reaction orders for the case of ethene.

Table 8.: Temperature dependent reaction orders regarding ethene and oxygen of total oxidation of ethene towards CO and CO_2 ($LiKCl/MgO + Dy_2O_3$)

T / °C	Ethane formation		CO_2 formation	
	RO ethane	RO oxygen	RO ethane	RO oxygen
500	—	—	—	—
550	—	—	—	—
600	-0.26	0.28	—	—
625	0.75	0.39	1.59	0.38
650	0.66	0.42	0.67	0.21

Reaction orders regarding ethane are higher than the reaction orders regarding oxygen for all temperatures.
Complete kinetic data can be found in the supplementary information in Tables 21, 22, 23 and 24.

3.3.2. Influence of carbon dioxide and water on ODH performance

To investigate to influence of the by-product carbon dioxide on the reactivity of the catalyst for ethane ODH, experiments with a co-feed of 10% CO_2 in total were performed. Results for ethene productivity can be found in Figure 25.

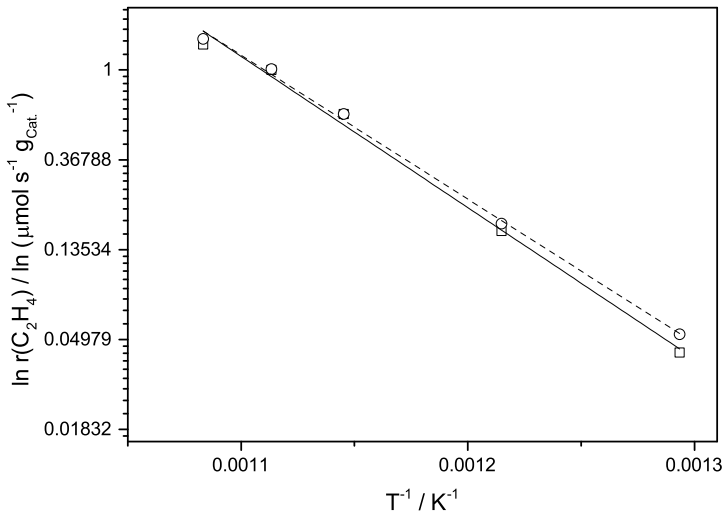

Figure 25.: Influence of CO_2 in the feed on reactivity (LiKCl/$MgO+Dy_2O_3$, $p_{total} = 1$ bar, $p_{Ethane} = p_{O2} = 70$ mbar, □: without CO_2-cofeed; ∘: with CO_2-cofeed ($p_{CO2} = 100$ mbar))

The presence of CO_2 does not decrease the ODH activity of the catalyst, thus the reaction order regarding carbon dioxide in the ODH reaction is zero.
The formation of carbonates and their role as active species, suggested for other similar catalysts, can thus be excluded. For example the reaction order of CO_2 for a LiDyMg mixed oxide catalyst is -0.5, suggesting that two active Li^+-sites are blocked by one CO_2-molecule.[19] For supported eutectic alkali chlorides, it can be speculated that CO_2 does not show an affinity towards the chloride melt, and it can neither adsorb on the suggested active site OCl^- nor block it. The adsorption of CO_2 on Li^+ or K^+ on the surface of the melt is not likely due to the dynamically rearranging surface, but can, however, not be excluded even for this supported chloride catalyst. As the cations are not the active centers of a supported alkali chloride catalyst, the non-existing blocking effect of CO_2 can be explained. Another hypothesis for the extraordinarily high selectivities of supported alkali chloides is the temporary absorption of CO_2 in the liquid melt, what would enhance the olefin selectivity for a limited time. By co-feeding CO_2 for a longer time, this effect can be excluded. Thus, supported molten alkali chlorides do not seem store carbon dioxide. For the kinetic model, the reaction is thus zero order in carbon dioxide. Thus, CO_2 does not have to be regarded in the derivation of the rate equation of ethane ODH.

Additionally, the influence of water, product of ODH and side reactions, has been inves-

tigated. Measurements have been performed at different temperatures, as summarized in Figure 26.

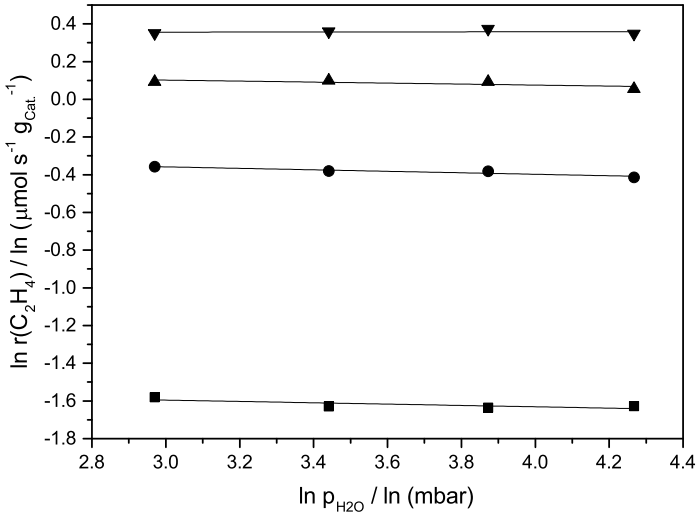

Figure 26.: Effect of water on ODH reaction: ■: 550°C; ●: 600°C; ▲: 625°C; ▼: 650°C;

Apparently, water does not influence the reactivity of the ODH reaction thus a reaction order of zero as well. Even water might be stored in low concentrations in the chloride melt (see Chapter 2), it does definitely not affect the activity in ethane ODH. A blocking of the active centers by water can thus be excluded. Furthermore, it can be excluded that OCl^-, the catalytically active intermediate, decomposes in the presence of water. ODH reactivities thus only depend on the partial pressures of the reactants ethane and oxygen.

3.3.3. Ethane ODH and its side reactions

In order to investigate whether CO_x is formed directly from ethane or via ethene, steady state experiments with different space velocities and conversion levels have been performed. Figure 27 presents the results of this study.

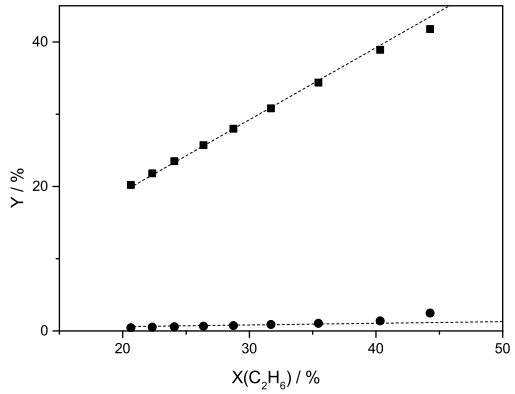

Figure 27.: Steady state experiment with $Li - K - Cl/MgO + Dy_2O_3$ with variable WHSV (T = 625°C, p_{total} = 1 bar, $p_{Ethane} = p_{O2}$ = 70 mbar, WHSV variable; ■: Ethene; ●: CO_2

Ethene yields increase linearly with conversion up to an ethane conversion of approximately 40%, thus the olefin selectivity is constant up to this conversion. At higher conversions, the linear trend slightly changes towards less olefin selectivity. Whereas the CO_2 curve also has a constant slope up to 40%, the yields at conversion levels over 40% increase less. Thus, CO_x is mainly formed from ethane directly. However, at higher ethene partial pressures in the gas phase, part of the formed ethene is converted to CO_x in a consecutive side reaction. CO_x formation pathways are further illustrated in Figure 28, where CO_x formation rates are presented, using both ethane and ethene as reactants together with oxygen.

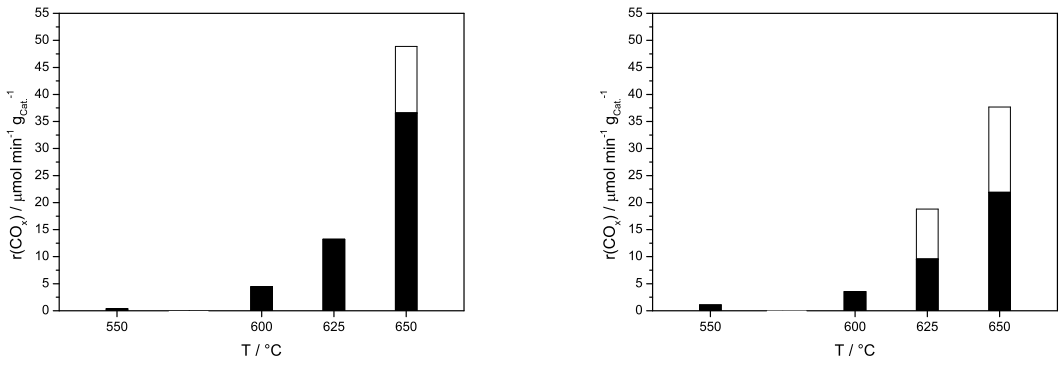

(a) (b)

Figure 28.: CO_x formation rates from ethane (a) and ethene (b) (black: CO_2, white: CO; WHSV = variable, $p_{O2} = p_{Ethane}$ = 80 mbar, p_{total}=1 bar)

Considerable CO_x formation starts at 600°C. CO_2 formation rates are in general higher for ethane as precursor. While CO is formed only at 650°C using ethane as pre-cursor, it can already be detected at 625°C for the case of ethene. Whereas the dominant total oxidation product is CO_2 for the case of ethane, CO is formed in more considerable amounts for the case of ethene as pre-cursor. For most of the temperatures studied, more by-products form in the case of ethane as pre-cursor. Only for the temperature of 625°C, CO starts forming for ethene as pre-cursor, the total amount of formed by-products is higher for the case of ethene in this case. Figure 29 presents the influence of ethene selectivitiy on the oxygen partial pressure. It can be observed that more oxygen in the feed leads to decreased selectivities. However, at 600°C ethene selectivities are still at very high levels.

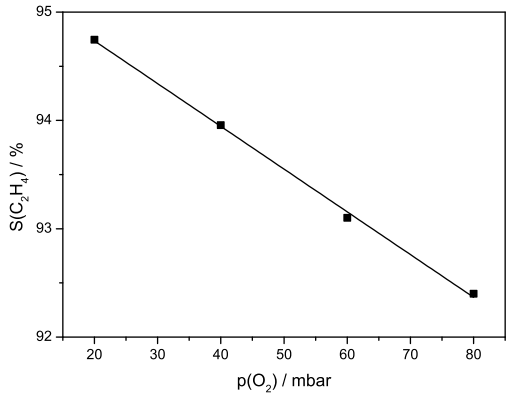

Figure 29.: Influence of oxygen/ethane ratio on ethene selectivity (WHSV variable, T=600°C, p_{Ethane} = 40 mbar, p_{total}=1 bar

It can be seen that the CO_x formation rate using ethene as reactant is slightly higher as the respective one with ethane as reactant. This explains why the olefin selectivity decreases slightly with increasing ethene partial pressures in the gas phase. Blank tests with only SiC in the reactor showed neglible ethane and ethene conversions in both studies.

3.3.4. Elementary steps of ODH

Transient experiments, as presented in the previous chapter, allow a decoupling of the oxygen activation, transport and hydrocarbon activation steps. As the oxygen loading of the catalyst was performed at the same conditions but different temperatures, the amount of stored oxygen for one temperature can be determined. The concentration of the active intermediate can be determined by integrating the amount of the whole

ethene formed after a step response, this value corresponds to the amount taken up by the catalyst at a certain temperature. Additionally, the initial ethene formation rate after a step response can be determined, which provides exact information for the hydrocarbon activation step. By varying ethene concentration the reaction order of the hydrocarbon activation step can be determined.
Figure 30 shows that the initial ethene formation rate after a step increases linearly with the ethane partial pressure, the reaction order as approximately 1 for all investigated temperatures.

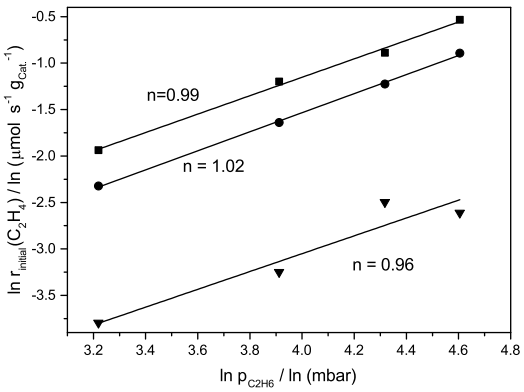

Figure 30.: Reaction orders of ethane activation after step experiment (▼: T = 575°C; ●: 600°C; ■: 625°C)

Transient step experiments allow a decoupling of the different elementary steps, thus kinetics of a single reaction step can be determined. Here, the kinetics of the hydrocarbon activation step could be probed. In the step experiment, the oxygen activation step was kept unchanged and the melt was saturated with oxygen, thereby forming the equilibrium concentration of active intermediates. As the active intermediate is formed during oxygen loading, oxygen activation is not rate determining after switching the effluent stream from oxygen to ethane in a step experiment. An evaluation of the initial ethene formation rates with different ethane partial pressures thus allows the determination of the true reaction order in ethane. Here, the reaction order is one compared to 0.5 in steady state operation mode, showing that ethane activation is an elementary step. Furthermore, it shows that reactivity linearly correlates with collision probability of ethane with an active intermediate species on the surface of the melt. Reaction orders for complex rate equations (i.e. Mars-van-Krevelen type rate equation) can depend on several kinetic parameters and partial pressures, thus they can change for different regimes.[189]

3.3.5. Kinetic model

3.3.5.1. Derivation of rate equation for ethane ODH

In Chapter 2, a comprehensive mechanistic model with 9 single steps was derived. For kinetic modeling, the mechanistic model is simplified, as kinetic information of each of the 9 steps cannot be measured. Thus, ethane ODH is formally divided into two elementary steps:

$$0.5\ O_2 + [Cl^-] \rightarrow [OCl^-] \tag{20}$$

$$[OCl^-] + C_2H_6 \rightarrow C_2H_4 + H_2O + [Cl^-] \tag{21}$$

Eq. 20 represents the oxygen activation step, eq. 21 represents the hydrocarbon activation step.

Rate equations can be written as following (eq. 22 for the oxygen activation step, eq. 24 for the hydrocarbon activation step):

$$r_1 = k_1 \cdot \sqrt{p_{O_2}} \cdot [Cl^-] \tag{22}$$

$$r_2 = k_2 \cdot p_{C_2H_6} \cdot [OCl^-] \tag{23}$$

A chloride balance completes the equation system:

$$[Cl^-] + [OCl^-] = 1 \tag{24}$$

In steady state, both steps must have the same rate:

$$k_1 \cdot \sqrt{p_{O_2}} \cdot [Cl^-] = k_2 \cdot p_{C_2H_6} \cdot [OCl^-] \tag{25}$$

Now, $[Cl^-]$ can be determined:

$$[Cl^-] = \frac{k_2 \cdot p_{C_2H_6} \cdot [OCl^-]}{k_1 \cdot \sqrt{p_{O_2}}} \tag{26}$$

Now, [OCl-] can be calculated (inserting expression for $[Cl^-]$ in chloride balance (eq. 24):

$$[OCl^-] + \frac{k_2 \cdot p_{C_2H_6} \cdot [OCl^-]}{k_1 \cdot \sqrt{p_{O_2}}} = 1 \tag{27}$$

$$k_1 \cdot \sqrt{p_{O_2}} - k_1 \cdot \sqrt{p_{O_2}} \cdot [OCl^-] = k_2 \cdot p_{C_2H_6} \cdot [OCl^-] \tag{28}$$

$$k_1 \cdot \sqrt{p_{O_2}} = [OCl^-] \cdot (k_2 \cdot p_{C_2H_6} + k_1 \cdot \sqrt{p_{O_2}}) \tag{29}$$

$$[OCl^-] = \frac{k_1 \cdot \sqrt{p_{O_2}}}{k_2 \cdot p_{C_2H_6} + k_1 \cdot \sqrt{p_{O_2}}} \tag{30}$$

$[OCl^-]$ can now be inserted into eq. 24:

$$r_2 = r_{total} = \frac{k_1 \cdot \sqrt{p_{O_2}} \cdot k_2 \cdot p_{C_2H_6}}{k_1 \cdot \sqrt{p_{O_2}} + k_2 \cdot p_{C_2H_6}} \tag{31}$$

3.3.5.2. Reaction network including side reactions

For kinetic modeling, the following reactions are taken into consideration:

$$1.\ \ C_2H_6 + 0.5\ O_2 \rightarrow C_2H_4 + H_2O \tag{32}$$

$$2.\ \ C_2H_6 + 3.5\ O_2 \rightarrow 2\ CO_2 + 3\ H_2O \tag{33}$$

$$3.\ \ C_2H_6 + 2.5\ O_2 \rightarrow 2\ CO + 3\ H_2O \tag{34}$$

$$4.\ \ C_2H_4 + 3\ O_2 \rightarrow 2\ CO_2 + 2\ H_2O \tag{35}$$

$$5.\ \ C_2H_4 + 2\ O_2 \rightarrow 2\ CO + 2\ H_2O \tag{36}$$

Both ethane and ethene can undergo total oxidation, thus both parallel (reactions 2 and 3) and consecutive (reactions 4 and 5) side reactions are possible. The reaction network of ODH and its side reactions is summarized in Figure 31.

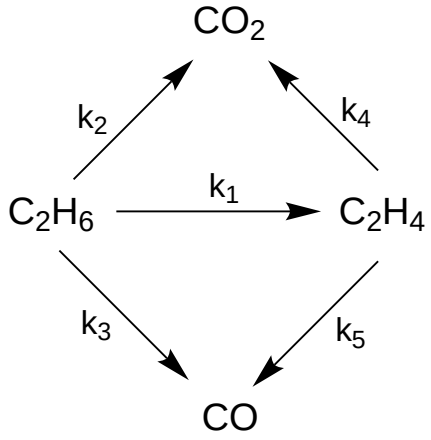

Figure 31.: Scheme of ethane ODH and its side reactions

Ethane is directly transformed to ethene via ODH, and both products can undergo total oxidation towards carbon monoxide and dioxide. Carbon monoxide has only been observed at high temperatures, mainly in the experiments with ethene in the feed. Thus, reaction 3 has been neglected in the modeling, as CO is only assumed to form directly from ethene. The modeling strategy involves two steps: At first, experiments with ethene and oxygen are taken into consideration. This allows to determine the kinetics of reactions 4 and 5 decoupled from the rest of the reaction network. As CO and CO_2 are assumed to form via a gas phase mechanism which is not known in detail, reactions 4 and 5 are modeled with power law equations.

$$r_4 = k_4 \cdot p_{O_2}^a \cdot p_{C_2H_4}^b \tag{37}$$

$$r_5 = k_5 \cdot p_{O_2}^c \cdot p_{C_2H_4}^d \tag{38}$$

The exponents are the average of the temperature dependent reaction orders in ethene and oxygen. Both rate constants are parametrized with activation energies and pre-exponential factors.

In a second step, experiments with ethane and oxygen in the feed are taken into consideration. The fitted parameters obtained in the first step (activation energies and pre-exponential factors of reactions 4 and 5) are used for the parameter fitting of reactions 1 and 2as fixed values. Now, parameters for reactions 1 and 2 can be fitted. The kinetic model for ODH is based on the chemistry and elementary steps suggested in Chapter 2. It contains two components: Oxygen activation (taking place at the interface between support and melt) and hydrocarbon activation (occurring at the surface of the melt). The equation derived above is similar to a Mars-van-Krevelen mechanism as

reported in literature.[24, 190] This model contains the separation of oxygen and hydrocarbon actvation. Thus, two rate constants are needed in this equation. Rate constants are parametrized each with an activation energy and a pre-exponential factor, which are optimized.

$$r_1 = \frac{k_{1,1} \cdot \sqrt{p_{O_2}} \cdot k_{1,2} \cdot p_{C_2H_6}}{k_{1,1} \cdot \sqrt{p_{O_2}} + k_{1,2} \cdot p_{C_2H_6}} \tag{39}$$

CO_2 formation, not assumed to proceed via the OCl^- species and assumed to form via a gas-phase mechanism, has been modeled with a power law equation. For the exponents of oxygen and hydrocarbon partial pressures, the average of the experimentally determined activation orders at different temperatures has been used.

$$r_2 = k_2 \cdot p_{O_2}^e \cdot p_{C_2H_6}^f \tag{40}$$

CO formation from ethane (reaction 3) is neglected, as CO mainly forma from ethene (see Figure 28).

3.3.6. Modeling results

3.3.6.1. Total oxidation of ethene

For reaction 4 (CO_2-formation from ethene), the following reaction orders have been used for the power-law-model: 0.7 for ethane, 0.41 in oxygen (average of experimentally determined temperature dependent reaction orders). For reaction 5 (CO-formation from ethene), the following reaction orders have been used for the power-law-model: 0.34 for ethane, 0.1 in oxygen (average of experimentally determined temperature dependent reaction orders). Figure 32 shows the parity plots for CO_2 and CO formation rates.

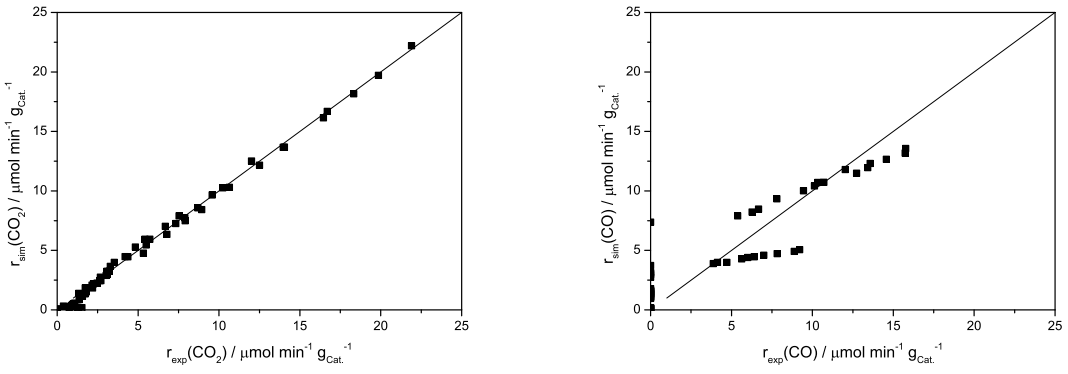

(a) (b)

Figure 32.: Parity plots of CO_2 and CO formation rates (experiment with oxygen and ethene in feed)

Despite a change in the reaction order of both reactants, CO_2 formation rates are described well by the power-law-model. For CO however, no good fit could be obtained. Compared to CO_2, CO formation rates are smaller and are not that fundamental for the modeling of the whole reaction system. Table 9 presents the optimized parameters for the formation of both carbon oxides.

Table 9.: Optimized parameters for total oxidation reactions with ethene as pre-cursor

C_2H_4 formation				CO_2 formation	
$E_{A,1}$ $kJ\ mol^{-1}$	A_1 -	$E_{A,2}$ $kJ\ mol^{-1}$	A_2 -	E_A $kJ\ mol^{-1}$	A - -
107.1	1.81E9	163.9	8.8E11	283.5	4.4E18

3.3.6.2. ODH of ethane and total oxidation of ethane towards CO_2

For reaction 2 (CO_2-formation from ethane), the following reaction orders have been used for the power-law-model: 0.79 for ethane, 0.41 in oxygen (average of experimentally determined temperature dependent reaction orders). Figure 33 shows the parity plots of ethene formation via ODH and CO_2 formation.

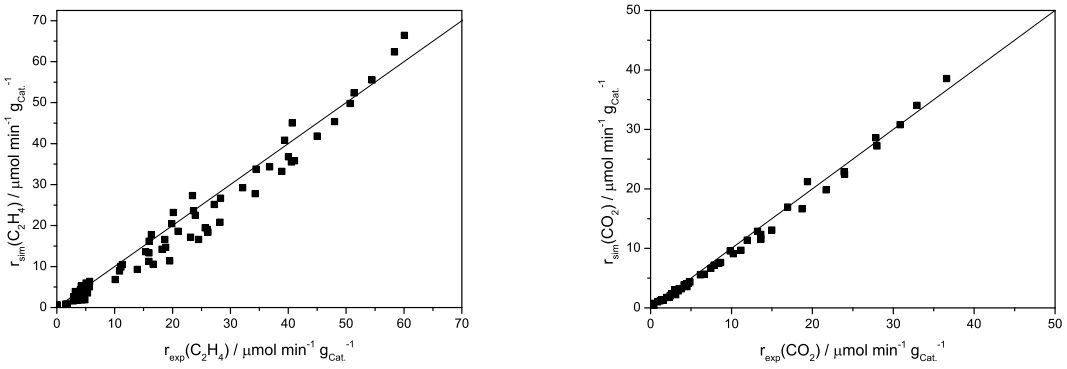

(a) (b)

Figure 33.: Parity plots of ethene and CO_2 formation rates (experiment with oxygen and ethane in feed)

For both products, experimental and simulated data fit reasonably well. The Mars-van-Krevelen model seems to describe a complex cascade of reaction steps well, despite the change in reaction orders of both reactants in temperature. Table 10 presents the optimized values for ODH and total oxidation of ethane towards CO_2.

Table 10.: Optimized parameters for ethene and CO_2 formation with ethane as precursor ($E_{A,1}$ and A_1 relate the to the rate constant $k_{1,1}$, $E_{A,2}$ and A_2 relate the to the rate constant $k_{1,2}$)

C_2H_4 formation				CO_2 formation	
$E_{A,1}$ / $kJ\ mol^{-1}$	A_1 / -	$E_{A,2}$ / $kJ\ mol^{-1}$	A_2 / -	E_A / $kJ\ mol^{-1}$	A / -
163.9	8.8E11	107.1	1.81E9	283.5	4.4E18

The activation energy for the oxygen activation is significantly higher than the one for the hydrocarbon activation, consistent with results presented in Chapter 2. Thus, the oxygen activation has the higher activation barrier compared to the hydrocarbon activation. Furthermore, oxygen activation shows a higher temperature dependence compared to the hydrocarbon activation. It lies in the range of the activation energy of the formation of the mixed oxygen isotope (190 kJ /mol) as showm in the TPIE experiment (see Chapter 2). Thereby, the activation energy of the oxidation step is validated by kinetic modeling. Under differential conditions with elevated flows through the reactor, the activation energy for CO_2 production is higher than for the case of lower flows. Total oxidation of ethane towards CO_2 is assumed to be a gas phase reaction, gas dynamics and back-mixing phenomena can play a role, which can explain the difference. At higher space velocities as used for the kinetic measurements, the formation of CO_2

can behave differently.

3.4. Summary and Conclusions

Ethane ODH reactivity over supported alkali chloride catalysts is neither influenced by water nor by CO_2, thus the reaction order of those molecules is zero. Reaction orders were lower for oxygen compared to ethane in the ODH reaction. Based on a complex mechanistic model presented in Chapter 2, a rate equation for ODH could be derived, both addressing an oxidation and hydrocarbon activation step. Furthermore, a complex kinetic model including ODH and its side reactions was used to fit kinetic parameters to experimental data for ODH, total oxidation of ethane and total oxidation of ethene. This model describes that data well. The activation energy of the oxidation step of the ODH reaction is higher compared to the one of the hydrocarbon activation step, which is consistent to previous results. Activation energies for total oxidation reactions, however, are higher compared to the ones of ODH, thereby reflecting the high olefin selectivities for catalysis over supported alkali chloride catalysts.

4. Tailoring of novel, highly selective supported melt catalysts for the oxidative dehydrogenation of ethane

Novel supported alkali chloride catalysts were investigated for the oxidative dehydrogenation of ethane as target reaction. Various factors have been varied to study the influence of certain properties on the catalytic performance: The influence of different oxides as supports, the influence of a different anion (bromide instead of chloride) in the melt and the influence of different cations in a chloride eutectic system. Also, dcatalysts prepared with different preparation methodes (chloride and nitrate precursors) have been investigated tested in long-term behavior. Metal oxides which could undergo a solid state reaction with chloride do not seem beneficial for the ODH performance, as substantial deactivation occurs. Especially supports forming volatile chlorides are not suitable for efficient ODH catalysts, as they would lead to irreversible chloride depletion. Bromides also tend to catalyze ODH, even with increased activities, but lower olefin selectivities. Thus, the formation of an oxo-halide species as catalytically active intermediate is also possible with other halogenides. Regarding the overlayer, ternary and quaternary chloride eutectic systems were explored, some of them with melting points below 300°C. Two of those catalysts show olefin selectivities up to 98%, being among the highest selectivities reported for ethane ODH. This work consists of characterization of the catalysts coupled with reaction studies, describing and discussing the requirements for good and efficient supported melt catalysts for ethane ODH.

4.1. Introduction

The growing market of light olefins spurs the development of novel technologies to selectively produce them from alternative feedstocks. Oxidative dehydrogenation of ethane towards ethene is a promising route, allowing very high olefin selectivities and lower process temperatures compared to stream cracking, the industrially well-established process for ethene production. Supported alkali chloride catalysts have been reported to be an excellent system for the oxidation of ethane, especially allowing outstandingly high selectivities (up to 95%).[51, 67] Specific feature of this class of catalysts is an alkali chloride layer on top of a solid support. This overlayer is molten under reaction conditions, thus rearranging dynamically. As alkali chlorides per se have a high melting point, eutectic mixtures of different alkali chlorides have been employed so far to decrease the melting point, i.e. LiCl-KCl, LiCl-NaCl, $LiCl - SrCl_2$. It has been reported that a low melting point of the overlayer leads to high olefin selectivities, thus being the aim for future catalyst development. In a previous chapter , the mechanism of ODH over LiKCl/MgDyO as a model system has been reported: Oxygen is absorbed by the molten overlayer of the catalyst, diffuses through it and is activated at the interface between the solid support and the melt. There, highly active intermediate species are formed (i.e. hypochlorite), which diffuse back to the surface of the overlayer. Here, the intermediate species catalyzes the C-H bond activation, leading to the cleavage of C-H bonds and subsequent ethene formation. It could thus be concluded that the ODH reaction on supported alkali chloride catalysts proceeds via a Pseudo Mars-van-Krevelen mechanism with spatial separation of the activation of oxygen and the activation of ethane. The mobility of the active species within the melt and site isolation is the key for the outstandingly selectivities that can be achieved. This chapter focuses on the design of novel catalysts with even higher activities and selectivities. This aim has been approached by varying both the overlayer and the support, while the support is known to mainly govern activity, while the overlayer tunes the selectivity. Thus, different novel supports and eutectic overlayers will be employed. The required features of support and overlayer will be examined and discussed. Thus, several factors for molten alkali chloride ODH catalysts will be introduced and discussed, and the requirements for tailoring new and efficient ODH catalysts will be defined.

4.2. Experimental

4.2.1. Catalyst preparation

Catalysts were prepared by wet impregnation in two different ways for different studies. One part of the catalysts was prepared via the addition of alkali chlorides to a slurry of the support material in 100 ml deionized water as described in Chapter 2. The reference catalyst (LiKCl supported on MgO) was prepared by adding the alkali chlorides (1.04 g LiCl (Aldrich, Reagent Plus) and 1.19 g KCl (Merck, 99.995%) to a slurry of 100 ml deionized water and 6.69 g MgO. For the study with different supports, 0.166 mol support were used for each synthesis (13.25 g TiO_2 Rutile (Aldrich, 99.99%), 9.97 g SiO_2 (Aldrich,99.5%), 38.47 g WO_3 (Aldrich, >99%)). 1.02 g LiCl (Aldrich, Reagent Plus) and 1.19 g KCl (Merck, >99.995%) were added to the slurry. For the study with different halides, 6.45 g MgO (Aldrich, 99.9%) and 0.6 g Dy_2O_3 (Aldrich,99,9%) were used as support materials. For the overlayer, 2.08 g LiBr (Aldrich, >99%) and 1.9 g KBr (Merck, 99.5%) were added to the slurry.
Another part of catalysts was prepared via a method using nitrates as pre-cursors.[51, 67] The reference catalyst (LiKCl supported on MgO) was prepared by adding the alkali nitrate precursors (1.66 g $LiNO_3$ (Aldrich, 99.99%) and 1.62 g KNO_3 (Merck, 99.995%) to a slurry of 100 ml deionized water and 6.69 g MgO. Additionally, 1.02 g of NH_4NO_3 (Aldrich, 99.99%) and 1.57 ml of HCl (Aldrich, ACS reagent 37%) were added to the slurry as chloride source. For the study with different chloride eutectica, 6,64 g MgO (Aldrich, >99%) and 0.6 g Dy_2O_3 (Aldrich,99,9%) were used as support materials, the chloride source remained unchanged. The different eutectic systems were established by mixing different alkali metal nitrates ($LiNO_3$ (Aldrich, 99.99%), KNO_3 (Aldrich, 99.99%), $NaNO_3$ (Aldrich, 99.995%), $RbNO_3$ (Aldrich, 99.7%), $CsNO_3$ (Aldrich, 99.99%), $Sr(NO_3)_2$ (Aldrich, >99%), $Ba(NO_3)_2$ (Aldrich, >99%)) . The compositions can be found in Table 11.

4.2.2. Elementary analysis

Solid catalysts were dried and solved in different acidic media. Cl^- was quantified by titration with $AgNO_3$, using a Metrohm Titrando 904. Mg, Li and K were quantified by AAS (Agilent AAS280FS). Ti, Si and W were quantified by photometry (Shimadzu UV-160 UV Spectrometer).

Table 11.: Synthesis of catalysts with novel eutectic systems as overlayer

Catalyst	molar composition (mol%)							g nitrate used for synthesis						
	Li	K	Na	Rb	Cs	Sr	Ba	Li	K	Na	Rb	Cs	Sr	Ba
LiKRbCs	55.5	18.7		1.4	24.3			1.53	0.76		0.08	1.89		
LiRb	54.9			45.1				1.51			2.65			
LiKNaRb	50.4	18.3	8	23				1.39	0.74	0.27	1.37			
LiRbCs	56.5			38.5	5			1.59			2,27	0.39		
LiNaRb	56.6		2.4	41				1.56		0.08	2.42			
LiKBa	54	40					6	1.49	1.62					0.63
LiCsSr	58.2				39.8	2		1.6				3.1	0.02	
LiNaCs	58		1.7		40.3			1,6		0,06		3.14		
LiCs	59.3				40.7			1,6				3.1		
LiKCs	57.5	13.3			29,2			1.59	0.54			2.28		
LiKNa	43	24	33					1.19	0.87	1.12				

4.2.3. Catalytic tests

Catalytic tests were performed in a plug flow reactor consisting of a catalyst fixed-bed in quartz tubes surrounded by heat distributor blocks and heating coils, using 300 mg of the catalysts diluted in 700 mg SiC to ensure a homogeneous temperature in the entire catalyst bed. Layers of SiC and quartz wool encased the catalyst bed to avoid dead volume and provide a mechanical fixation. The product gas stream was analyzed by a Maxum edition II Process gas chromatograph (Siemens) equipped with TCD detectors. Oxygen, carbon monoxide and methane were separated on a Molesieve 5A column and the other hydrocarbons were separated on a HayeSep Q column combined with a HayeSep T precolumn. A Poraplot Q column was used to resolve additional products. Steady state kinetic experiments were performed at atmospheric pressure, using partial pressures of ethane (99.5%) and oxygen (10.1% in He) of 70 mbar each and balance He (99.99%). The WSHV was 0.8 h^{-1} and reactions were performed in a temperature window between 450°C and 650°C. For the step transient experiments, the catalyst was heated to the reaction temperature in He and then 10% O_2 in He was subsequently supplied for 45 min. After a short He purge (0.25 min), the probe reaction with ethane (10% C_2H_6 in He) followed, detecting the ethane consumption and ethene and CO_2 formation by MS analysis. Ethane and ethene were quantified by linear deconvolution of different MS signals m/z = 26, 27, 28, 29, 30.

4.2.4. BET analysis

BET surface areas and pore size distributions were determined by N_2 adsorption-desorption at 77 K using a PMI Automated BET Sorptomatic 1900 Series instrument. Prior to the adsorption, the samples were evacuated at 250°C for 2 h.

4.2.5. DSC analysis

DSC analysis was performed with a SenSys EVO 3D TGA/DSC setup, using quartz crucibles. A helium flow of 20 ml/min was applied during the whole experiment. To remove water and other adsorbed species, the sample was activated by heating it up to 500°C with a temperature ramp of 10 K/min. At 500°C, the temperature was kept constant for 5 h before cooling down. At room temperature, the sample was kept for 3 h. After this activation, the experiment could be started. The sample was heated with a rate of 2 K/min up to 500°C, monitoring the DSC signals.

4.2.6. XRD

XRD measurements were performed on a Philips X'Pert Pro System (CuKα1-radiation, 0.154056 nm) in Bragg-Brentano geometry in the range 2θ = 5-70° with a step size of 0.017°/s, operating at 45 kV/40 mA.

4.3. Results

4.3.1. Catalyst preparation methods

Supported alkali chloride catalysts are reported to be prepared via wet impregnation of alkali/alkali earth nitrates together with HCl/NH_4Cl as chloride source. After drying the residues are calcined in a stream of synthetic air to remove the nitrates in order to form stable chlorides. [51, 67] To simplify the synthesis, a novel method was developed as explained in Chapter 2. In this new method, the support material and alkali chlorides were solved in water, thus being directly impregnated without the deposition of any precursors. The subsequent drying and calcination were kept unchanged. As the chemical composition of the catalyst should be identical, no differences in reactivity are assumed. Figure 34 shows the time resolved conversion of ethane ODH with the two different catalysts.

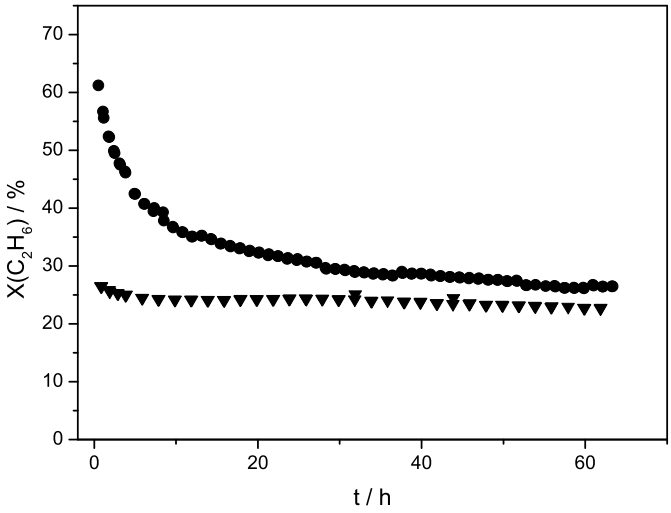

Figure 34.: Time resolved ethane conversion over LiKCl- catalyst prepared with different precursors (▼:nitrates as precursors; •:chlorides as precursors; T=625°C, WHSV = 0.8 h^{-1}, p_{total} = 1 bar , $p_{Ethane} = p_{O2}$ = 70 mbar)

However, a difference in activity was observable: The catalyst prepared with the new method starts with a very high activity followed by a decay in activity before reaching an asymptotic value, despite its chemical composition being identical to the one prepared with nitrates as pre-cursors. The conversion after 50 h, however, is nearly identical. In order to check for chloride loss, elementary analysis of the catalyst prepared via the chloride method (fresh catalyst and a sample after 50 h TOS) was performed. The results are summarized in Table 12.

Table 12.: Elementary analysis of LiKCl/MgO prepared with chlorides as precursors (fresh and after 50 TOS)

	LiKCl/MgO calcined	LiKCl/MgO after 50 h TOS
Mg (wt%)	35.8	40.4
Li (wt%)	1.5	1.5
K (wt%)	2.2	2.5
Cl (wt%)	13.25	13.3

No substantial changes in the elementary composition of the catalysts before and after the reaction can be observed. BET areas of the catalyst did not vary substantially (13.6

m^2g^{-1} for the fresh one vs. 12.1 m^2g^{-1} for the one after 50 h TOS).

4.3.2. Tuning the catalyst performance by support variation

Different common metal oxide supports have been tested as support material to anchor an eutectic alkali chloride mixture. LiKCl has served as a model system for the overlayer in all cases. In this study, TiO_2, SiO_2 and WO_3 have been employed as supports, all known as common catalyst supports. Figure 35 shows the time dependent conversion of the three catalysts with different supports.

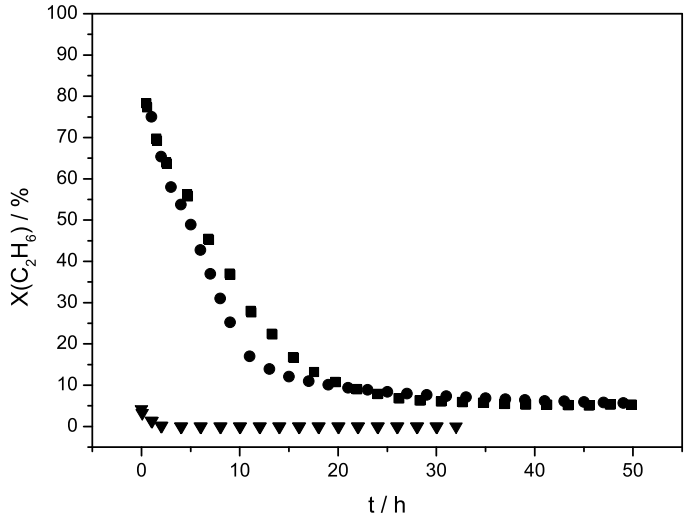

Figure 35.: Time resolved ethane conversion over LiKCl- catalyst with different supports (▼:WO_3; •: SiO_2; ■: TiO_2; T=625°C, WHSV = 0.8 h^{-1}, p_{total} = 1 bar , $p_{Ethane} = p_{O2}$ = 70 mbar)

Surprisingly, all catalysts lose most of their activity within the first 25 h on stream. The catalysts supported on TiO_2 and SiO_2 have an initial conversion of around 80%, decreasing to around 5% after 25 h on stream. The catalyst supported on WO_3, however, starts with an ethane conversion of around 5%, losing all activity within 5 h.

MgO, as presented in Figure 1, seems to be a stable support, allowing stable conversion levels for the synthesis method with nitrates as precursors, as well being stable after 50 h for the synthesis method with chlorides as precursors. Due to those experiments, the supports for the alkali chloride catalysts can be classified into two additional types: Titania and silica have a high initial activity, the decrease in reactivity occurs during the first 20 h of the ODH reaction. However, the tungsten oxide supported system shows hardly any activity at the beginning of the ODH reaction.

The first type is analyzed and discussed first. To further rationalize the chemical processes responsible for the deactivation, elementary analysis of Si (Table 13) and Ti (Table 14) based systems was performed.

Table 13.: Elementary analysis of $LiKCl/SiO_2$ prepared with chlorides as precursors (fresh and after 50 TOS)

	$LiKCl/SiO_2$ theoretical	$LiKCl/SiO_2$ calcined	$LiKCl/SiO_2$ after react.
Si (wt%)	38.25	36.7	37.2
Li (wt%)	1.37	0.9	1.3
K (wt%)	5.12	3.7	3.3
Cl (wt%)	11.66	5.6	2.1

Table 14.: Elementary analysis of LiKCl/TiO_2 prepared with chlorides as precursors (fresh and after 50 TOS)

	$LiKCl/TiO_2$ theoretical	$LiKCl/TiO_2$ calcined	$LiKCl/TiO_2$ after react.
Ti (wt%)	51.4	47	55.3
Li (wt%)	1.1	0.9	0.9
K (wt%)	4	3.7	4.1
Cl (wt%)	9.2	2.9	0.7

It is interesting to note that the calcined catalysts show a deviation from the theoretically calculated values. In the case of the silica supported system, the weight percentage of all overlayer components has decreased. The loss of chloride is most obvious, as its amount decreased to half of its theoretical value. The loss of lithium and potassium is less pronounced. The titania supported system shows a smaller loss of lithium and potassium. The weight percentages of those two components is close to the theoretically calculated value. However, the weight percentage of chloride is about one third of its theoretically calculated value. A different result can be obtained after the ODH test reaction with both catalysts. While the weight percentage of lithium and potassium changes only marginally after 50 h on stream, the chloride amount decreases further. In the case of silica, more than half of the chloride still being present after calcination has disappeared, in the case of titania, only one third of the chloride being present after

calcination is still present. However, it is important to note that the amount of chloride has not decreased to zero.
The other type of support, represented with WO_3 in this study, will now be discussed. The fact that WO_3 does not even show a notable initial activity leads to the assumption that no active intermediate species can be formed utilizing WO_3 as a support. Thus, the question whether a chloride phase remains on the support after the synthesis arises. In order to answer this question, both elementary analyses (Table 15) and XRD (Figure 36) of the catalyst have been performed before and after calcination. In this case, elementary analysis has been performed also for the case of an uncalcined catalyst, however not for a catalyst after 50 h on stream, as no activity can be observed only after few hours on stream.

Table 15.: Elementary analysis of uncalcined and calcined $LiKCl/WO_3$

	$LiKCl/WO_3$ theoretical	$LiKCl/WO_3$ uncalc.	$LiKCl/WO_3$ calc.
W (wt%)	75	70.1	75.58
Li (wt%)	0.4	0.5	<0.1
K (wt%)	1.6	1.6	1
Cl (wt%)	3.5	4.1	0

While the uncalcined catalyst shows values close to the theoretical value, the calcined one does not contain any chloride and nearly any lithium. Potassium is present, but only about 63% compared to the uncalcined one. Thus, the calcination of the catalyst seems to be the reason for the loss of lithium and chloride and part of the potassium. Two decisive differences can be seen in comparison to silica and titania: All the chloride is already lost during calcination, furthermore a larger decay in Li and K can be observed. To further investigate the chemical processes occurring during calcination, XRD analyses of the uncalcined and calcined WO_3-supported catalyst are presented in Figure 36. It can be observed that potassium tungstates and lithium tungstates form during calcination of the catalyst. All chlorine containing components (LiCl, KCl), however, disappear, confirming the result of the elementary analysis that all chlorine is lost during calcination.

4.4. Variation of the overlayer

Besides the properties of the support, the overlayer can be varied as well. In order to systematically study the influence of its properties, both the anion and the cations are

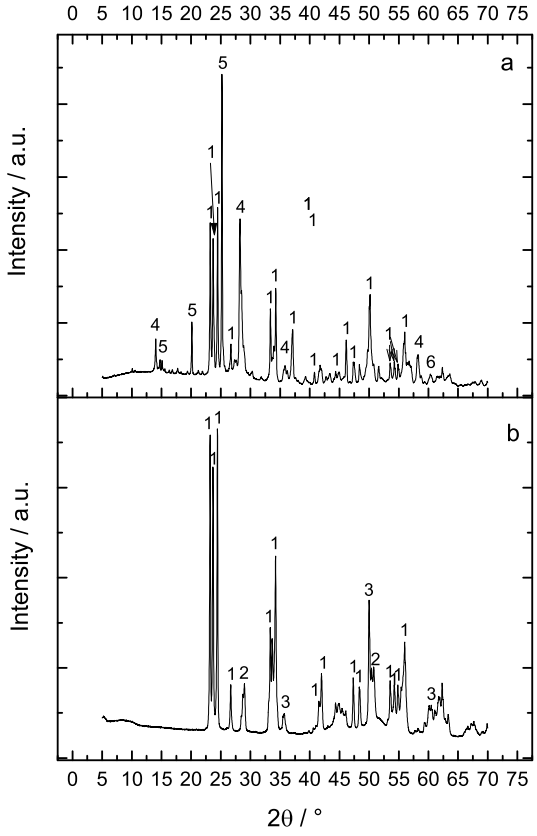

Figure 36.: XRD of calcined and uncalcined LiKCl/WO_3 (1: WO_3; 2: KCl; 3: LiCl; 4: $K_{0.33}W_{0.944}O_3$; 5: Li_6WO_6; 6 $KClO_4$)

varied.

4.4.1. Influence of the halide anion on the catalytic performance

Besides chlorides, bromides can potentially serve as overlayer on a stable support as ODH catalyst. An eutectic mixture of LiBr and KBr has been used as model system for bromides, as it can be compared to the respective eutectic system utilizing chlorides. Also the melting temperature of this system is comparable (T_{melt}=329°C compared to 353°C for LiKCl). Figure 16 shows ethane conversion and ethene selectivities for LiKBr in comparison to LiKCl.

The chloride system shows almost no ethane conversion between 450°C and 550°C. Notable conversion starts around 550°C and reaches a value of around 50% at 625°C. The bromide system, however, shows a much higher ethane conversion over the whole temperature range. At 450°C, the system already shows an ethane conversion of 8% and

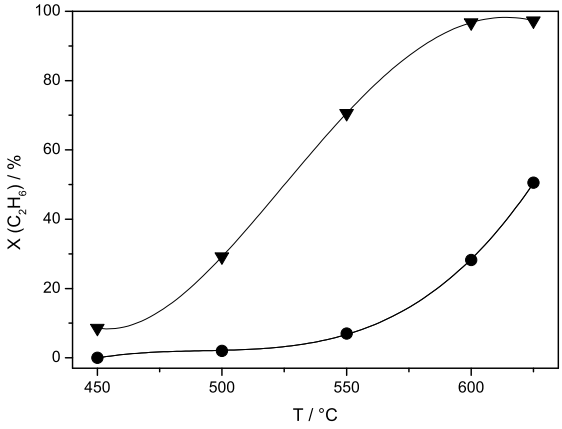

(a)

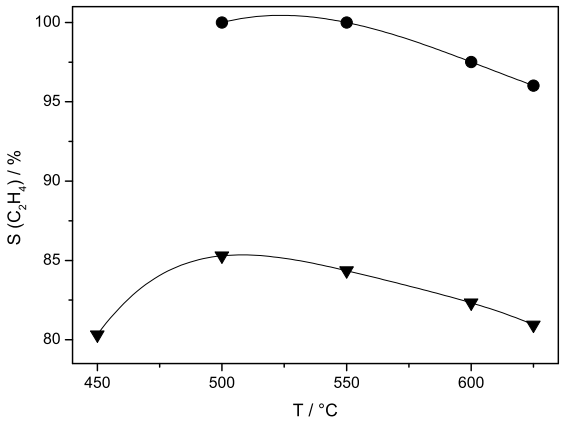

(b)

Figure 37.: Catalytic performance of LiKCl (•) and LiKBr (▼); WHSV = 0.8 h^{-1}, p_{total} = 1 bar , $p_{Ethane} = p_{O_2}$ = 70 mbar

reaches a value of 97% at 625°C. While the chloride system shows an ethylene selectivity of 100% at 500°C, it decreases to 95% at 625°C. In contrast, the ethylene selectivity of the bromide system is lower over the whole temperature range. It shows a maximum of around 85% at 500°C before decreasing to 81%. A transient step experiment was performed as well, investigating the transient step response of ethane over an oxygen-loaded LiKBr, as already investigated with chloride catalysts (see Chapter 2). Figure 38 shows the ethene and CO_2 signals. It becomes obvious that both species can be detected.

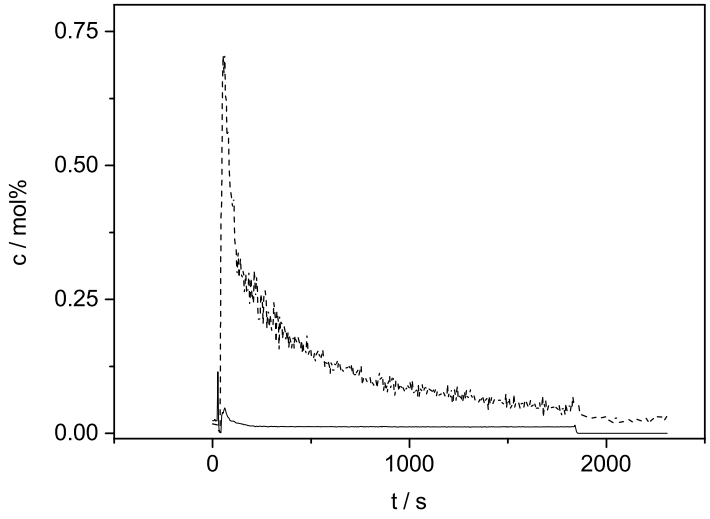

Figure 38.: Responses of step experiment with LiKBr (T = 625°C): dashed line: Ethene; solid line: CO_2

Table 16 compares the stored oxygen, initial ethene formation rate of the step and the initial ethene formation rate divided by the total amount of active intermediates in thr melt to the respective chloride catalyst.

Table 16.: Step experiment of LiKBr compared to LiKCl

Catalyst	stored O $g_{Cat.}^{-1}$	Initial ethene rate after step $g_{Cat.}^{-1} s^{-1}$	Initial ethene rate after step / stored O s^{-1}
LiKBr	195.1	0.72	0.0036
LiKCl	75.5	0.3	0.0039

The bromide system stores more oxygen than the chloride system. Therefore, also the initial ethene formation rates after the step are higher. Initial ethene rates after a step

divided by the total amount stored O, representing turnover frequencies over the active sites (OBr^- and OBr^-), however, are in the same range.

4.4.2. Controlling selectivity by novel eutectic systems as catalyst overlayer

Mixtures of different eutectic chlorides have been used for this study. [191] The catalysts used have been prepared with nitrates as precursors in order to obtain stable activity from the beginning of the experiment.

4.4.2.1. DSC analysis

To verify the melting point of the novel eutectic systems reported in literature, DSC measurements of the catalysts were performed. Each negative peak in a DSC signal represents a heat flow into the system, which can either be needed for the desorption of certain components or to provide the heat needed for melting the system. The experimentally determined melting points of the different eutectica are compiled in Figure 39 and compared to literature in Table 17.

Table 17.: Experimentally determined melting points of different chloride eutectica compared to literature values

Eutectic system	mp via DSC / °C	mp literature / °C	Reference
LiCl/KCl/CsCl	262	265	[192]
LiCl/KCl/RbCl/CsCl	no clear mp observable	258	[193]
LiCl/RbCl	275	325	[194]
LiCl/KCl/NaCl/RbCl	288	297	[194]
LiCl/RbCl/CsCl	293	290	[194]
LiCl/NaCl/RbCl	294	318	[195]
LiCl/KCl/BaCl	298	290	[196]
LiCl/CsCl/SrCl	306	298	[194]
LiCl/NaCl/CsCl	311	320	[195]
LiCl/CsCl	319	323	[192]
LiCl/KCl/NaCl	333	367	[195]

The DSC signals show different peaks in the temperature range between 30°C and 500°C. Signals at 100°C are attributed to the evaporation of water, signals below 100°C are attributed to the desorption of carbon dioxide. The big, sharp peaks above 200°C represent

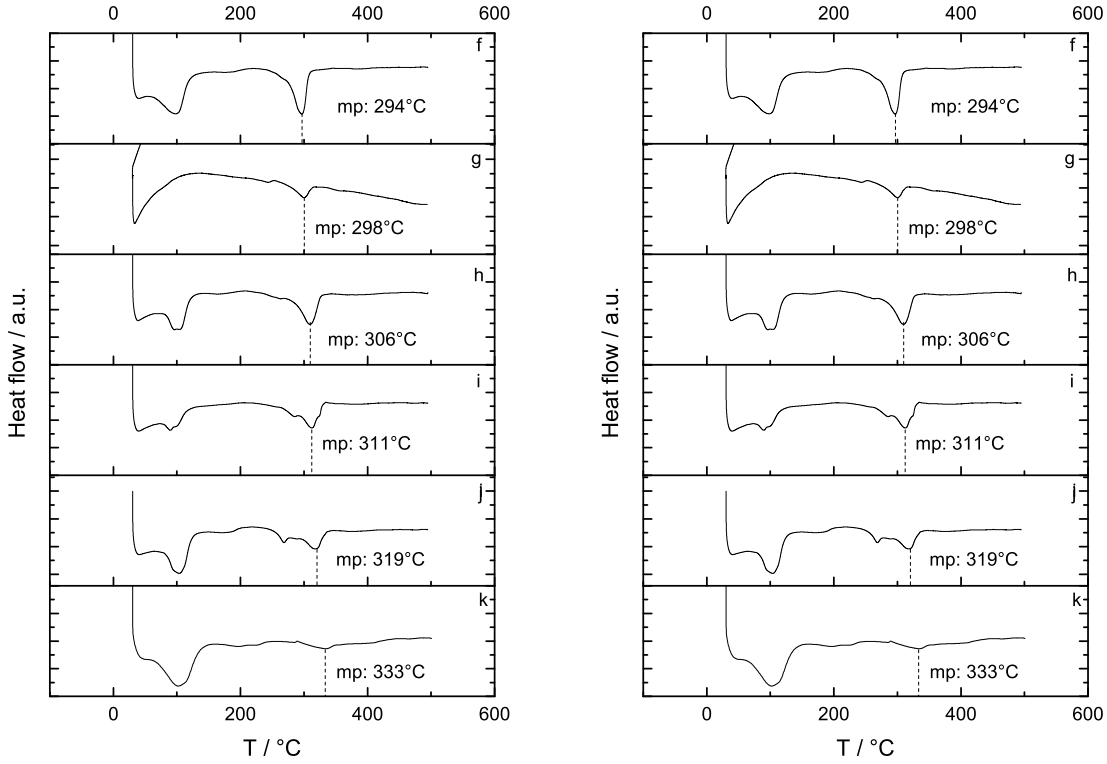

(a) (b)

Figure 39.: Determination of the melting point of novel eutectic systems via DSC (a: LiKCsCl; b: LiKRbCsCl; c: LiRbCl; d: LiKNaRbCl; e: LiRbCsCl; f:LiNaRbCl; g: LiKBaCl; h: LiCsSrCl; i: LiNaCsCl; j:LiCsCl; k: LiKNaCl

the heat needed for melting a system. The measured melting point is very similar to the one reported in literature in most of the cases. Only in the cases of LiCl/RbCl, LiCl/NaCl/RbCl and LiCl/KCl/NaCl, a deviation can be observed. However, the measured melting point is lower in all of the cases. The system LiCl/KCl/RbCl/CsCl does not show a clear melting point in the DSC measurements. Thus, it cannot be assumed that this eutectic system is molten under reaction conditions.

4.4.3. Reactivity studies

Reactivity tests for the catalysts with the eutectic systems listed in Table 17 are compiled in Figure 40 (eutectica with lower melting points) and Figure 41 (eutectica with higher melting points).

Whereas the eutectic systems with the lower melting points allow ethene selectivities over 95%, the ones with the higher melting point do not exceed 90% olefin selectivity. The highest selectivities can be achieved with LiRbCl and LiKNaRbCl (LiRb shows an olefin selectivity above 97% at 625°C and LiKNaRb an olefin selectivity above 96%). Those new eutectic systems are an improvement for tailoring new catalysts that are even more selective than the ones reported in literature.[51, 67]

4.5. Discussion

4.5.1. Influence of the catalyst synthesis method

Initial hyperactivity of the catalyst prepared with chlorides as pre-cursors can be observed, starting with very high conversion levels, followed by a rapid decrease before reaching an asymptotic value. Interestingly, the catalyst with an identical chemical composition but prepared with nitrates as pre-cursors, shows a stable ethane conversion, being almost identical with the asymptotic value that the catalyst with chloride pre-cursors reached. Thus, properties of the chloride catalyst change in the first 50 hours of the reaction. Potential reasons for the decay in activity could be chloride loss to the gas phase, sintering or a change of the support properties during the first 50 hours on stream. The support properties are known to mainly control the catalytic activity. (see Chapter 2). Elementary analysis of the fresh chloride catalyst and another one after 50 hours on stream did not show a substantial change in the chemical composition. Thus, no component of the overlayer is prone to leaching, and the results do not confirm a substantial loss of chloride, which thus cannot be the reason for the decay in activity. Sintering can also be excluded as the reason for the decay in activity, as the BET areas remain nearly constant. Thus, only structural changes in the support can be the reason

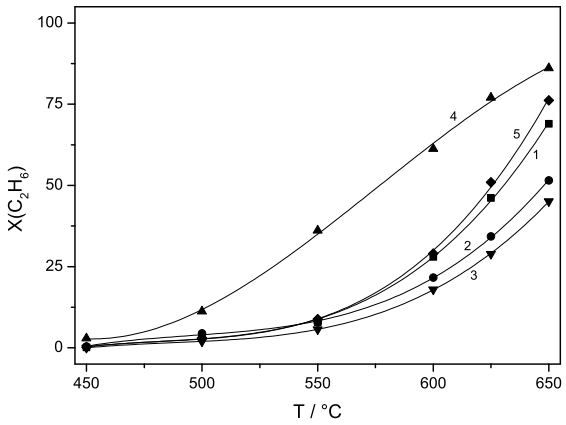

(a)

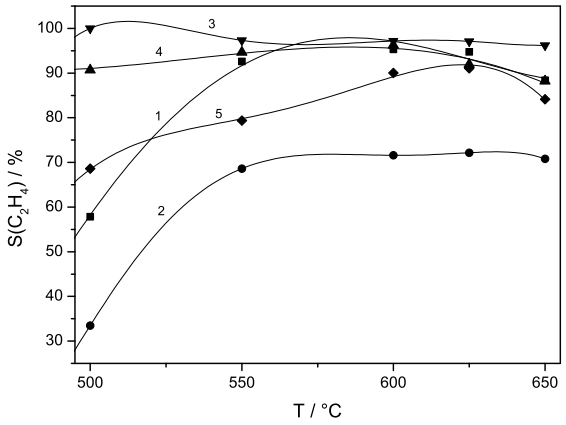

(b)

Figure 40.: Performance of catalysts with lower melting eutectic systems (1: LiKCs; 2: LiKRbCs; 3: LiRbCl; 4: LiKNaRbCl 5: LiRbCsCl; WHSV = 0.8 h^{-1}, p_{total} = 1 bar , $p_{Ethane} = p_{O2}$ = 70 mbar

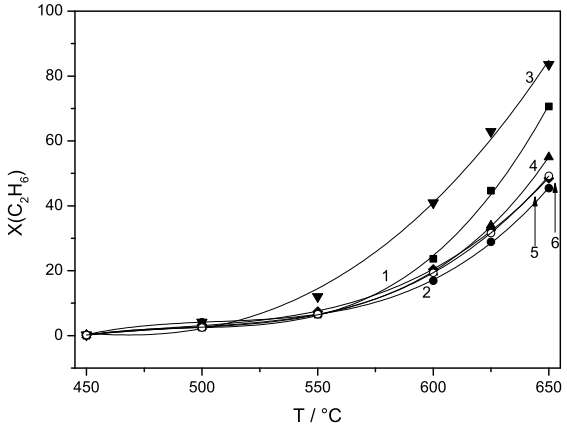

(a)

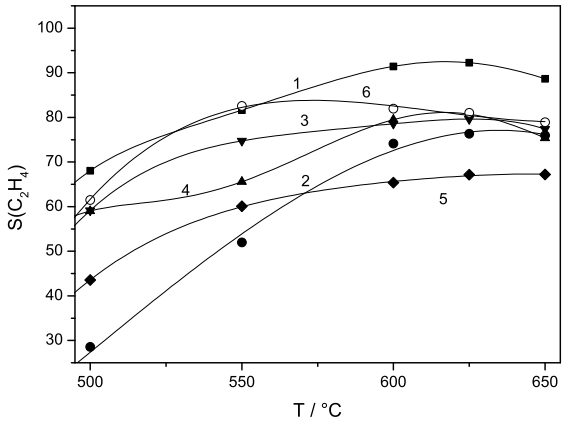

(b)

Figure 41.: Performance of catalysts with higher melting eutectic systems (1: LiNaRbCl; 2: LiKBaCl; 3: LiCsSrCl; 4 LiNaCs; 5: LiCsCl; 6: LiKNaCl; WHSV = 0.8 h^{-1}, p_{total} = 1 bar , $p_{Ethane} = p_{O2}$ = 70 mbar

for the decay in activity. HCl is one precursor for the overlayer formation using the nitrate method. In the chloride method, however, no HCl is added at any point in the synthesis. It can be speculated that HCl is responsible for avoiding initial hyperactivity. In the nitrate method, it is present in the synthesis. In the chloride method, however, the catalyst is exposed the first time to HCl during the ODH reaction, as it forms at one step. Thus, it is possible that it takes 50 hours to form enough HCl to stabilize the conversion at an asymptotic value. HCl could for example block active centers at the support. a potential blocking of active sites on the support would happen during synthesis in the nitrate method, but only during reaction in the chloride method.

4.5.2. Requirements for a good support for an alkali chloride catalyst for ethane ODH

MgO seems to be a stable support for anchoring an alkali chloride overlayer which can be molten under reaction conditions. Even the activity of catalysts with chloride precursors is not constant, it stabilizes at an asymptotic value that still allows reasonable conversion levels. However, other metals like titania, silica and tungsten oxide do not show a stable behavior, as their activity decreases drastically, allowing only conversion levels below 5% after 50 h TOS. Tungsten oxide is the worst support, as reasonable conversion levels are not attainable with a calcined catalyst. In order to investigate the reason for this decay, different reasons could be found, as already introduced in the previous chapter. As the chemical composition of all three catalysts changes, this reason is more obvious in this case. Chloride, key component of the supported alkali chloride catalysts and guarantor for the formation of a liquid melt on top of the support, is lost during calcination and during reaction. The chloride loss has to be caused by the formation of volatile compounds. One possibility is the hydrolysis of chloride with formed water, forming volatile HCl, observed at a similar catalyst.[169] The results of this study contradict this possibility, as no chloride loss can be observed with MgO as a support, and furthermore the degree of chloride loss is dependent on the support material. Thus, a different route for chloride loss has to be opened, and it is obvious that the support material is involved in this route. This route can be rationalized with reactions of cations of the support with chloride. In the case of tungsten oxide, a solid state reaction between the support WO_3 and chloride is suggested, which can lead to the formation of tungsten hexachloride which melts at 275°C and evaporates at 337°C.[197] The formation of this volatile species can explain the loss of chloride even during calcination. Lithium and potassium remain in the catalyst, forming tungstates in another solid state reaction. For the case of silica and titania, similar solid state reactions could occur. Titanium tetrachloride melts at -24.1°C and has a boiling point

of 136.5°C. This molecule can easily react with water, forming TiO_2 and HCl, which can also explain the chloride loss pathway.[197] Silicium tetrachloride has a melting point of -70.4°C and a boiling point of 57.57°C. It can also react with water, forming silicium hydroxide and HCl, again opening a pathway for chlorine loss.[197] Regarding those results, a stable catalyst with a molten chloride layer cannot be tailored with WO_3, silica or titania as support materials, as those materials seem to react with chloride and form volatile compounds. Thus, a chloride loss is inevitable. A dense chloride overlayer, however, is guarantor for the excellent performance of supported alkali chloride catalysts, as a molten overlayer of chlorides enables the formation of the intermediate oxo-chloride anions. This overlayer furthermore enables the diffusion of those intermediates through the melt and also stores the reactive hypochlorite species, needed at the surface of the melt to initiate the ODH reaction. Thus, materials that do not easily react with chloride should be used. For a good support, even if such a reaction is theoretically possible, the formed metal-chloride must not be volatile. MgO is thus an excellent candidate, as $MgCl_2$ remains solid up to 708°C, which is outside the temperature window of ethane ODH over this class of catalysts.

4.5.3. Influence of the anion in the overlayer

Besides chlorides, supported bromides seem to be suitable materials for good ODH catalysts as well. Activity and selectivity of both systems can be related to the reactivity of the intermediate species, the oxo-halide-anions which are formed at the support-melt interface. Apparently, the route with bromides proceeds along the formation of an hypobromite species. The bromide system can apparently store more oxygen than chloride. Thus, the concentration of the reactive intermediate is higher, also at the surface of the melt where the ethane is activated. This can explain the higher activities for bromides in the steady state operation mode. As a consequence, the initial ethene formation rate directly after the step is higher than for chloride. Interestingly, the turnover frequencies lie in the same range. Thus, the reactivity of the active intermediate OBr- is comparable to OCl^-. Regarding the selectivity, there is one important difference compared to the chloride system. CO_2 can be detected in the step experiment with the bromide system. This could have two reasons: Either the higher concentration of the active intermediate makes the isolation of sites less likely. Two hypobromite species might thus attack one ethane molecule, leading to oxygen insertion and total oxidation. Another reason could be a difference in the stability of the intermediate (according to the Hammond postulate)[198], leading to different selectivities. As the initial ethene concentration divided by the total number of active intermediates of both hypohalogenites is very similar, this option is less likely, as a different transition state would probably cause different values in this case. As reactivity is much higher in

the steady state experiment, it can be speculated that also the formation of the active intermediate is faster compared to chloride. This effect is however less obvious in the step experiment, as here equilibrium concentrations of the active intermediates are measured. Form the step experiment, it can be derived that CO_2 formation starts after the ethene formation. Thus, CO_2 is a secondary product in this case. This could either be related to the higher density of active intermediates in the melt or caused by a higher reactivity for oxygen insertion (leasing to total oxidation) for the case of bromide.

4.5.4. Influence of different cations in the overlayer of a supported alkali chloride catalyst

A variety of different eutectic systems has been tested in order to understand the influence of cations present in the melt and the melting point of the eutectic system. Tope [67] has shown a correlation between the melting point of an eutectic system and the olefin selectivity of the respective supported catalyst. It would now be desirable to understand the link between overlayer composition, melting point and olefin selectivity. In Figure 42, olefin selectivities at 625°C are illustrated as a function of the melting point of the eutectic system.

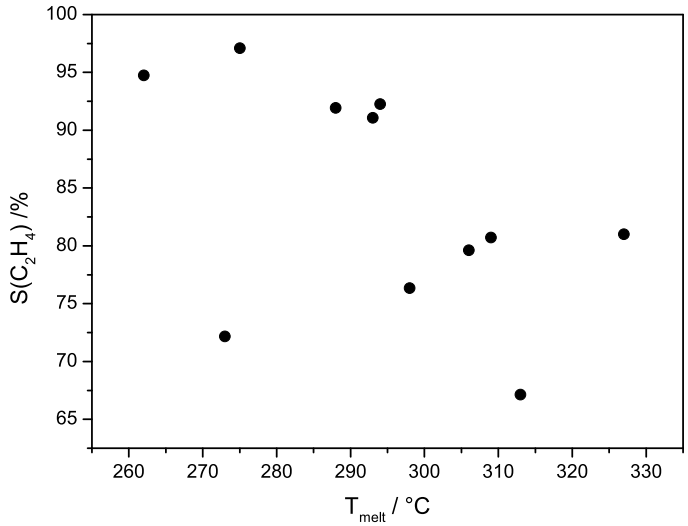

Figure 42.: Ethene selectivities at 625°C as a function of the melting point of the overlayer eutectic system

Olefin selectivities over 90% can only be observed using eutectic systems with a melting point below 300°C for the systems studied in this work. However, a linear correlation between olefin selectivity and melting point of the eutectic system cannot be seen. The

linear correlation found by Tope [67] does not hold true for the systems studied in this work and can thus not be extended to eutectic systems with three or more different cations. Furthermore, it is worth to note that LiKCl, as reported in previous publications [51, 67], shows a higher selectivity than most of the systems shown in Figure 42, even having a higher melting point than all of the studied systems. LiKRbCsCl, with a reported melting point of 258°C, cannot be assumed to be molten at this temperature, as there is no clear sign of melting in the DSC signal. Olefin selectivities remain very low for this system, leading to the conclusion that a molten system is required for outstanding selectivities. Thus, this system is out of the trend in Figure 42. The presence of a molten phase is essential for high olefin selectivities, as OCl^- ,the reactive intermediate species, is formed at the interface between support and melt before diffusing through the molten overlayer to the surface, where it activates the hydrocarbon. If a molten phase is not present, the reaction cannot proceed via this pathway, as OCl^- cannot diffuse through the molten overlayer. Furthermore, the surface of the catalyst could not dynamically rearrange, which prevents the exposure of metal cations to the gas phase, which could easily lead to re-adsorption of ethane, followed by total oxidation. This would lead to decreased olefin selectivities. The necessity of a molten overlayer is nicely illustrated by the example of LiKRbCsCl. Apparently, no clear correlation can be found regarding different eutectic systems. According to the mechanistic understanding, two features of an eutectic layer are important for reactivity and selectivity: Solubility and diffusion coefficient of OCl^- in the melt and the surface concentration of the alkali cations at the melt-gas interface. The diffusion coefficient of OCl^- through the molten overlayer is assumed to be dependent on the cations in the melt, as a counter-cation has to diffuse through the layer as well. Due to ion radii, different local concentrations of chloride and its counter-ions are possible. The concentration of metal ions on the surface of the melt is thus a key factor for olefin selectivity, as metal cations can catalyze total oxidation.

4.6. Conclusions

The properties of the support have a large effect on the performance of supported alkali chloride catalysts for ODH, even never exposed to the gas phase reactants. Supports need to form surface defect sites, as this is supposed to be the active center where the catalytically active intermediate is formed (see Chapter 2). This contribution has shown that there is an additional requirement for a suitable support, as the support has furthermore to be stable against any solid state reaction of the support metal cation with the chloride overlayer, leading to chloride loss. Especially, the formation of a volatile chloride compound like WCl_6, $TiCl_4$ and $SiCl_4$ should not occur, as this would open a path for chloride loss via the gas phase, finally leading to a chloride depletion. Depletion

of chloride prevents the formation of a molten overlayer on top of the surface of the oxide support, which is the key factor for very high olefin selectivties. We could show that chlorides are not the only materials that can serve as an overlayer for ODH catalysts. Apparently, other halides besides chloride are also capable of polarizing oxygen by the formation of a hypohalogenide species. The assumption that the the halogenide and not any metal cation in the melt is the key species for the intermediate formation is thus confirmed (see Chapter 2). Bromides show a good ODH activity as well, however a worse olefin selectivity compared to chlorides. This can be explained with a higher concentration of intermediate species, thus lowering the effect of site isolation (see Chapter 1). Replacing the chlorides by bromides is a means to improve the activity, however hazarding a worse olefin selectivity. Better olefin selectivities can be achieved by tailored multi-component alkali chloride eutectic systems, consisting of up to 4 different cations. The melting point of those eutectica can be decreased down to 250°C. We could show that the formation of an eutectic system is crucial for obtaining very high olefin selectivities. Systems consisting of different alkali chlorides, however without melting at a certain temperature, showed inferior selectivity compared to systems for which the formation of a melt could be proven. Reactivity tests, however, could not confirm a linear correlation between melting point and selectivity. LiRbCl and LiKNaRbCl have been found to be the best systems regarding olefin selectvities. Olefin selectivities up to 98% are the highest ones compared to the ones reported in literature (see Chapter 1).

This chapter is based on:
Christian A. Gärtner, Andre C. van Veen, Johannes A. Lercher: Highly selective supported alkali chloride catalysts for the oxidative dehydrogenation of ethane, *Top.Catal.*, 57, 2014, pp. 1236-1247

Parts of this chapter are base on the following patent applications:
Christian A. Gärtner, Andre C. van Veen, Johannes A. Lercher: Catalyst, process for catalyst manufacture and process for catalytic oxidative dehydrogenation, WO2013/092179, PCT/EP/2012/.074212

Christian A. Gärtner, Andre C. van Veen, Johannes A. Lercher Catalyst, process for catalyst manufacture and process for catalytic oxidative dehydrogenation, WO2013/092180, PCT/EP/2012/074214

Christian A. Gärtner, Andre C. van Veen, Johannes A. Lercher: Catalyst, process for catalyst manufacture and process for catalytic oxidative dehydrogenation, EP 2 606 963 A1

5. Suitability of Supported Alkali Chloride Catalysts for the Oxidative Coupling of Methane

Surprisingly high C_2-selectvitities for methane coupling over supported alkali chloride catalysts are reported in this chapter, thus enabling an efficient valorization of this large volume chemical. A novel catalyst system has been found which combines two groundbreaking new principles for selective activation of methane and coupling it oxidatively to ethane. Chemically, the catalyst is based on the highly selective redox capabilities of oxidized chloride anions generated transiently by the catalytic oxidation of chloride anions with oxygen in a molten layer of alkali chlorides. This generation of the catalytically active species by oxidation is facilitated or catalyzed at the interface between the chloride melt and the support, which consists of any oxide capable of activating oxygen into an electrophilic species able to oxidize Cl^- and generating a redox active anion. The formed anion diffuses through the molten chloride layer to the surface of the melt, stabilized there in low concentrations of isolated species. Isolation of catalytically active species enables the highly selective activation of the C-H bond of methane, generating a radical that either recombines with another nearby methyl radical or cleaves off spontaneously a second hydrogen, forming a surface carbene, which recombines to ethene. Formed ethene rapidly desorbs under reaction conditions and is hardly re-adsorbed allowing to achieve high olefin selectivities. The dynamic rearrangement of the surface of the molten overlayer prevents the exposure of metal cations, known to interact with ethene, which would drastically enhance the probability of ethene to be further oxidized. As the catalyst is also known to efficiently catalyze oxidative dehydrogenation form ethane towards ethane, it is a bifunctional one which is able to convert both the C_1- and C_2 paraffin towards ethylene

5.1. Introduction

Methane, major component of natural gas, is mostly used as a clean-burning fuel. However, it would be desirable to convert methane into more valuable chemicals and fuels.[199] Possible valuable products are synthesis gas, methanol, acetic acid, but also hydrocarbons with a longer chain like ethane and ethylene.[200] An elegant and intensively studied process for the conversion of methane to ethane and ethylene is the oxidative coupling of methane, being able to convert the abundantly available methane towards ethane and ethylene, the latter being the mostly produced organic chemical and in important building block for other products. A good coupling catalyst must have sites able to activate the C-H bond of methane (bond energy: 425 kJ/mol). The main problem of this highly attractive reaction is that the products ethane and ethene also have C-H bonds (weakest bond 419.5 kJ/mol for ethane, 444 kJ/mol for ethene [22]) which are prone to activation by those active centers as well, leading to oxygen insertion followed by combustion. An ideal OCM catalyst would be active for the activation of the C-H bond in methane, but not in ethane and ethylene. This is however very problematic, as the dissociation energy for the C-H bond in methane and ethane is very similar. OCM is a mildly exothermic reaction, the combustion reactions are however strongly exothermic. Thus, combustion inside the reactor does not only impose a selectivity problem, but also a problem with the heat management in the reactor.[200] The reaction mechanism proceeds via the generation of methyl radicals at the surface of the heterogeneous catalyst, those being bounced into the gas phase where they couple to ethane. As a gas phase reaction is involved, the formation of COx in the gas phase is also likely [200], depending on the reaction conditions. A formation of surface carbenes followed by a coupling towards ethene is theoretically possible, is however unlikely and could not be proven by an isotopic tracer study.[201] Different catalysts have been employed for this reaction, the research was mainly driven into the direction of catalyst screening. LaSrCaO[201, 202], Na-W-Mn/SiO_2[203**?**], $Mn - Na_2WO_4/SiO_2$ [204] and Li-MgO [142] are well-known examples for OCM-active catalysts. Maximum single-pass C_2-yields using catalytic fixed bed processes are reported lie around 25% at a C_2-selectivity of around 80%.[200] In practice, temperatures above 700°C are needed. The maximum theoretical C_2-yield has been estimated to be around 30%.[205, 206, 207] However, ceramic membranes make single pass C_2-yields of 35% possible, however at temperatures around 900°C.[200] Thus, it would be desirable to find catalysts with a better performance, ideally working at low temperatures and reaching high C_2-selectivities. In the last two decades, many research activities could be observed for methane OCM. High throughput screening is a valid approach for OCM catalysts and has been done extensively, but a rational catalyst design is also an attractive alternative. The latter has also been reported for oxidative dehydrogenation reactions. As many good cata-

lysts for ODH seem also attractive for OCM, this work focuses on one excellent ODH system, trying to be transferred to OCM. Supported alkali chloride catalysts have been reported to efficiently catalyze the oxidative dehydrogenation of ethane, allowing the production of ethene with outstandingly high selectivities.[51, 67, 177] In a previous publication, we have reported a detailed reaction mechanism for ethane ODH over this type of catalysts, linking its high selectivity with the transient formation of oxidizing O-Cl species, i.e. hypochlorite. This species is reported to be ideally selective for the ODH of ethane, not catalyzing any combustion reaction. Thus, the selectivity problem of OCM could be circumvented, as the C-H bond in the desired product ethene is not attacked to a great extent. Thus, the OCM performance of this class of catalysts is in the scope of this present work. Most of the reported supported alkali chloride catalysts are eutectic mixtures of two chlorides, one of them being lithium chloride. A detailed review presents a nice overview about similar materials - Li-MgO - and correlates its properties to OCM activity.[142] Among those systems, the maximum C_2-selectivity is 80% at a conversion of around 25%. The OCM activity of Li-MgO is clearly linked to lithium related sites due to that review, either as $[Li^+O^-]$ or Li_2O_3. It also addresses the effect of chlorine on Li-MgO, leading to the conclusion that chlorine containing promotors lead to a suppression of carbon oxide formation, i.e. by reducing to CO_2 uptake of the catalyst, where to CO_2 acts as a catalyst poison. Another theory is the formation of a $[Li^+Cl^-]$ defect cluster in MgO. As the main feature of the new supported alkali chloride catalysts is a molten alkali chloride overlayer on a solid support, they differ a lot from simple doping MgO with Li. The present publication aims on testing supported alkali chloride catalysts and addressing the mechanism of OCM over supported alkali chloride catalysts.

5.2. Experimental

Catalysts were prepared by wet impregnation. The support material, a physical mixture of MgO (6.45 g, Aldrich >99%) and Dy_2O_3 (0.6 g, Aldrich, 99,9%), was added to a 100 ml of deionized water, followed by the addition of chloride salts forming the overlayer(LiCl (1.02 g, Aldrich >99%) , KCl (1.19 g, Merck 99,5%) or CsCl (4.38 g, Aldrich â¥ 99.5%) and NaCl (0.82 g, Aldrich â¥99.8%)). The slurry was stirred at 80° C for 2 h, followed by the evaporation of water at reduced pressure. The residue was dried at 120 °C for 12 h and calcined in synthetic air (100 ml/min) at 650 °C for 12 h. OCM experiments were performed in a plug flow reactor system described in Chapter 2. For steady state experiments, the product stream analysis was performed with a Siemens Maxum II GC (described elsewhere). For step experiments, the outlet stream was performed with a Pfeiffer Omni StarTM GSD 320 OC mass spectrometer system. Standard conditions for

steady state experiments were performed with a methane partial pressure of 70 mbar and an oxygen partial pressure of 35 or 70 mbar each with balance He (99.99%) at atmospheric pressure. A temperature range between 450°C and 750°C was explored at a WSHV of 0.7 h^{-1}. For the measurement of the OCM activation energy, the WHSV levels were adapted to keep methane conversions low. Step experiments with subsequent reactant dosing were performed by exposing the catalyst to oxygen (10.1% in He) before a short flushing period with inert He (0.25 min). Afterwards, the catalyst was exposed to the hydrocarbon (10% methane in He). For step experiments with an abrupt dosing of both reactants, the catalyst was heated up in He to the respective reaction temperature (650°C, 700°C or 750°C), followed by dosing a gas mixture with partial pressures of 70 mbar for oxygen and methane at a total pressure of 1 bar (balance He).

5.3. Results and discussion

Steady state reactivity tests of a supported alkali chloride catalyst (Li-K-Cl in eutectic composition (mp=353°C [67]) supported on MgO/Dy_2O_3) as depicted in figures 43 and 44 show surprisingly high performances.

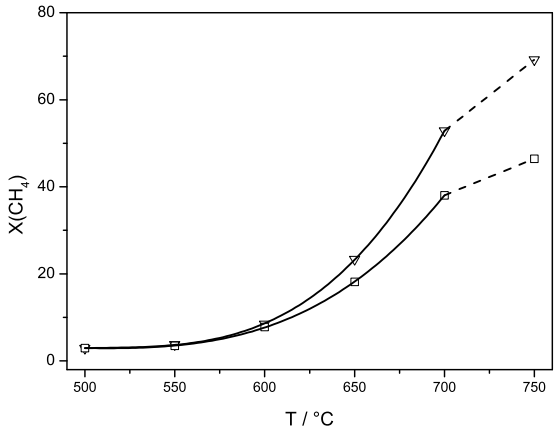

(a)

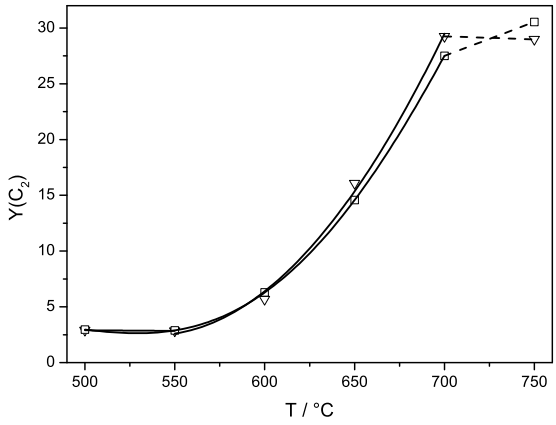

(b)

Figure 43.: Methane conversions (a) and C_2-yields (b); LiKCl, WHSV = 0.7 h^{-1}, p_{ges} = 1 bar, $p_{Methane}$ = 70 mbar, ∇ : p_{Oxygen} = 70 mbar, $\square$: p_{Oxygen} =35 mbar.

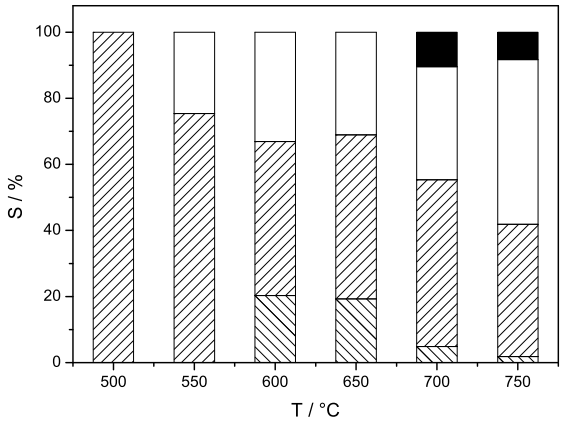

(a)

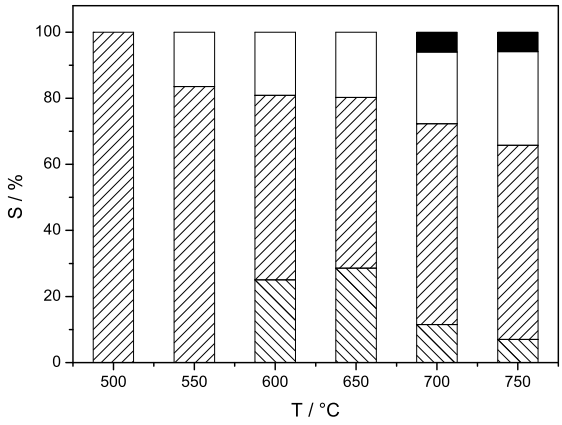

(b)

Figure 44.: Product selectivies (LiKCl, WHSV = 0.7 h^{-1},p_{ges}= 1 bar, $p_{Methane}$ = 70 mbar; (a): p_{Oxygen} = 70 mbar; (b) p_{Oxygen} = 35 mbar; white: CO_2, black: CO, /: ethene, \: ethane)

Conversions up to approx. 70% (with a CH_4/O_2 ratio of 2:1) or approx. 40% (with a CH_4/O_2 ratio of 1:1) can be reached. Unlike other known OCM catalysts, the OCM reaction starts already at comparatively low temperatures: At 600°C, already a conversion of around 10% methane can be observed. Figure 44 additionally presents the product selectivities at different oxygen-methane ratios. Selectivities towards ethane and ethene largely vary with temperature. Compared to the experiments with the higher oxygen content, elevated C_2-selectivities can be observed at the lower oxygen partial pressure. This can be attributed to lower total oxidation rates of methane, ethane and ethene. The highest C_2-selectivities (around 80%) can be achieved at between 550°C and 650°C

with 3,5% oxygen in the feed stream. C_2-yields increase with temperature for both methane-oxygen ratios. Conversion and selecticity levels compensate each other, therefore the C_2-yields are very similar. With the methane-oxygen ratio of 1:1, the C_2-yields reaches its maximum at 700°C, while with the methane-oxygen ratio of 2:1 the C_2-yield even increases at a temperature of 750°C, thereby exceeding the 30% level. Thus, this catalyst outperforms the abovementioned OCM catalyst system. To understand the different behavior of the different methane-oxygen ratios and to identify primary, secondary and side products of OCM, a space time velocity variation as depicted in Figure 45 has been performed.

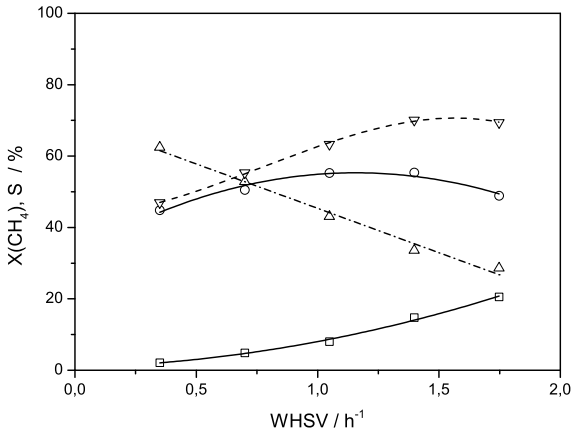

(a)

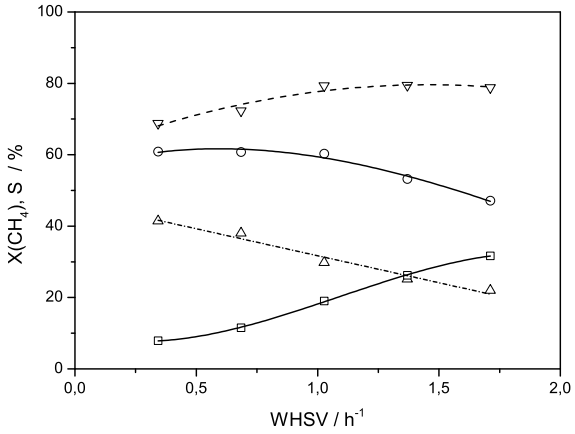

(b)

Figure 45.: Space time variation, LiKCl/MgDyO, T=700°C, p_{ges}= 1 bar, $p_{Methane} = 70$ mbar, (a): p_{Oxygen}=70 mbar, (b): p_{Oxygen}=35 mbar. ($\triangle : CH_4$ conversion, $\triangledown$: C_2-selectivity, $\square$: C_2H_6 selectivity, $\circ$: C_2H_4 selectivity)

Increasing the space velocity leads to lower methane conversions, but higher C_2-selectivities. Thus, it can be concluded that at least part of the formed C_2-components undergo total oxidation reactions. Another interesting finding is that at elevated space velocities, a larger fraction of ethane can be detected in the product stream. A lower space velocities, ethene is the major compound. Those findings clearly indicate that ethane is the primary product of the methane coupling, part of it subsequently converted to ethene at higher temperatures via oxidative dehydrogenation. Interestingly, the same trend can be observed for both different oxygen partial pressures. As mentioned in the introduction, the bond dissociation energy of the first C-H bond is very similar for methane and ethane. Thus, the activation of OCM over LiKCl/MgDyO energy was measured and compared to ethane ODH (figure 46).

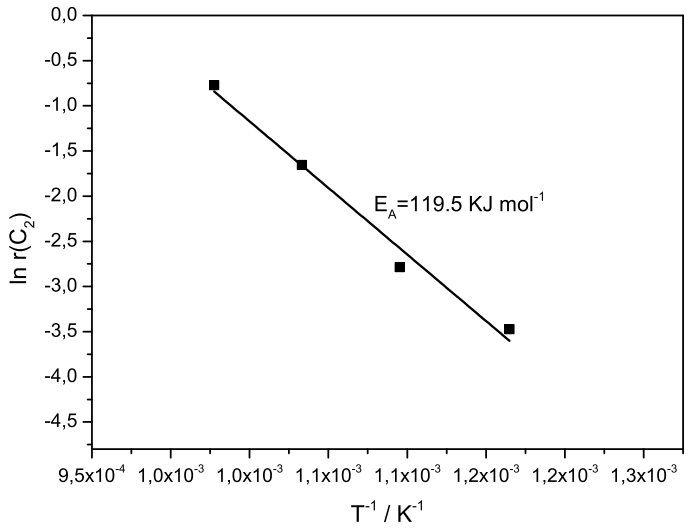

Figure 46.: Determination of activation energy of OCM over LiKCl/MgDyO

The value of approx. 120 kJ/mol for OCM is very similar to the value for ethane ODH over the same catalyst (approx. 130 kJ/mol as reported in chapter 2). This trend clearly confirms the similar bond dissociation energies of both components. Additionally, it suggests that the same active site is responsible for the activation of the first C-H bond in both molecules. Similarly to ODH, several authors have suggested lithium containing sites as active centers.[199] Thus, another Li-free eutectic system (Na-Cs-Cl in eutectic composition, mp = 486°C) was checked for suitability of OCM. As depicted in Figure 5 and Figure 6, a Li-free system is also active and selective for OCM. However, the C_2-selectivities are around 10%-20% below the ones for the Li-containing system, but maximum C_2-yields of 20% can be reached.

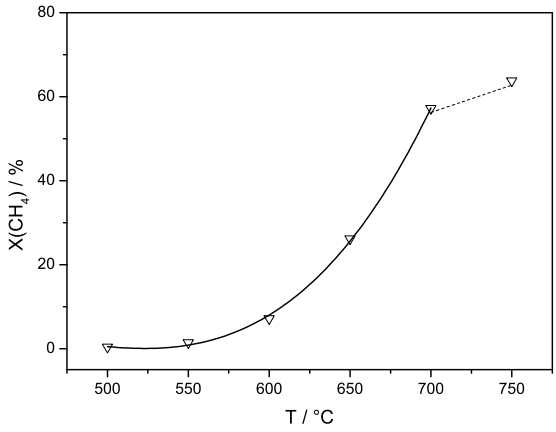

(a)

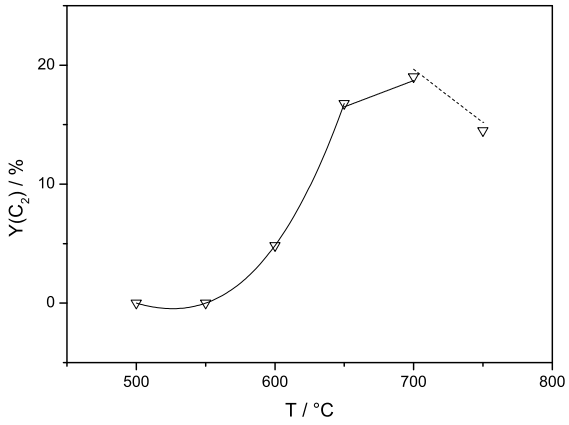

(b)

Figure 47.: Methane conversions (a) and C_2-yields (b); NaCsCl, WHSV = 0.7 h^{-1}, p_{ges} = 1 bar, $p_{Methane}$ = 70 mbar, $\triangledown$: p_{Oxygen} = 70 mbar

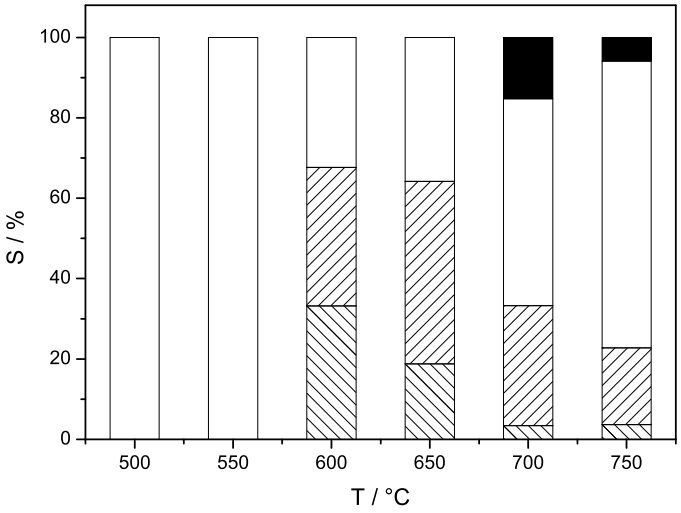

Figure 48.: Product selectivies (NaCcCl, WHSV = 0.7 h^{-1},p_{ges}= 1 bar, $p_{Methane}$ = p_{Oxygen}= 70 mbar; white: CO_2, black: CO, /: ethene, \: ethane

However, it could clearly be shown that no Li is necessary for a good OCM performance. Thus, the catalytic activity for OCM cannot be related to lithium oxides in supported alkali chloride systems. Similarly to ethane ODH using those systems, an anionic O-Cl species (i.e. hypochlorite) is suggested to be catalytically active. To further prove this concept and to further elucidate the mechanism of methane OCM by addressing the influence of gas-phase oxygen and by studying the consecutive reaction steps from methane towards ethylene, a step experiment with subsequent dosing of both reactants was performed. The step response of the oxygen-loaded catalyst after methane exposure as depicted in Figure 49 shows a significant formation of ethane, persisting approx. 30 minutes.

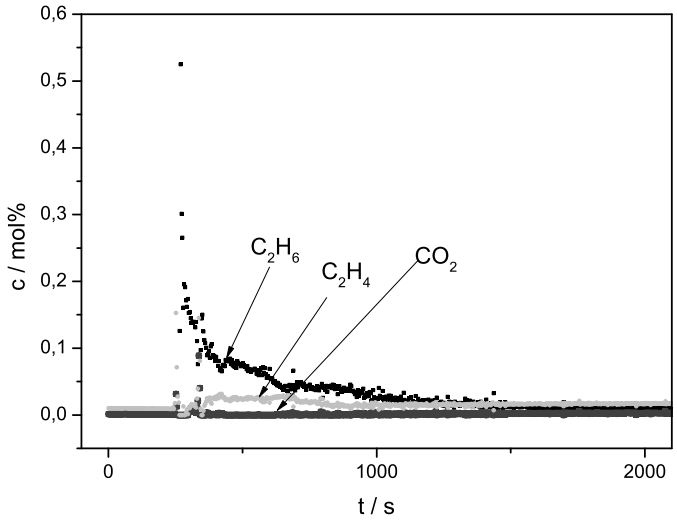

Figure 49.: OCM step experiment with LiKCl/MgDyO at 650°C

After an induction period, additionally the formation of ethylene can be observed, however in lower concentrations compared to ethane. This is another proof for ethane being the primary reaction product. Those results furthermore link the catalytic activity for OCM and stored O-Cl species, which efficiently catalyze the coupling of methane towards ethane. As those species are also known to efficiently catalyze the oxidative dehydrogenation of ethane with outstanding selectivities, the subsequent formation of ethylene can be explained as well. Interestingly, the stored O-Cl species show an ideal selectivity towards C_2-products, as no CO_2 can be detected in the step experiment. Thus it can be followed that the active O-Cl species do not catalyze the total oxidation of methane, ethane or ethylene. Total oxidation can thus only be initiated by gas-phase oxygen. To further confirm the sequence of the different products, Figure 50 shows the step responses of a different experiment in which the catalyst was heated up in He to the reaction temperature, followed by an abrupt dosing of both reactants.

At 650°C, ethene is the first product to be detected, the concentration of ethane is only marginal. After a short induction time (approx. 25 s), the total oxidation product CO_2 can be detected, suggesting that the major part of this undesired product is formed via the combustion of ethene. A similar behavior can be detected for the experiment with 700°C as reaction temperature. However, the step response of oxygen differs for the previous experiment. Its concentration goes through a maximum, followed by a decay before reaching an asymptotic value. The decrease in oxygen after reaching its maximum concentration starts simultaneously with the increase in the CO_2 concentration. Thus, the initiation of total oxidation can be clearly attributed to the availability of gas-phase

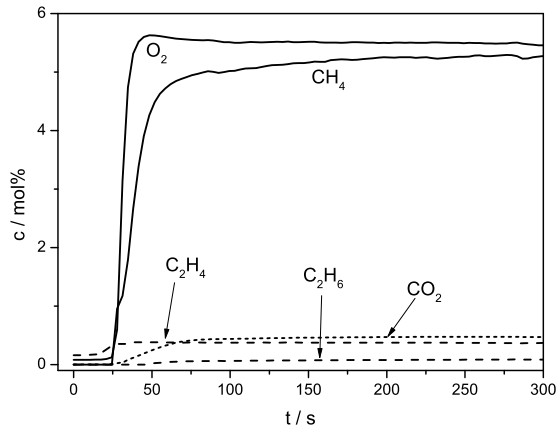

(a)

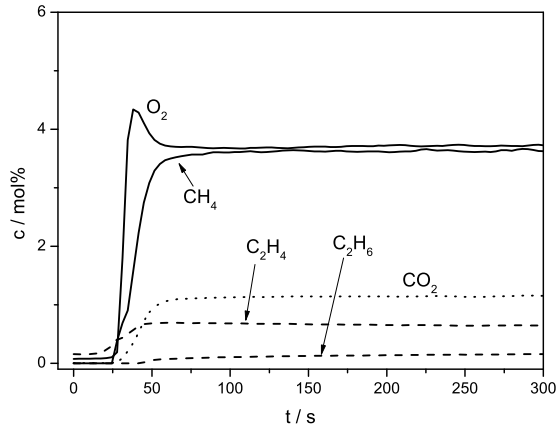

(b)

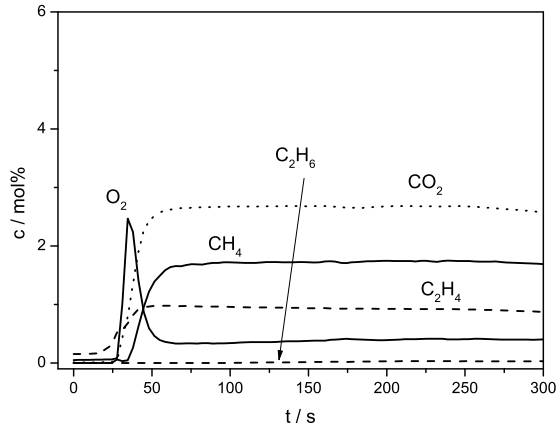

(c)

Figure 50.: Step experiment with reaction mixture (7% O_2 and 7% methane diluted in He); (a): 650°C; (b):700°C; (c):750°C

oxygen. The maximum peak of O_2 becomes even more dominant at 750°C, where CO_2 is the main product in the outlet stream.

5.4. Summary and conclusion

Supported alkali chlorides seem to be a very attractive system for the oxidative coupling of methane. C_2-yields of over 30% are definitively possible with those systems, thus being among the best catalysts reported for OCM. Similarly to the oxidative dehydrogenation of ethane (see chapter 2), oxygen-chlorine species (i.e. hypochlorite) are supposed to be formed transiently at the surface of the support, diffuse through the melt and react with methane at the surface of the melt, spontaneously abstracting one hydrogen atom (see chapter 2). The similar activation energies suggest an identical activation of the first C-H bond in both methane and ethane. The good performance is based on the highly selective redox potential of oxidized chloride anions. A molten chloride layer is the common feature of both studied systems, thus the catalytically active site has to be related to these anions. The alkali chloride cations present in the melt influence activity and selectivity, but lithium can be excluded to be essential for the OCM reaction. Thus, this catalyst is a new system for OCM compared to the ones already reported in literature, where Li is mostly incorporated in the MgO lattice.[142] It has been shown that ethane is the primary coupling product, which is in good accordance with recent literature.[208] As this catalyst system is also known to show excellent properties for the oxidative dehydrogenation of ethane, part of the formed ethane is converted via oxidative dehydrogenation to ethene. Thus, this class of catalysts is capable of activating the C-H bond in methane and ethane, which is an excellent candidate to selectively produce ethene from natural gas which contains methane and ethane.

6. Summary and Conclusions

6.1. Summary

Ethane ODH is an industrially promising reaction to selectively produce ethene. Compared to steam cracking, a narrow product spectrum can be obtained (only CO, CO_2 and methane in traces, however no aromatics), and the temperature window of the reaction is comparatively low.
Several different catalyst systems catalyze ODH efficiently: Vanadia based systems, rare earth oxides, alkali oxides and supported alkali chlorides. All those catalyst systems work via different mechanisms: Both radical and redox processes can be involved in ODH over different catalysts. Optimization in ethane ODH in has not only been performed by tailoring new catalysts, also the reactor configuration plays a key role, as membrane reactors or reactors with a very short contact time could lead to substantial improvements compared to conventional plug flow reactors.
Supported alkali chloride catalysts have been subject of this thesis, as they convince with very high olefin selectivities. Those catalysts consist of a solid support and an alkali chloride film, which is molten under reaction conditions. Mechanistically, the ODH reaction proceeds via a Pseudo-Mars-van-Krevelen reaction mechanism, as the reaction can be separated in an oxidation and reduction step. Oxygen from the gas phase is absorbed into the melt and is transformed into catalytically active oxygen-chlorine species at the interface between support and melt via the oxidation of chloride. The formed intermediates diffuse back to the interface between melt and gas phase, where they catalyze ethane ODH towards ethene, while the intermediate is simultaneously reduced. In contrast to oxygen, ethane cannot be solved in the melt, thus ethane is not exposed to the oxidation site. The shielding chloride layer nearly prevents total oxidation of ethane and ethene at the defect sites on the support, resulting in very high olefin selectivities. Interestingly, the oxygen activation step has been found to be rate determining. SSTIKA studies revealed that ODH proceeds via a bulk species stored in the liquid melt, via total oxidation reactions proceed via a different pathway.
Kinetically, it could be shown that ethane ODH over supported alkali chloride catalysts can be described with a Mars-van-Krevelen type equation. The reaction order of water and CO_2 is zero, thus the presence of those molecules in the reactor does not

influence ODH performance. Regarding the side reactions (total oxidation towards CO and CO_2), it could be shown that those products are both formed from ethane and ethene. However, the reactivitiy of ethane in those side reactions is slightly higher compared to ethene. ODH and its side reactions could be fitted via a complex reaction network using a plug flow reactor model. ODH of ethane was described with a Pseudo Mars-van-Krevelen approach, while the side reactions were described with power-law rate equations.

Many variables exist in tayloring new supported alkali chloride catalysts, as both support and the overlayer material can be varied. The support material both has to be stable against solid state reaction with chloride and has to have enough oxygen defect sites to efficiently form enough intermediate species. Regarding the overlayer, high selectivities can only be achieved if the overlayer is molten under reaction conditions. Mechanistically, this can be explained with the fact that the overlayer stores the catalytically active intermediates. Furthermore, a dynamically rearranging surface prevents the readsorption of ethene on metal cations, which would lead to enhanced total oxidation rates. The rate of the rearrangement of the molten film depends on its composition, the rate of the rearrangement is faster or slower. Thus, the overlayer composition influences the rate of total oxidation of ethane and ethene, thereby tuning the olefin selectivity. In this work, catalysts with extraordinarily high olefin selectivities (over 97%) could be tailored.

Finally, supported alkali chloride catalysts have been shown to be suitable for the Oxidative Coupling of Methane (OCM) as well. For this reaction, a temperature window between 700°C and 750°C was necessary to obtain reasonable C_2-yields over LiKCl/MgO + Dy_2O_3 as model catalyst. C_2-yields around 30% were attainable. Mechanistically, OCM over supported alkali chloride catalysts is also based on the highly selective redox potential of oxidized chloride anions stored in the liquid melt. Lithium, as claimed in literature, can be excluded to be the crucial element of an OCM catalyst, as a Li-free eutectic system works well for OCM as well. It has also be shown that ethane is the primary coupling product in the OCM reaction. As supported alkali chloride catalysts are excellent candidates for the oxidative dehydrogenation of ethane as well, ethene is a secondary product, generated via ODH. Regarding OCM and ODH, supproted alakli chloride catalysts are bi-functional ones, as they can perform both reactions.

Future work could include a detailed characterization of a supported alkali chloride catalyst under reaction conditions, aiming on the in-situ monitoring of the generation of the catalytically active sites. From a reaction engineering site, the yield of ODH and OCM could be optimized by using different reactor systems, i.e. reactors with staged feed of oxygen or even membrane reactors.

6.2. Zusammenfassung

Die oxidative Dehydrierung von Ethan (ODH) ist eine für die Industrie relevante Reaktion, um Ethen selektiv herzustellen. Im Vergleich zum *steam cracking* entstehen wenige Nebenprodukte (nur CO und CO_2 sowie Methan in Spuren, jedoch keine Aromaten), und die Reaktionstemperatur ist vergleichsveise gering.
In der Literatur sind verschiedene für die oxidative Dehydrierung von Ethane geeignete Katalysatorsysteme bekannt: Vanadium-basierte Systeme, Oxide von seltenen Erden, Alkalimetalloxide sowie geträgerte Alkalimetallchloride. Alle Katalysatorsysteme basieren auf unterschiedlichen Reaktionsmechanismen: Sowie Radikalmechanismen als auch Redoxprozesse sind für die ODH möglich. Eine Optimierung der Reaktion konnte nicht nur durch Modifikationen an den Katalysatoren, sondern auch durch reaktionstechnische Massnahmen wie dem Einsatz spezieller Reaktoren, wie z.B. Membranreaktoren sowie Reaktoren mit einer sehr kurzen Kontaktzeit, erzielt werden, welche im Vergleich mit herkömmlichen Rohrreaktoren eine deutliche Verbesserung darstellen konnten.
Gegenstand dieser Arbeit sind geträgerte Alkalimetallkatalysatoren, welche durch sehr hohe Olefinselektivität überzeugen konnten. Diese zeichnen sich dadurch aus, dass unter Reaktionsbedingungen ein geschmolzener Alkalimetallchloridfilm auf einem festen Träger vorliegt. Was den Reaktionsmechanismus betrifft, läuft die ODH nach einem modifizierten Mars-van-Krevelen-Mechanismus ab, da die Reaktion in einen Oxidations- und Reduktionsschritt unterteilt werden kann. Sauerstoff aus der Gasphase wird in die Schmelze absorbiert. An der Grenzfläche von festem Träger und Schmelze wird der Sauerstoff durch Oxidation von Chlorid zu einer katalytisch aktiven Sauerstoff-Chlor-Spezies umgewandelt. Das gebildete Intermediat diffundiert zurück zur Grenzfläche von Schmelze und Gasphase, wo es die ODH von Ethan zu Ethen katalysiert, wobei das Intermediat gleichzeitig reduziert wird. Im Gegensatz zu Sauerstoff kann sich Ethan nicht in der Gasphase lösen, daher kommt Ethan mit dem Oxidationszentrum nicht in Kontakt. Die schützende Chloridschicht unterdrückt die Totaloxidation von Ethan und Ethen and den Fehlstellen des Trägers fast komplett, was zu sehr hohen Olefinselektivitäten führt.
Interessanterweise ist der Sauerstoffaktivierungsschritt ratenbestimmend. SSTIKA-Erperimente haben zudem gezeigt, dass die ODH über eine Spezies, welche in der Schmelze gespeichert ist, abläuft, während die Totaloxidationsreaktionen über einen anderen Reaktionspfad abläuft.
Bezüglich der Kinetik konnte gezeigt werden, dass die oxidative Dehydrierung von Ethan mit einer Mars-Van-Krevelen-Gleichung beschrieben werden kann. Die Reaktionsordnung oder ODH bezüglich Wasser und CO_2 ist null, daher beeinflusset die Anwesenheit beider Moleküle die Reaktionsgeschwindigkeit der ODH nicht. Was die

Nebenreaktionen (Totaloxidation zu CO und CO_2) anbetrifft, konnte gezeigt werden, dass sich diese Produkte sowohl aus Ethan wie auch Ethen bilden können. Jedoch ist die Reaktivität von Ethan in diesen Nebenreaktionen geringfügig höher als die von Ethen. Die ODH und deren Nebenreaktionen konnten mit einem komplexen Reaktionsnetzwerk unter Verwendung eines Rohhreaktormedells beschrieben werden. Während die oxidative Dehydrierung mit einem Pseudo Mars-van-Krevelen-Ansatz beschrieben wurden, wurden die Nebenreaktionen mit einem Exponentialansatz beschrieben.
Bei der Entwicklung neuer Katalysatoren existieren viele Freiheitsgrade, da sowohl die Zusammensetzung des Trägers als auch des Alkalichlorid-Films verändert werden können. Der Träger muss gegenüber einer Festkörperreaktion mit Chlorid stabil sein und muss genügend Sauerstofffehlstellen besitzen, um genug Intermediat bilden zu können. Was den Chloridfilm anbetrifft können hohe Olefinselektivitäten nur dann erzielt werden, wenn dieser Film unter Reaktionsbedingungen in geschmolzenem Zustand vorliegt. In mechanistischer Hinsicht kan dies damit erklärt werden, dass dieser Film die katalytisch aktiven Intermediate speichert. Des weiteren verhindert eine sich dynamisch neu anordnende Oberfläche die Re-Adsorption von Ethen auf Metallkationen, was zu verstärkter Totaloxidation führen würde. Je nach Zusammensetzung des Chloridfilms ist die Rate der Neuanordnung schneller oder langsamer. Daher beeinflusst die Filmzusammensetzung die Rate der Totaloxidation von Ethan und Ethen, welche wiederum die Olefinselektivität beeinflussen. In der vorliegenden Arbeit konnten Katalysatoren mit erstaunlich hoher Olefinselektivität (über 97%) entwickelt werden.
Es konnte ebenfalls gezeigt werden, dass geträgerte Alkalimetallchloridkatalysatoren für die oxidative Kupplung von Methan (OCM) ebenfalls geeignet sind. Für diese Reaktion war ein Temperaturfenster zwischen 700°C und 750°C notwendig, um annehmbare C_2-Ausbeuten bei Verwendung eines LiKCl/MgO + Dy_2O_3-Modellkatalysators zu erreichen. C_2-Ausbeuten von ca. 30% konnten erreicht werden. In mechanistischer Hinsicht basiert die oxidative Kupplung von Methan über geträgerten Alkalimetallchloridkatalysatoren ebenfalls auf dem hochselektiven Redoxpotential von oxidierter Chloridanionen, welche in der flüssigen Schmelze gespeichert sind. Jedoch kann ausgeschlossen werden, dass Lithium, wie in einschlägiger Literatur beschrieben, das entscheidende Element eines OCM-Katalysators ist, da lithium-freie Chloridsysteme ebenfalls für die OCM funktionieren. Ebenfalls konnte gezeigt werden, dass Ethan das primäre Kupplungsprodukt der OCM-Reaktion ist. Da geträgerte Alkalimetallchloride exzellente ODH-Katalysatoren sind, ist Ethen ein sekundäres Produkt, welches durch die oxidative Dehydrierung von Ethan gebildet wird. Somit sind geträgerte Alkalimetallchloride bifunktionale Katalysatoren, welche sowohl ODH als auch OCM katalysieren.
Künftige Arbeiten könnten eine detaillierte Charakterisierung eines geträgerten

Aklalimetallkatalysators unter Reaktionsbedingungen beinhalten mit dem Ziel, die Bildung der katalytisch aktiven Intemrediate in-situ zu messen. Von einer reaktionstechnischen Seiten könnte die Ethenausbeute bei ODH und OCM durch Verwendung von verschiedenen Reaktorsystemen, z.B. Reaktoren mit stufenweiser Sauerstoffzufuhr oder Membranreaktoren, optimiert werden.

Bibliography

[1] H. Zimmermann, R. Walzl, Ethylene, in: Ullmann's Encyclopedia of Industrial Chemistry, Wiley-VCH Verlag GmbH & Co. KGaA, Weinheim, 2000.

[2] M. A. Banares, Supported metal oxide and other catalysts for ethane conversion: a review, Catalysis Today 51 (2) (1999) 319–348.

[3] F. Cavani, F. Trifiro, The oxidative dehydrogenation of ethane and propane as an alternative way for the production of light olefins, Catalysis Today 24 (3) (1995) 307–313.

[4] F. Cavani, F. Trifiro, Selective oxidation of light alkanes: interaction between the catalyst and the gas phase on different classes of catalytic materials, Catalysis Today 51 (3-4) (1999) 561–580.

[5] E. A. Mamedov, V. Cortes Corberan, Oxidative dehydrogenation of lower alkanes on vanadium oxide-based catalysts. The present state of the art and outlooks, Applied Catalysis A: General 127 (1995) 1–40.

[6] F. Cavani, N. Ballarini, A. Cericola, Oxidative dehydrogenation of ethane and propane: How far from commercial implementation?, Catalysis Today 127 (1-4) (2007) 113.

[7] H. H. Kung, D. Eley, H. Pines, W. O. Haag, Oxidative Dehydrogenation of Light (C_2 to C_4) Alkanes, in: Advances in Catalysis, Vol. Volume 40, Academic Press, 1994, pp. 1–38.

[8] A. S. Bodke, D. A. Olschki, L. D. Schmidt, E. Ranzi, High Selectivities to Ethylene by Partial Oxidation of Ethane, Science 285 (5428) (1999) 712–715.

[9] M. M. Bhasin, J. H. McCain, B. V. Vora, T. Imai, P. R. Pujado, Dehydrogenation and oxydehydrogenation of paraffins to olefins, Applied Catalysis A: General 221 (1-2) (2001) 397–419.

[10] F. M. Ashmawy, Catalytic dehydrogenation of propane on chromia, palladium and platinum supported catalysts, Journal of Applied Chemistry and Biotechnology 27 (1) (1977) 137–142.

[11] J. D. Arndt, S. Freyer, R. Geier, O. Machhammer, J. Schwartze, M. Volland, R. Diercks, Rohstoffwandel in der chemischen Industrie, Chemie Ingenieur Technik 79 (5) (2007) 521–528.

[12] M. Stöcker, Biofuels and Biomass-To-Liquid Fuels in the Biorefinery: Catalytic Conversion of Lignocellulosic Biomass using Porous Materials, Angewandte Chemie International Edition 47 (48) (2008) 9200–9211.

[13] G. W. Huber, S. Iborra, A. Corma, Synthesis of Transportation Fuels from Biomass: Chemistry, Catalysts, and Engineering, Chemical Reviews 106 (9) (2006) 4044–4098.

[14] S. Golay, R. Doepper, A. Renken, In-situ characterisation of the surface intermediates for the ethanol dehydration reaction over γ-alumina under dynamic conditions, Applied Catalysis A: General 172 (1) (1998) 97–106.

[15] I. Takahara, M. Saito, M. Inaba, K. Murata, Dehydration of Ethanol into Ethylene over Solid Acid Catalysts, Catalysis Letters 105 (3) (2005) 249–252.

[16] E. Heracleous, A. A. Lemonidou, Ni-Nb-O mixed oxides as highly active and selective catalysts for ethene production via ethane oxidative dehydrogenation. Part I: Characterization and catalytic performance, J. Catal. 237 (1) (2006) 162–174.

[17] J. A. Lercher, F. N. Naraschewski, C-H Activation of Alkanes in Selective Oxidation Reactions on Solid Oxide Catalysts, in: C. Hess, R. Schlögl (Eds.), Nanostructured Catalysts - Selective Oxidations, RSC Nanoscience & Nanotechnology, Royal Society of Chemistry, Cambridge, 2011, pp. 5–32.

[18] T. Xie, K. B. McAuley, J. C. C. Hsu, D. W. Bacon, Gas Phase Ethylene Polymerization: Production Processes, Polymer Properties, and Reactor Modeling, Industrial & Engineering Chemistry Research 33 (3) (1994) 449–479.

[19] S. Fuchs, L. Leveles, K. Seshan, L. Lefferts, A. Lemonidou, J. Lercher, Oxidative dehydrogenation and cracking of ethane and propane over LiDyMg mixed oxides, Topics in Catalysis 15 (2-4) (2001) 169–174.

[20] K. Chen, S. Xie, A. T. Bell, E. Iglesia, Structure and Properties of Oxidative Dehydrogenation Catalysts Based on MoO_3/Al_2O_3, Journal of Catalysis 198 (2) (2001) 232–242.

[21] P. Viparelli, P. Ciambelli, L. Lisi, G. Ruoppolo, G. Russo, J. C. Volta, Oxidative dehydrogenation of propane over vanadium and niobium oxides supported catalysts, Applied Catalysis A: General 184 (2) (1999) 291–301.

[22] C. Batiot, B. K. Hodnett, The role of reactant and product bond energies in determining limitations to selective catalytic oxidations, Applied Catalysis A: General 137 (1) (1996) 179–191.

[23] S. Albonetti, F. Cavani, F. Trifiro, Key Aspects of Catalyst Design for the Selective Oxidation of Paraffins, Catalysis Reviews 38 (4) (1996) 413–438.

[24] R. Grabowski, Kinetics of Oxidative Dehydrogenation of C_2-C_3 Alkanes on Oxide Catalysts, Catalysis Reviews 48 (2) (2006) 199–268.

[25] J.-A. Dalmon, A. Cruz-Lopez, D. Farrusseng, N. Guilhaume, E. Iojoiu, J.-C. Jalibert, S. Miachon, C. Mirodatos, A. Pantazidis, M. Rebeilleau-Dassonneville, Y. Schuurman, A. C. van Veen, Oxidation in catalytic membrane reactors, Appl. Catal., A 325 (2) (2007) 198–204.

[26] M. Rebeilleau-Dassonneville, S. Rosini, A. C. van Veen, D. Farrusseng, C. Mirodatos, Oxidative activation of ethane on catalytic modified dense ionic oxygen conducting membranes, Catal. Today 104 (2-4) (2005) 131–137.

[27] F. Khorasheh, M. R. Gray, High-pressure thermal cracking of n-hexadecane, Industrial & Engineering Chemistry Research 32 (9) (1993) 1853–1863.

[28] P. Ciambelli, L. Lisi, R. Pirone, G. Ruoppolo, G. Russo, Comparison of behaviour of rare earth containing catalysts in the oxidative dehydrogenation of ethane, Catalysis Today 61 (1-4) (2000) 317–323.

[29] S. Gaab, J. Find, R. K. Grasselli, J. A. Lercher, X. Bao, X. Yide, Oxidative ethane activation over oxide supported molten alkali metal chloride catalysts, in: Studies in Surface Science and Catalysis, Vol. Volume 147, Elsevier, 2004, pp. 673–678.

[30] S. Gaab, J. Find, T. E. Mueller, J. A. Lercher, Kinetics and mechanism of the oxidative dehydrogenation of ethane over Li/Dy/Mg/O/(Cl) mixed oxide catalysts, Top. Catal. 46 (1-2) (2007) 101–110.

[31] L. Leveles, K. Seshan, J. A. Lercher, L. Lefferts, Oxidative conversion of propane over lithium-promoted magnesia catalyst. I. Kinetics and mechanism, Journal of Catalysis 218 (2) (2003) 296–306.

[32] L. Leveles, K. Seshan, J. A. Lercher, L. Lefferts, Oxidative conversion of propane over lithium-promoted magnesia catalyst. II. Active site characterization and hydrocarbon activation, Journal of Catalysis 218 (2) (2003) 307–314.

[33] P. Myrach, N. Nilius, S. Levchenko, A. Gonchar, T. Risse, K.-P. Dinse, L. A. Boatner, W. Frandsen, R. Horn, H.-J. Freund, R. Schlögl, M. Scheffler, Temperature-Dependent Morphology, Magnetic and Optical Properties of Li-Doped MgO, ChemCatChem 2 (7) (2010) 854–862.

[34] A. Beretta, P. Forzatti, E. Ranzi, Production of Olefins via Oxidative Dehydrogenation of Propane in Autothermal Conditions, Journal of Catalysis 184 (2) (1999) 469–478.

[35] M. Y. Sinev, V. Y. Bychkov, V. N. Korchak, O. V. Krylov, Oxidative coupling of methane with participation of oxide catalyst lattice oxygen, Catalysis Today 6 (4) (1990) 543–549.

[36] J. Le Bars, A. Auroux, M. Forissier, J. C. Vedrine, Active Sites of V2O5/[gamma]-Al2O3Catalysts in the Oxidative Dehydrogenation of Ethane, Journal of Catalysis 162 (2) (1996) 250–259.

[37] X. Rozanska, J. Sauer, Oxidative conversion of $C_1 - C_3$ alkanes by vanadium oxide catalysts. DFT results and their accuracy, International Journal of Quantum Chemistry 108 (12) (2008) 2223–2229.

[38] Z.-S. Chao, E. Ruckenstein, Noncatalytic and catalytic conversion of ethane over V—Mg oxide catalysts prepared via solid reaction or mesoporous precursors, Journal of Catalysis 222 (1) (2004) 17–31.

[39] E. M. Thorsteinson, T. P. Wilson, F. G. Young, P. H. Kasai, The oxidative dehydrogenation of ethane over catalysts containing mixed oxides of molybdenum and vanadium, Journal of Catalysis 52 (1) (1978) 116–132.

[40] P. Mars, D. W. van Krevelen, Oxidations carried out by means of vanadium oxide catalysts, Chemical Engineering Science 3 (Supplement 1) (1954) 41–59.

[41] M. V. Martinez-Huerta, X. Gao, H. Tian, I. E. Wachs, J. L. G. Fierro, M. A. Banares, Oxidative dehydrogenation of ethane to ethylene over alumina-supported vanadium oxide catalysts: Relationship between molecular structures and chemical reactivity, Catalysis Today 118 (3-4) (2006) 279–287.

[42] J. Le Bars, J. C. Vedrine, A. Auroux, S. Trautmann, M. Baerns, Microcalorimetric and infrared studies of the acid-base properties of V_2O_5/ γ-Al_2O_3 catalysts, Applied Catalysis A: General 119 (2) (1994) 341–354.

[43] T. Blasco, J. M. Lopez Nieto, Oxidative dyhydrogenation of short chain alkanes on supported vanadium oxide catalysts, Applied Catalysis A: General 157 (1-2) (1997) 117–142.

[44] J. M. Lopez Nieto, A. Dejoz, M. I. Vazquez, W. O'Leary, J. Cunningham, Oxidative dehydrogenation of n-butane on MgO-supported vanadium oxide catalysts, Catalysis Today 40 (2-3) (1998) 215–228.

[45] M. A. Banares, M. V. Martinez-Huerta, X. Gao, J. L. G. Fierro, I. E. Wachs, Dynamic behavior of supported vanadia catalysts in the selective oxidation of ethane: In situ Raman, UV-Vis DRS and reactivity studies, Catalysis Today 61 (1-4) (2000) 295–301.

[46] K. Chen, A. T. Bell, E. Iglesia, The Relationship between the Electronic and Redox Properties of Dispersed Metal Oxides and Their Turnover Rates in Oxidative Dehydrogenation Reactions, Journal of Catalysis 209 (1) (2002) 35 – 42.

[47] G. Centi, F. Trifiro, J. R. Ebner, V. M. Franchetti, Mechanistic aspects of maleic anhydride synthesis from C_4 hydrocarbons over phosphorus vanadium oxide, Chemical Reviews 88 (1) (1988) 55.

[48] A. E. Schweizer, M. E. Jones, D. A. Hickman, Oxidative halogenation of C_1 hydrocarbons to halogenated C_1 hydrocarbons and integrated processes related thereto, US Patent US 6,452,058 B1 (2002).

[49] A. E. Schweizer, M. E. Jones, D. A. Hickman, Oxidative halogenation and optinal dehydrogenation of C_3-hydrocarbons, US Patent US 6,984,763 B2 (2006).

[50] A. E. Schweizer, M. E. Jones, D. A. Hickman, Oxidative halogenation of C_1 hydrocarbons to halogenated C_1 hydrocrabons and integrated processes related thereto, European Patent EP1395536 (2007).

[51] C. Kumar, S. Gaab, T. Müller, J. Lercher, Oxidative Dehydrogenation of Light Alkanes on Supported Molten Alkali Metal Chloride Catalysts, Top. Catal. 50 (1) (2008) 156–167.

[52] M. P. Woods, B. Mirkelamoglu, U. S. Ozkan, Oxygen and Nitrous Oxide as Oxidants: Implications for Ethane Oxidative Dehydrogenation over Silica-Titania-Supported Molybdenum, Journal of Physical Chemistry C 113 (23) (2009) 10112–10119.

[53] M.-J. Cheng, K. Chenoweth, J. Oxgaard, A. van Duin, W. A. Goddard, Single-Site Vanadyl Activation, Functionalization, and Reoxidation Reaction Mechanism for Propane Oxidative Dehydrogenation on the Cubic V_4O_{10} Cluster, The Journal of Physical Chemistry C 111 (13) (2007) 5115–5127.

[54] C. Hess, Highly Dispersed Vanadium Oxide Catalysts, in: C. Hess, R. Schlögl (Eds.), Nanostructured Catalysts - Selective Oxidations, RSC Nanoscience & Nanotechnology, Royal Society of Chemistry, Cambridge, 2011, pp. 299–325.

[55] J. E. Molinari, I. E. Wachs, Presence of Surface Vanadium Peroxo-oxo Umbrella Structures in Supported Vanadium Oxide Catalysts: Fact or Fiction?, Journal of the American Chemical Society 132 (36) (2010) 12559–12561.

[56] X. Rozanska, E. V. Kondratenko, J. Sauer, Oxidative dehydrogenation of propane: Differences between N_2O and O_2 in the reoxidation of reduced vanadia sites and consequences for selectivity, Journal of Catalysis 256 (1) (2008) 84 – 94.

[57] R. K. Grasselli, Fundamental Principles of Selective Heterogeneous Oxidation Catalysis, Topics in Catalysis 21 (1-3) (2002) 79–88.

[58] P. Concepcion, A. Galli, J. M. L. Nieto, A. Dejoz, M. I. Vazquez, On the influence of the acid-base character of catalysts on the oxidative dehydrogenation of alkanes, Top. Catal. 3 (3,4) (1996) 451–460.

[59] O. R. Evans, A. T. Bell, T. D. Tilley, Oxidative dehydrogenation of propane over vanadia-based catalysts supported on high-surface-area mesoporous $MgAl_2O_4$, Journal of Catalysis 226 (2) (2004) 292.

[60] J. L. Callahan, R. K. Grasselli, A selectivity factor in vapor-phase hydrocarbon oxidation catalysis, AIChE Journal 9 (6) (1963) 755–760.

[61] H. Dai, A. T. Bell, E. Iglesia, Effects of molybdena on the catalytic properties of vanadia domains supported on alumina for oxidative dehydrogenation of propane, Journal of Catalysis 221 (2) (2004) 491 – 499.

[62] E. V. Kondratenko, M. Cherian, M. Baerns, D. Su, R. Schlögl, X. Wang, I. E. Wachs, Oxidative dehydrogenation of propane over V/MCM-41 catalysts: comparison of {O2} and {N2O} as oxidants, Journal of Catalysis 234 (1) (2005) 131 – 142. doi:http://dx.doi.org/10.1016/j.jcat.2005.05.025.
URL `http://www.sciencedirect.com/science/article/pii/S0021951705002307`

[63] E. Kondratenko, M. Cherian, M. Baerns, Oxidative dehydrogenation of propane over differently structured vanadia-based catalysts in the presence of O_2 and N_2O, Catalysis Today 112 (1-4) (2006) 60 – 63.

[64] P. Botella, A. Dejoz, J. M. Lopez Nieto, P. Concepcion, M. I. Vazquez, Selective oxidative dehydrogenation of ethane over MoVSbO mixed oxide catalysts, Appl. Catal., A 298 (2006) 16–23.

[65] P. Botella, A. Dejoz, M. C. Abello, M. I. Vazquez, L. Arrua, J. M. Lopez Nieto, Selective oxidation of ethane: Developing an orthorhombic phase in Mo-V-X (X=Nb, Sb, Te) mixed oxides, Catalysis Today 142 (3-4) (2009) 272.

[66] A. Trunschke, Propane-Selective Oxidation to Acrylic Acid, in: C. Hess, R. Schlögl (Eds.), Nanostructured Catalysts - Selective Oxidations, RSC Nanoscience & Nanotechnology, Royal Society of Chemistry, Cambridge, 2011, pp. 299–325.

[67] B. Tope, Y. Zhu, J. A. Lercher, Oxidative dehydrogenation of ethane over Dy_2O_3/MgO supported LiCl containing eutectic chloride catalysts, Catal. Today 123 (1-4) (2007) 113–121.

[68] R. K. Grasselli, Genesis of site isolation and phase cooperation in selective oxidation catalysis, Top. Catal. 15 (2) (2001) 93–101.

[69] R. Schlögl, C. Hess, Characteristics of Selective Oxidation Reactions, in: R. Schlögl, C. Hess (Eds.), Nanostructured Catalysts - Selective Oxidations, Royal Society of Chemistry, Cambridge, 2011, pp. 355–397.

[70] M. D. Argyle, K. Chen, A. T. Bell, E. Iglesia, Ethane Oxidative Dehydrogenation Pathways on Vanadium Oxide Catalysts, The Journal of Physical Chemistry B 106 (21) (2002) 5421–5427.

[71] I. E. Wachs, Recent conceptual advances in the catalysis science of mixed metal oxide catalytic materials, Catalysis Today 100 (1-2) (2005) 79–94.

[72] G. Bergeret, P. Gallezot, K. V. R. Chary, B. R. Rao, V. S. Subrahmanyam, Structure of monolayer type vanadium pentoxide, supported on γ-alumina, Applied Catalysis 40 (1988) 191–196.

[73] J. Haber, A. Kozlowska, R. Kozlowski, The structure and redox properties of vanadium oxide surface compounds, Journal of Catalysis 102 (1) (1986) 52–63.

[74] H. Tian, E. I. Ross, I. E. Wachs, Quantitative Determination of the Speciation of Surface Vanadium Oxides and Their Catalytic Activity, The Journal of Physical Chemistry B 110 (19) (2006) 9593–9600.

[75] X. Gao, M. A. Banares, I. E. Wachs, Ethane and n-Butane Oxidation over Supported Vanadium Oxide Catalysts: An in Situ UV-Visible Diffuse Reflectance Spectroscopic Investigation, Journal of Catalysis 188 (2) (1999) 325–331.

[76] Z. Zhao, X. Gao, I. E. Wachs, Comparative Study of Bulk and Supported V-Mo-Te-Nb-O Mixed Metal Oxide Catalysts for Oxidative Dehydrogenation of Propane to Propylene, The Journal of Physical Chemistry B 107 (26) (2003) 6333–6342.

[77] S. Feyel, D. Schröder, X. Rozanska, J. Sauer, H. Schwarz, Gas-Phase Oxidation of Propane and 1-Butene with $[V_3O_7]^+$: Experiment and Theory in Concert, Angewandte Chemie International Edition 45 (28) (2006) 4677.

[78] S. Feyel, D. Schröder, H. Schwarz, Gas-Phase Oxidation of Isomeric Butenes and Small Alkanes by Vanadium-Oxide and -Hydroxide Cluster Cations, The Journal of Physical Chemistry A 110 (8) (2006) 2647.

[79] A. Klisinska, S. Loridant, B. Grzybowska, J. Stoch, I. Gressel, Effect of additives on properties of V_2O_5/SiO_2 and V_2O_5/MgO catalysts: II. Structure and physicochemical properties of the catalysts and their correlations with oxidative dehydrogenation of propane and ethane, Applied Catalysis A: General 309 (1) (2006) 17–27.

[80] I. E. Wachs, B. M. Weckhuysen, Structure and reactivity of surface vanadium oxide species on oxide supports, Applied Catalysis A: General 157 (1997) 67 – 90.

[81] P. Knotek, L. Capek, R. Bulanek, J. Adam, Vanadium supported on hexagonal mesoporous silica: active and stable catalysts in the oxidative dehydrogenation of alkanes, Topics in Catalysis 45 (1) (2007) 51–55.

[82] A. Klisinska, K. Samson, I. Gressel, B. Grzybowska, Effect of additives on properties of V_2O_5/SiO_2 and V_2O_5/MgO catalysts: I. Oxidative dehydrogenation of propane and ethane, Applied Catalysis A: General 309 (1) (2006) 10–16.

[83] F. Cavani, G. Centi, F. Trifiro, R. K. Grasselli, A dynamic approach to selectivity in heterogeneous partial oxidation, Catalysis Today 3 (2-3) (1988) 185–198.

[84] A. Galli, J. M. Lopez Nieto, A. Dejoz, M. I. Vazquez, The effect of potassium on the selective oxidation of n-butane and ethane over Al_2O_3-supported vanadia catalysts, Catal. Lett. 34 (1,2) (1995) 51–8.

[85] P. Concepcion, T. Blasco, J. M. Lopez Nieto, A. Vidal-Moya, A. Martinez-Arias, Preparation, characterization and reactivity of V- and/or Co-containing AlPO-18 materials (VCoAPO-18) in the oxidative dehydrogenation of ethane, Microporous Mesoporous Mater. 67 (2-3) (2004) 215–227.

[86] P. Concepcion, A. Corma, J. M. L. Nieto, J. Perez-Pariente, Selective oxidation of hydrocarbons on V- and/or Co-containing aluminophosphate (MeAPO-5) using molecular oxygen, Appl. Catal., A 143 (1) (1996) 17–28.

[87] P. Concepcion, J. M. Lopez Nieto, J. Perez-Pariente, Oxidative dehydrogenation of ethane on a magnesium-vanadium aluminophosphate (MgVAPO-5) catalyst, Catalysis Letters 28 (1) (1994) 9–15.

[88] D. B. Akolekar, Catalytic Properties and Deactivation Behavior of Crystalline Microporous MAPO-36, Journal of Catalysis 144 (1) (1993) 148–159.

[89] P. Concepcion, J. M. Lopez Nieto, J. Perez-Pariente, The selective oxidative dehydrogenation of propane on vanadium aluminophosphate catalysts, Catalysis Letters 19 (4) (1993) 333–337.

[90] B. Solsona, T. Blasco, J. M. Lopez Nieto, M. L. Pena, F. Rey, A. Vidal-Moya, Vanadium Oxide Supported on Mesoporous MCM-41 as Selective Catalysts in the Oxidative Dehydrogenation of Alkanes, Journal of Catalysis 203 (2) (2001) 443–452.

[91] P. Concepcion, J. M. Lopez Nieto, A. Mifsud, J. Perez-Pariente, Synthesis, characterization and catalytic properties of microporous MgVAPO-5, Applied Catalysis A: General 151 (2) (1997) 373–392.

[92] T. Blasco, L. Fernandez, A. Martinez-Arias, M. Sanchez-Sanchez, P. Concepcion, J. M. Lopez Nieto, Magnetic resonance studies on V-containing, and V,Mg-containing AFI aluminophosphates, Microporous and Mesoporous Materials 39 (1-2) (2000) 219–228.

[93] P. M. Michalakos, M. C. Kung, I. Jahan, H. Kung, Selectivity Patterns in Alkane Oxidation over $Mg_3(VO_4)_2$-MgO, $Mg_2V_2O_7$, and $(VO)_2P_2O_7$, Journal of Catalysis 140 (1) (1993) 226–242.

[94] P. Ciambelli, P. Galli, L. Lisi, M. A. Massucci, P. Patrono, R. Pirone, G. Ruoppolo, G. Russo, TiO_2 supported vanadyl phosphate as catalyst for oxidative dehydrogenation of ethane to ethylene, Applied Catalysis A: General 203 (1) (2000) 133–142.

[95] B. Solsona, A. Dejoz, T. Garcia, P. Concepcion, J. M. L. Nieto, M. I. Vazquez, M. T. Navarro, Molybdenum-vanadium supported on mesoporous alumina catalysts for the oxidative dehydrogenation of ethane, Catal. Today 117 (1-3) (2006) 228–233.

[96] M. C. Abello, M. F. Gomez, O. Ferretti, $Mo/\gamma - Al_2O_3$ catalysts for the oxidative dehydrogenation of propane.: Effect of Mo loading, Applied Catalysis A: General 207 (1-2) (2001) 421–431.

[97] E. Heracleous, M. Machli, A. A. Lemonidou, I. A. Vasalos, Oxidative dehydrogenation of ethane and propane over vanadia and molybdena supported catalysts, J. Mol. Catal. A: Chem. 232 (1-2) (2005) 29–39.

[98] E. Heracleous, A. A. Lemonidou, J. A. Lercher, Mechanistic features of the ethane oxidative dehydrogenation by in situ FTIR spectroscopy over a MoO_3/Al_2O_3 catalyst, Appl. Cat. A 264 (1) (2004) 73.

[99] A. Christodoulakis, E. Heracleous, A. A. Lemonidou, S. Boghosian, An operando Raman study of structure and reactivity of alumina-supported molybdenum oxide catalysts for the oxidative dehydrogenation of ethane, Journal of Catalysis 242 (1) (2006) 16.

[100] R. B. Watson, U. S. Ozkan, K/Mo Catalysts Supported over Sol-Gel Silica-Titania Mixed Oxides in the Oxidative Dehydrogenation of Propane, Journal of Catalysis 191 (1) (2000) 12–29.

[101] R. B. Watson, U. S. Ozkan, Mo Loading Effects over Mo/Si: Ti Catalysts in the Oxidative Dehydrogenation of Ethane, Journal of Catalysis 208 (1) (2002) 124–138.

[102] R. B. Watson, U. S. Ozkan, Propane and propylene adsorption effects over MoOx-based catalysts induced by low levels of alkali doping, Journal of Molecular Catalysis A: Chemical 194 (1-2) (2003) 115–135.

[103] R. B. Watson, S. L. Lashbrook, U. S. Ozkan, Chlorine modification of Mo/silica-titania mixed-oxide catalysts for the oxidative dehydrogenation of ethane, Journal of Molecular Catalysis A: Chemical 208 (1-2) (2004) 233–244.

[104] C. Liu, U. S. Ozkan, Effect of chlorine on redox and adsorption characteristics of Mo/Si:Ti catalysts in the oxidative dehydrogenation of ethane, Journal of Molecular Catalysis A: Chemical 220 (1) (2004) 53–65.

[105] C. Liu, S. Ozkan Umit, Spectroscopic and structural characterization of chlorine loading effects on Mo/Si:Ti catalysts in oxidative dehydrogenation of ethane, The journal of physical chemistry. A 109 (6) (2005) 1260–8.

[106] J. M. Lopez Nieto, P. Botella, M. I. Vazquez, A. Dejoz, The selective oxidative dehydrogenation of ethane over hydrothermally synthesised MoVTeNb catalysts, Chemical Communications (17) (2002) 1906.

[107] P. Botella, E. Garcia-Gonzalez, A. Dejoz, J. M. Lopez Nieto, M. I. Vazquez, J. Gonzalez-Calbet, Selective oxidative dehydrogenation of ethane on MoVTeNbO mixed metal oxide catalysts, Journal of Catalysis 225 (2) (2004) 428–438.

[108] T. Konya, T. Katou, T. Murayama, S. Ishikawa, M. Sadakane, D. Buttrey, W. Ueda, An orthorhombic Mo_3VO_x catalyst most active for oxidative dehydro-

genation of ethane among related complex metal oxides, Catalysis Science Technology 3 (2013) 380–387.

[109] N. Fang Chen, W. Ueda, K. Oshihara, Hydrothermal synthesis of Mo-V-M-O complex metal oxide catalysts active for partial oxidation of ethane, Chemical Communications (6) (1999) 517–518.

[110] J. M. Lopez Nieto, B. Solsona, P. Concepcion, F. Ivars, A. Dejoz, M. I. Vazquez, Reaction products and pathways in the selective oxidation of C2-C4 alkanes on MoVTeNb mixed oxide catalysts, Catalysis Today 157 (1-4) (2010) 291–296.

[111] A. A. Adesina, N. W. Cant, A. Saberi-Moghaddam, C. H. L. Szeto, D. L. Trimm, Structural effects in oxidative dehydrogenation of hydrocarbons over a vanadia-molybdena-niobia catalyst, Journal of Chemical Technology & Biotechnology 72 (1) (1998) 19–22.

[112] P. Botella, E. Garcia-Gonzalez, J. M. Lopez Nieto, J. M. Gonzalez-Calbet, MoVTeNbO multifunctional catalysts: Correlation between constituent crystalline phases and catalytic performance, Solid State Sciences 7 (5) (2005) 507–519.

[113] W. Ueda, K. Oshihara, Selective oxidation of light alkanes over hydrothermally synthesized Mo-V-M-O (M=Al, Ga, Bi, Sb, and Te) oxide catalysts, Applied Catalysis A: General 200 (1-2) (2000) 135–143.

[114] J. Guan, S. Wu, H. Wang, S. Jing, G. Wang, K. Zhen, Q. Kan, Synthesis and characterization of MoVTeCeO catalysts and their catalytic performance for selective oxidation of isobutane and isobutylene, Journal of Catalysis 251 (2) (2007) 354–362.

[115] E. Heracleous, A. F. Lee, K. Wilson, A. A. Lemonidou, Investigation of Ni-based alumina-supported catalysts for the oxidative dehydrogenation of ethane to ethylene: structural characterization and reactivity studies, J. Catal. 231 (1) (2005) 159–171.

[116] S. Wang, K. Murata, T. Hayakawa, S. Hamakawa, K. Suzuki, Selective oxidation of ethane and propane over sulfated zirconia-supported nickel oxide catalysts, Journal of Chemical Technology & Biotechnology 76 (3) (2001) 265.

[117] E. Heracleous, A. A. Lemonidou, Ni-Nb-O mixed oxides as highly active and selective catalysts for ethene production via ethane oxidative dehydrogenation. Part II: Mechanistic aspects and kinetic modeling, J. Catal. 237 (1) (2006) 175–189.

[118] B. Solsona, J. M. Lopez Nieto, P. Concepcion, A. Dejoz, F. Ivars, M. I. Vazquez, Oxidative dehydrogenation of ethane over Ni-W-O mixed metal oxide catalysts, Journal of Catalysis 280 (1) (2011) 28–39.

[119] B. Solsona, P. Concepcion, S. Hernandez, B. Demicol, J. M. Lopez Nieto, Oxidative dehydrogenation of ethane over NiO-CeO_2 mixed oxides catalysts, Catalysis Today 180 (1) (2012) 51–58.

[120] B. Solsona, P. Concepcion, B. Demicol, S. Hernandez, J. J. Delgado, J. J. Calvino, J. M. Lopez Nieto, Selective oxidative dehydrogenation of ethane over SnO_2-promoted NiO catalysts, Journal of Catalysis 295 (0) (2012) 104.

[121] M. Iwamoto, Y. Yoda, M. Egashira, T. Seiyama, Study of metal oxide catalysts by temperature programmed desorption. 1. Chemisorption of oxygen on nickel oxide, The Journal of Physical Chemistry 80 (18) (1976) 1989–1994.

[122] H. Zhu, S. Ould-Chikh, D. H. Anjum, M. Sun, G. Biausque, J.-M. Basset, V. Caps, Nb effect in the nickel oxide-catalyzed low-temperature oxidative dehydrogenation of ethane, Journal of Catalysis 285 (1) (2012) 292.

[123] Z. Skoufa, E. Heracleous, A. A. Lemonidou, Unraveling the contribution of structural phases in Ni-Nb-O mixed oxides in ethane oxidative dehydrogenation, Catalysis Today 192 (1) (2012) 169.

[124] B. Savova, S. Loridant, D. Filkova, J. M. M. Millet, Ni-Nb-O catalysts for ethane oxidative dehydrogenation, Applied Catalysis A: General 390 (2010) 148.

[125] Y. Brik, M. Kacimi, M. Ziyad, F. Bozon-Verduraz, Titania-Supported Cobalt and Cobalt-Phosphorus Catalysts: Characterization and Performances in Ethane Oxidative Dehydrogenation, Journal of Catalysis 202 (1) (2001) 118–128.

[126] S.-W. Ho, J. M. Cruz, M. Houalla, D. M. Hercules, The structure and activity of titania supported cobalt catalysts, Journal of Catalysis 135 (1) (1992) 173–185.

[127] X. Zhang, Q. Ye, B. Xu, D. He, Oxidative dehydrogenation of ethane over $Co - BaCO_3$ catalysts using CO2 as oxidant: effects of Co promoter, Catal. Lett. 117 (3-4) (2007) 140–145.

[128] E. M. Kennedy, N. W. Cant, Comparison of the oxidative dehydrogenation of ethane and oxidative coupling of methane over rare earth oxides, Applied Catalysis 75 (1) (1991) 321–330.

[129] E. M. Kennedy, N. W. Cant, Oxidative dehydrogenation of ethane and the coupling of methane over sodium containing cerium oxides, Applied Catalysis A: General 87 (2) (1992) 171–183.

[130] E. Reverchon, G. D. Porta, D. Sannino, L. Lisi, P. Ciambelli, Supercritical Anti-Solvent precipitation: a novel technique to produce catalyst precursors. Preparation and characterization of samarium oxide nanoparticles, in: Studies in Surface Science and Catalysis, Vol. Volume 118, Elsevier, 1998, pp. 349–358.

[131] L. Ji, J. Liu, X. Chen, M. Li, The oxidative dehydrogenation of ethane over alkali-doped lanthanum-calcium oxide catalysts, Catalysis Letters 39 (3) (1996) 247–252.

[132] R. X. Valenzuela, G. Bueno, V. Cortes Corberan, Y. Xu, C. Chen, Selective oxidehydrogenation of ethane with CO_2 over CeO_2-based catalysts, Catal. Today 61 (1-4) (2000) 43–48.

[133] R. X. Valenzuela, G. Bueno, A. Solbes, F. Sapina, E. Martinez, V. Cortes Corberan, Nanostructured ceria-based catalysts for oxydehydrogenation of ethane with CO_2, Top. Catal. 15 (2-4) (2001) 181–188.

[134] V. R. Choudhary, S. A. R. Mulla, V. H. Rane, Oxidative coupling of methane and oxidative dehydrogenation of ethane over strontium-promoted rare earth oxide catalysts, J. Chem. Technol. Biotechnol. 71 (2) (1998) 167–172.

[135] V. Cortes Corberan, Novel approaches for the improvement of selectivity in the oxidative activation of light alkanes, Catalysis Today 99 (1-2) (2005) 33.

[136] C. T. Au, K. D. Chen, H. X. Dai, Y. W. Liu, C. F. Ng, The modification of Ho_2O_3 with $BaCl_2$ for the oxidative dehydrogenation of ethane, Appl. Catal., A 177 (2) (1999) 185–191.

[137] J. Z. Luo, X. P. Zhou, Z. S. Chao, H. L. Wan, Oxidative dehydrogenation of ethane over BaF_2 promoted Sm_2O_3-LaF_3 catalysts, Appl. Catal., A 159 (1-2) (1997) 9–19.

[138] H. X. Dai, C. F. Ng, C. T. Au, Raman spectroscopic and EPR investigations of oxygen species on $SrCl_2$-promoted Ln_2O_3 (Ln=Sm and Nd) catalysts for ethane-selective oxidation to ethene, Appl. Catal., A 202 (1) (2000) 1–15.

[139] S. Sugiyama, K. Sogabe, T. Miyamoto, H. Hayashi, J. B. Moffat, Oxidative dehydrogenation of ethane on rare earth oxides: effects of chlorine additives in gas and solid phase on the oxidation over cerium oxide, Catalysis Letters 42 (3) (1996) 127–133.

[140] E. Morales, J. H. Lunsford, Oxidative dehydrogenation of ethane over a lithium-promoted magnesium oxide catalyst, Journal of Catalysis 118 (1) (1989) 255–65.

[141] D. Wang, M. P. Rosynek, J. H. Lunsford, The role of Cl- in a Li+-ZnO-Cl- catalyst on the oxidative coupling of methane and the oxidative dehydrogenation of ethane, Chemical Engineering & Technology 18 (2) (1995) 118–24.

[142] S. Arndt, G. Laugel, S. Levchenko, R. Horn, M. Baerns, M. Scheffler, R. Schlögl, R. Schomäcker, A Critical Assessment of Li/MgO-Based Catalysts for the Oxidative Coupling of Methane, Catalysis Reviews 53 (4) (2011) 424–514.

[143] E. Finazzi, C. DiValentin, G. Pacchioni, M. Chiesa, E. Giamello, H. Gao, J. Lian, T. Risse, H.-J. Freund, Properties of Alkali Metal Atoms Deposited on a MgO Surface: A Systematic Experimental and Theoretical Study, Chemistry - A European Journal 14 (14) (2008) 4404–4414.

[144] J. C. Lian, E. Finazzi, C. Di Valentin, T. Risse, H. J. Gao, G. Pacchioni, H. J. Freund, Li atoms deposited on single crystalline MgO(001) surface. A combined experimental and theoretical study, Chemical Physics Letters 450 (2008) 308–311.

[145] L. Leveles, S. Fuchs, K. Seshan, J. A. Lercher, L. Lefferts, Oxidative conversion of light alkanes to olefins over alkali promoted oxide catalysts, Appl. Catal., A 227 (1-2) (2002) 287–297.

[146] M. Machli, C. Boudouris, S. Gaab, J. Find, A. A. Lemonidou, J. A. Lercher, Kinetic modelling of the gas phase ethane and propane oxidative dehydrogenation, Catalysis Today 112 (1-4) (2006) 53–59.

[147] V. L. Cherginets, T. P. Rebrova, Studies of some acid-base equilibria in the molten eutectic mixture KCl-LiCl at 700°C, Electrochimica Acta 45 (3) (1999) 469–476.

[148] V. A. Volkovich, T. R. Griffiths, D. J. Fray, M. Fields, Increased oxidation of UO_2 in molten alkali-metal carbonate based mixtures by increasing oxygen solubility and by controlled generation of superoxide ions, and evidence for a new sodium uranate, Journal of the Chemical Society, Faraday Transactions 93 (21) (1997) 3819–3826.

[149] V. A. Volkovich, T. R. Griffiths, D. J. Fray, R. C. Thied, A new method for determining oxygen solubility in molten carbonates and carbonate-chloride mixtures using the oxidation of UO_2 to uranate reaction, Journal of Nuclear Materials 282 (2-3) (2000) 152–158.

[150] X. Lin, C. A. Hoel, W. M. H. Sachtler, K. R. Poeppelmeier, E. Weitz, Oxidative dehydrogenation (ODH) of ethane with O_2 as oxidant on selected transition metal-loaded zeolites, Journal of Catalysis 265 (1) (2009) 54.

[151] G. Busca, E. Finocchio, V. Lorenzelli, G. Ramis, M. Baldi, IR studies on the activation of C-H hydrocarbon bonds on oxidation catalysts, Catalysis Today 49 (4) (1999) 453–465.

[152] B. Frank, M. Morassutto, R. Schomäcker, R. Schlögl, D. S. Su, Oxidative Dehydrogenation of Ethane over Multiwalled Carbon Nanotubes, ChemCatChem 2 (6) (2010) 644.

[153] E. Heracleous, A. A. Lemonidou, Ni-Me-O mixed metal oxides for the effective oxidative dehydrogenation of ethane to ethylene - Effect of promoting metal Me, Journal of Catalysis 270 (1) (2010) 67–75.

[154] S. J. Conway, D. J. Wang, J. H. Lunsford, Selective oxidation of methane and ethane over lithium($^{1+}$)-magnesia-chloride catalysts promoted with metal oxides, Applied Catalysis A: General 79 (1) (1991) L1–L5.

[155] M. L. Rodriguez, D. E. Ardissone, E. Heracleous, A. A. Lemonidou, E. Lopez, M. N. Pedernera, D. O. Borio, Oxidative dehydrogenation of ethane to ethylene in a membrane reactor: A theoretical study, Catalysis Today 157 (1-4) (2010) 303–309.

[156] M. L. Rodriguez, D. E. Ardissone, E. Lopez, M. N. Pedernera, D. O. Borio, Reactor Designs for Ethylene Production via Ethane Oxidative Dehydrogenation: Comparison of Performance, Industrial & Engineering Chemistry Research 50 (2010) 2690–2697.

[157] T. Waku, M. D. Argyle, A. T. Bell, E. Iglesia, Effects of O_2 Concentration on the Rate and Selectivity in Oxidative Dehydrogenation of Ethane Catalyzed by Vanadium Oxide: Implications for O_2 Staging and Membrane Reactors, Industrial & Engineering Chemistry Research 42 (22) (2003) 5462–5466.

[158] F. Klose, T. Wolff, S. Thomas, A. Seidel-Morgenstern, Concentration and residence time effects in packed bed membrane reactors, Catalysis Today 82 (1-4) (2003) 25–40.

[159] A. L. Y. Tonkovich, J. L. Zilka, D. M. Jimenez, G. L. Roberts, J. L. Cox, Experimental investigations of inorganic membrane reactors: A distributed feed approach for partial oxidation reactions, Chemical Engineering Science 51 (5) (1996) 789–806.

[160] A. C. van Veen, M. Rebeilleau, D. Farrusseng, C. Mirodatos, Studies on the performance stability of mixed conducting barium cobalt iron strontium oxide membranes in medium temperature oxygen permeation, Chemical Communications (1) (2003) 32–33.

[161] M. Huff, L. D. Schmidt, Ethylene formation by oxidative dehydrogenation of ethane over monoliths at very short contact times, The Journal of Physical Chemistry 97 (45) (1993) 11815–11822.

[162] B. Silberova, M. Fathi, A. Holmen, Oxidative dehydrogenation of ethane and propane at short contact time, Applied Catalysis A: General 276 (1-2) (2004) 17–28.

[163] M. C. Huff, I. P. Androulakis, J. H. Sinfelt, S. C. Reyes, The Contribution of Gas-Phase Reactions in the Pt-Catalyzed Conversion of Ethane-Oxygen Mixtures, Journal of Catalysis 191 (1) (2000) 46–54.

[164] F. Donsi, K. A. Williams, L. D. Schmidt, A Multistep Surface Mechanism for Ethane Oxidative Dehydrogenation on Pt- and Pt/Sn-Coated Monoliths, Industrial & Engineering Chemistry Research 44 (10) (2005) 3453–3470.

[165] A. Beretta, E. Ranzi, P. Forzatti, Oxidative dehydrogenation of light paraffins in novel short contact time reactors. Experimental and theoretical investigation, Chemical Engineering Science 56 (3) (2001) 779.

[166] E. V. Kondratenko, Mechanistic Aspects of Short Contact Time Oxidative Functionalization of Propane and Ethane from Temporal Analysis of Products, in: C. Hess, R. Schlögl (Eds.), Nanostructured Catalysts - Selective Oxidations, Royal Society of Chemistry, Cambridge, 2011, pp. 340–354.

[167] S. J. Conway, J. H. Lunsford, Oxidative dehydrogenation of ethane over chlorine-promoted lithium-magnesium oxide catalysts, J. Catal. 131 (2) (1991) 513–22.

[168] S. A. R. Mulla, O. V. Buyevskaya, M. Baerns, A comparative study on non-catalytic and catalytic oxidative dehydrogenation of ethane to ethylene, Appl. Catal., A 226 (1-2) (2002) 73–78.

[169] S. Gaab, M. Machli, J. Find, R. K. Grasselli, J. A. Lercher, Oxidative Dehydrogenation of Ethane Over Novel Li/Dy/Mg Mixed Oxides: Structure-Activity Study, Top. Catal. 23 (1-4) (2003) 151–158.

[170] D. J. Wang, M. P. Rosynek, J. H. Lunsford, The Effect of Chloride Ions on a Li^+-MgO Catalyst for the Oxidative Dehydrogenation of Ethane, Journal of Catalysis 151 (1) (1995) 155–167.

[171] S. Wang, K. Murata, T. Hayakawa, K. Suzuki, Oxidative Dehydrogenation of Ethane Over Zirconia-Supported Lithium Chloride Catalysts, Chemical Engineering & Technology 23 (12) (2000) 1099–1103.

[172] C. T. Au, X. P. Zhou, H. L. Wan, The activation of O_2 and the oxidative dehydrogenation of C_2H_6 over SmOF catalyst, Catalysis Letters 40 (1) (1996) 101–104.

[173] D. A. Goetsch, L. D. Schmidt, Microsecond Catalytic Partial Oxidation of Alkanes, Science 271 (5255) (1996) 1560–1562.

[174] O. Czuprat, S. Werth, S. Schirrmeister, T. Schiestel, J. Caro, Oxidative dehydrogenation of lower alkanes in a selective membrane reactor with stepwise oxygen feed and in situ hydrogen oxidation, Chem. Ing. Tech. 81 (10) (2009) 1591–1597.

[175] O. Czuprat, S. Werth, S. Schirrmeister, T. Schiestel, J. Caro, Olefin Production by a Multistep Oxidative Dehydrogenation in a Perovskite Hollow-Fiber Membrane Reactor, ChemCatChem 1 (3) (2009) 401–405.

[176] T. Blasco, A. Galli, J. M. Lopez Nieto, F. Trifiro, Oxidative dehydrogenation of ethane and n-butane on VO_x/Al_2O_3 catalysts, J. Catal. 169 (1) (1997) 203–211.

[177] C. A. Gärtner, A. C. van Veen, J. A. Lercher, Oxidative Dehydrogenation of Ethane: Common Principles and Mechanistic Aspects, ChemCatChem 5,11 (2013) 3196–3217.

[178] M. V. Landau, A. Gutman, M. Herskowitz, R. Shuker, Y. Bitton, D. Mogilyansky, The role and stability of Li_2O_2 phase in supported LiCl catalyst in oxidative dehydrogenation of n-butane, Journal of Molecular Catalysis A: Chemical 176 (2001) 127.

[179] [link].
URL `http://www.crct.polymtl.ca/fact/documentation/FTsalt/FTsalt_Figs.htm`, `accessed 1.5.2013`

[180] Y.-H. Chin, C. Buda, M. Neurock, E. Iglesia, Reactivity of Chemisorbed Oxygen Atoms and Their Catalytic Consequences during CH_4-O_2 Catalysis on Supported Pt Clusters, Journal of the American Chemical Society 133 (2011) 15958–15978.

[181] B. Grzybowska-Swierkosz, Thirty years in selective oxidation on oxides: What have we learned?, Topics in Catalysis 11-12 (1-4) (2000) 23–42.

[182] K. Chen, E. Iglesia, A. T. Bell, Isotopic Tracer Studies of Reaction Pathways for Propane Oxidative Dehydrogenation on Molybdenum Oxide Catalysts, The Journal of Physical Chemistry B 105 (3) (2000) 646.

[183] M. Sterrer, E. Fischbach, T. Risse, H.-J. Freund, Geometric Characterization of a Singly Charged Oxygen Vacancy on a Single-Crystalline MgO(001) Film by Electron Paramagnetic Resonance Spectroscopy, Physical Review Letters 94 (18) (2005) 186101.

[184] J. Carrasco, N. Lopez, F. Illas, First Principles Analysis of the Stability and Diffusion of Oxygen Vacancies in Metal Oxides, Physical Review Letters 93 (22) (2004) 225502.

[185] A. M. Ferrari, G. Pacchioni, Electronic Structure of F and V Centers on the MgO Surface, The Journal of Physical Chemistry 99 (46) (1995) 17010.

[186] A. M. Ferrari, G. Pacchioni, Surface reactivity of MgO oxygen vacancies: electrostatic mechanisms in the formation of O_2^- and CO^- species, The Journal of Chemical Physics 107 (6) (1997) 2066.

[187] M. Wakao, K. Minami, A. Nagashima, Viscosity measurements of molten LiCl in the temperature range 886-1275 K, International Journal of Thermophysics 12 (2) (1991) 223–230.

[188] C. T. Adams, S. G. Brandenberger, J. B. DuBois, G. S. Mill, M. Nager, D. B. Richardson, Dehydrogenation and coupling reactions in the presence of iodine and molten salt hydrogen iodide acceptors, J. Org. Chem. 42 (1) (1977) 1–6.

[189] I. Chorkendorff, J. Niemantsverdriet, Concepts of Modern Catalysis and Kinetics, Wiley-VCH Verlag GmbH, 2007.

[190] F. Klose, M. Joshi, C. Hamel, A. Seidel-Morgenstern, Selective oxidation of ethane over a VO_x/Al_2O_3 catalyst - investigation of the reaction network, Applied Catalysis A: General 260 (1) (2004) 101 – 110.

[191] (2013).

[192] H. Ito, Y. Hasegawa, Y. Ito, Densities of Eutectic Mixtures of Molten Alkali Chlorides below 673 K, Journal of Chemical & Engineering Data 46 (5) (2001) 1203–1205.

[193] D. L. Thomas, J.-Y. Cherng, D. N. Bennion, Thermodynamic and Transport Properties of a Four-Component Alkali-Metal Chloride Electrolyte, Journal of The Electrochemical Society 135 (1988) 2674–2678.

[194] [link].
URL `hht://ras.material.tohoku.ac.jp/∼olten/molten_eut_queryl1.php, accessed 15.10.2010`

[195] G. Janz, Molten salts handbook, Acedemic Press, 1967.

[196] J. Grosbois, J.-Y. Dumousseau (1983).

[197] N. Wiberg, E. Wiberg, A. F. Holleman, Lehrbuch der Anorganischen Chemie, de Gruyter, 2007.

[198] C. Janiak, Nichtmetallchemie: Grundlagen und Anwendungen, Shaker Verlag, 2007.

[199] J. H. Lunsford, The Catalytic Oxidative Coupling of Methane, Angewandte Chemie International Edition in English 34 (9) (1995) 970.

[200] A. Holmen, Direct conversion of methane to fuels and chemicals, Catalysis Today 142 (1-2) (2009) 2.

[201] L. Olivier, S. Haag, H. Pennemann, C. Hofmann, C. Mirodatos, A. C. van Veen, High-temperature parallel screening of catalysts for the oxidative coupling of methane, Catalysis Today 137 (1) (2008) 80 – 89.

[202] J. W. Thybaut, J. Sun, L. Olivier, A. C. van Veen, C. Mirodatos, G. B. Marin, Catalyst design based on microkinetic models: Oxidative coupling of methane, Catalysis Today 159 (1) (2011) 29 – 36.

[203] Z. C. Jiang, C. J. Yu, X. P. Fang, S. B. Li, H. L. Wang, Oxide/support interaction and surface reconstruction in the sodium tungstate(Na_2WO_4)/silica system, The Journal of Physical Chemistry 97 (49) (1993) 12870–12875.

[204] S. Arndt, T. Otremba, U. Simon, M. Yildiz, H. Schubert, R. Schomäcker, $MnNa_2WO_4/SiO_2$ as catalyst for the oxidative coupling of methane. What is really known?, Applied Catalysis A: General 425-426 (0) (2012) 53 – 61.

[205] Y. S. Su, J. Y. Ying, W. H. G. Jr., Upper bound on the yield for oxidative coupling of methane, Journal of Catalysis 218 (2) (2003) 321 – 333.

[206] J. Sun, J. W. Thybaut, G. B. Marin, Microkinetics of methane oxidative coupling, Catalysis Today 137 (2008) 90 – 102.

[207] J. A. Labinger, Methane activation in homogeneous systems, Fuel Processing Technology 42 (2-3) (1995) 325 – 338.

[208] P. F. Nelson, C. A. Lukey, N. W. Cant, Isotopic evidence for direct methyl coupling and ethane to ethylene conversion during partial oxidation of methane over lithium/magnesium oxide, The Journal of Physical Chemistry 92 (22) (1988) 6176–6179.

[209] F. H. Westheimer, The Magnitude of the Primary Kinetic Isotope Effect for Compounds of Hydrogen and Deuterium., Chemical Reviews 61 (3) (1961) 265–273.

[210] P. W. Atkins, Physikalische Chemie, VCH Verlagsgesellschaft mbH, Weinheim, 1996.

[211] [link].
URL `http://www.chemgapedia.de, accessed 29.6.2012`

A. Appendix

A.1. Publications

C. A. Gärtner, A.C. van Veen, J.A. Lercher: "Oxidative Dehydrogenation of Ethane: Common Principles and Mechanistic Aspects", ChemCatChem (2013), 11, 3196-3217

C. A. Gärtner, A.C. van Veen, J. A. Lercher: "Oxidative Dehydrogenation of Ethane on Dynamically Rearranging Supported Chloride Catalysts", J. Am. Chem. Soc. (2014), 136(36), 12691-12701

C. A. Gärtner, A. C. van Veen, J. A. Lercher: "Highly selective supported alkali chloride catalysts for the oxidative dehydrogenation of ethane", Top.Catal. (2014), 57, 1236-1247

A.2. Patent applications

C. A. Gärtner, A. C. van Veen, J. A. Lercher: Catalyst, process for catalyst manufacture and process for catalytic oxidative dehydrogenation, WO2013/092179, PCT/EP/2012/.074212

C. A. Gärtner, A. C. van Veen, J. A. Lercher: Catalyst, process for catalyst manufacture and process for catalytic oxidative dehydrogenation, WO2013/092180, PCT/EP/2012/074214

C. A. Gärtner, A. C. van Veen, J. A. Lercher: Catalyst, process for catalyst manufacture and process for catalytic oxidative dehydrogenation, EP 2 606 963 A1

A.3. Conference contributions

A.3.1. Oral presentations

C.A.Gärtner, A. C. van Veen, J. A. Lercher: "Unravelling the reaction mechanism of the highly selective oxidative dehydrogenation of ethane over supported molten alkali chloride catalysts", 11. Europacat, Lyon, France, 1.9.-6.9.2013

C.A.Gärtner, A. C. van Veen, J. A. Lercher: "Mechanistic understanding of the highly selective oxidative dehydrogenation of ethane over supported molten alkali chloride catalysts", 23. Meeting of the North American Catalysis Society, Louisville, KY, USA, 2.6.-7.6.2013

J. A. Lercher, C.A.Gärtner, A. C. van Veen: "Oxidative dehydrogenation of ethane on supported chloride catalysts", 245^{th} ACS National Meeting, New Orleans, LA, USA, 7.4.-11.4.2013

C.A.Gärtner, A. C. van Veen, J. A. Lercher: "Mechanism of ethane oxidative dehydrogenation over supported alkali-chloride catalysts", 46. Jahrestreffen Deutscher Katalytiker, Weimar, 13.3.-15.3.2013

C.A.Gärtner, A. C. van Veen, J. A. Lercher: "Highly selective oxidehydrogenation of ethane via supported molten alkali chloride catalyts", 6^{th} IDECAT/ERIC-JCAT Conference, Brixen, Italy, 3.3.-6.3.2013

C.A.Gärtner, A. C. van Veen, J. A. Lercher: "Mechanistic understanding of the highly selective oxidative dehydrogenation of ethane via novel supported alkali chloride catalysts", AIChE Annual Meeting, Pittsburgh, PA, USA, 28.10.-2.11.2012

C.A.Gärtner, A. C. van Veen, J. A. Lercher: "Oxidative dehydrogenation of ethane over supported liquid phase catalysts", Jahrestreffen Reaktionstechnik, Wärzburg, 14.5.-16.5.2012

C.A.Gärtner, A. C. van Veen, J. A. Lercher: "Highly selective oxidative dehydrogenation of ethane with supported molten chloride catalysts", X. Europacat, Glasgow, Scotland, 28.8.-2.9.2011

A.3.2. Poster presentations

C. A. Gärtner, A. C. van Veen, J. A. Lercher: "Mechanistic and kinetic analysis of the oxidative dehydrogenation of ethane via novel supported alkali chloride catalysts ", International DGMK-Conference "Shale Gas, Heavy Oils and Coal-Implications on Refining and Petrochemistry " Dresden, 9.10.-11.10.2013

C. A. Gärtner, A. C. van Veen, J. A. Lercher: "Kinetic analysis of the oxidative dehydrogenation of ethane over supported alkali chloride catalysts", Jahrestreffen Reaktionstechnik, Würzburg, 6.5.-8.5.2013

C. A. Gärtner, A. C. van Veen, J. A. Lercher: "Mechanistic understanding and kinetic studies of highly selective oxidative dehydrogenation of ethane over novel supported molten chloride catalysts", International DGMK-Conference "'Reducing the Carbon Footprint of Fuels and Petrochemicals - Alternative Feedstocks and Innovative Technologies", Berlin, 8.10.-10.10.2012

C. A. Gärtner, A. C. van Veen, J. A. Lercher: "Supported liquid phase catalysis as a novel concept for oxidative dehydrogenation of ethane", ProcessNet Jahrestagung 2012, Karlsruhe,11.9.-13.9.2012

C. A. Gärtner, S. Müller, A. C. van Veen, J. A. Lercher: "Mechanistic understanding of the oxidative dehydrogenation of ethane over supported molten alkali chloride catalysts", 15^{th} International Congress on Catalysis, München, 1.07.-6.07.2012

C. A. Gärtner, M.F. Wagenhofer, S. Müller, A. C. van Veen, J. A. Lercher: "Kinetic and mechanistic aspects of the oxidative dehydrogenation of ethane over supported eutectic alkali-chloride catalysts", 45. Jahrestreffen Deutscher Katalytiker, Weimar, 14.3.-16.3.2012

C. A. Gärtner, A. C. van Veen, J. A. Lercher: "Highly Selective Oxidative Dehydrogenation of Ethane with Supported Molten Chloride Catalysts", International DGMK-Conference "Catalysis - Innovative Applications in Petrochemistry and Refining", Dresden, 4.10.-6.10.2011

C. A. Gärtner, D. Hartmann, A. C. van Veen, J. A. Lercher: "Highly Selective Oxidative Dehydrogenation of Light Alkanes", Joint Workshop on Energy and Sustainability: Materials and Processes (Chemistry Department, Northwestern University, and Catalysis Research Center, Technische Universität München), München, 13.5.-14.5.2011

C. A. Gärtner, B. Tope, J. A. Lercher: "Oxidative dehydrogenation of ethane on supported eutectic alkali-chloride catalysts", 44. Jahrestreffen Deutscher Katalytiker und Jahrestreffen Reaktionstechnik, Weimar, 16.-18.3.2011

Table 18.: Pore volume of catalysts with different chloride loadings (*: pore volume of the support where that chloride overlayer was washed off)

mol% overlayer	cumulative pore volume / $cm^3g{-}1]$
0	0.3518
1,27	0.0177
3,4	0.0141
5,57	0.0299
10,67	0.0265
19,23	0.019
32,23	0.0192
0*	0.1263

Table 19.: BET analysis of selected supports and respective catalysts

	refractory oxide		catalyst with chloride overlayer	
Support	specific surface area m^2g^{-1}	pore volume cm^3g^{-1}	specific surface area m^2g^{-1}	pore volume cm^3g^{-1}
MgO900	10	0.0218	4.73	n.r.
ZnO	7.55	0.0073	1.4	n.r.

A.4. Supplementary material

A.4.1. Supplementary material for Chapter 2

A.4.1.1. Additional information on physicochemical properties

A.4.1.2. In-situ XRD of $LiKCl/MgO + Dy_2O_3$

XRD measurements were performed on a Philips XPert Pro System (CuKα1-radiation, 0.154056 nm) in Bragg-Brentano geometry in the range 2θ = 5-70 ° with a step size of 0.017°/s, operating at 45 kV/40 mA. In-situ experiments were conducted utilizing an Anton Paar HTK 1200 chamber under controlled gas atmosphere of 100 mL/min synthetic air. The heating rate was 10 K/min. Diffractograms were recorded at 303 K and within 373 K to 973 K every 100 K. The last measurement was performed after cooling to 202 K. Figure 51 shows the result of this experiment.

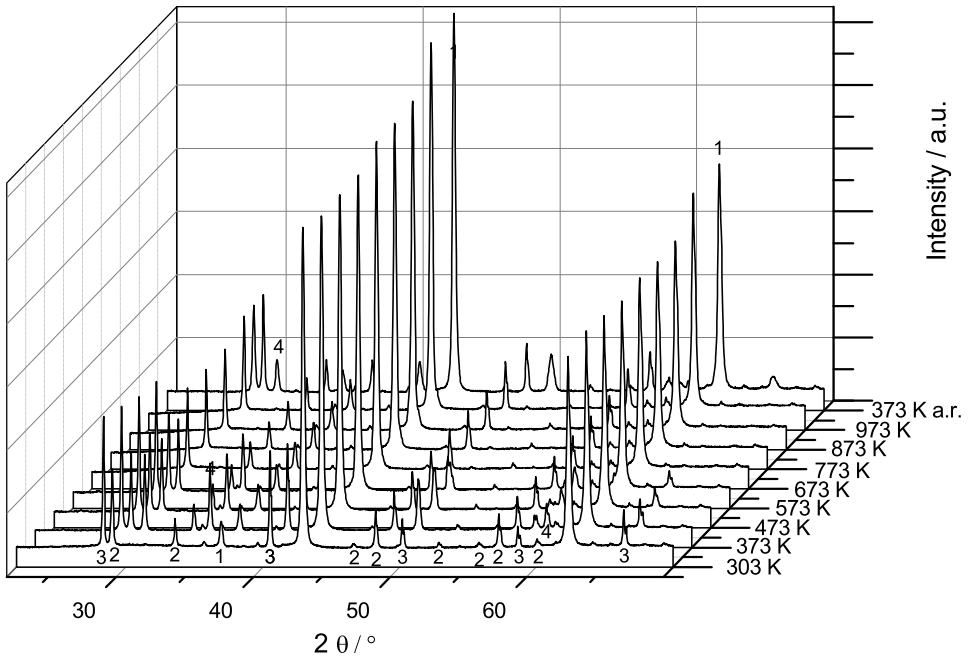

Figure 51.: Insitu-XRD of $LiKCl/MgO + Dy_2O_3$ (row 6 in table 4; 1: MgO; 2:Dy_2O_3; 3: KCl; 4: LiCl; a.r.:after reaction

It becomes obvious that LiCl cannot be detected in the first measurement, as it is hygroscopic and thus forms hydrates which cannot be detected via XRD. However, at higher temperatures and at 373 K after the measurements at higher temperatures, a LiCl reflection can be seen. Furthermore, it can be seen that at 673 K, LiCl and KCl reflections cannot be observed any more due to the melting of the eutectic system, thus losing its crystallinity. However, in the measurement at 373 K after the other measurements, the reflections can be observed again.

A.4.1.3. Additional information on reactivity

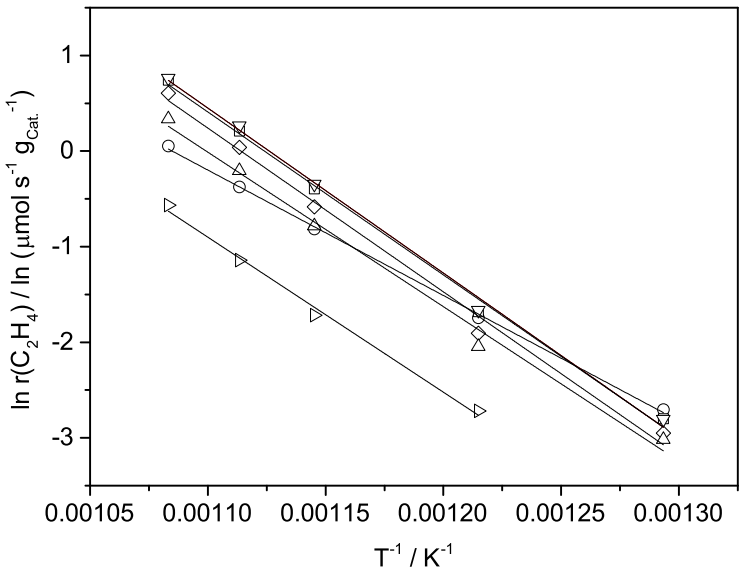

(a)

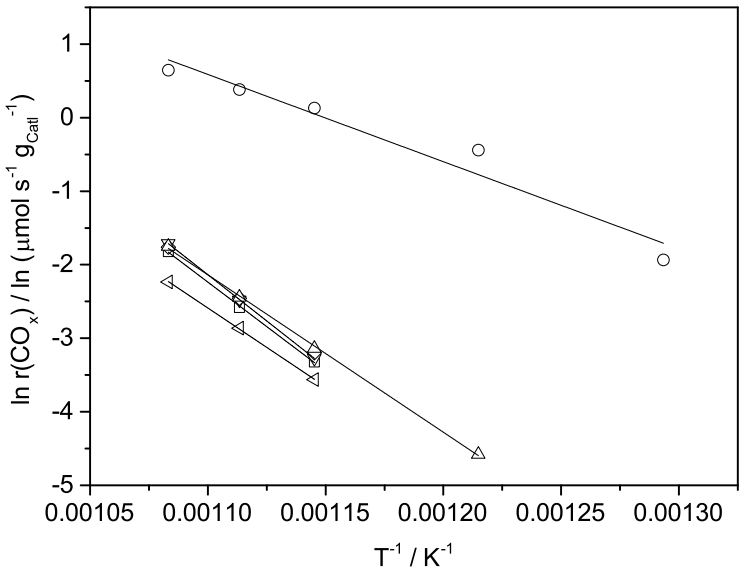

(b)

Figure 52.: Graphical determination ((a): Ethene production, (b): CO_2 production; ○: 0 mol% overlayer; □:5.57 mol% overlayer; ▽: 10.67 mol% overlayer; ◇: 19.23 mol% overlayer; △: 32.23 mol% overlayer; ◁: 41.65 mol% overlayer)

A.4.1.4. Kinetic isotope effect (KIE)

For mechanistic studies, the kinetic isotope effect is useful method, as it allows the analysis of the elementary steps of a reaction mechanism [209]. Here, this method was used to check if the cleavage of a C-H bond in ethane is rate determining step for the ODH reaction. A kinetic isotope effect can be observed when one reactant (i.e. ethane) is substituted by an isotope (i.e. perdeuterated ethane) which influences the reaction kinetics, but only if the substituted element (H in this case) is involved in the rate determining step. A KIE bases on reaction rate constant k, to be more specific in the activation energy E_A which is given in the Arrhenius law.
The difference in the reaction rate of the reactant and its substituting isotope can be estimated by the use of equation (41) [210]. X,Y and Z represent elements, X and Y are isotopes of the same element and Z is any element bonded either to X or Y.

$$\frac{k(\mathrm{Z}-\mathrm{Y})}{k(\mathrm{Z}-\mathrm{X})} = exp(-\lambda) \tag{41}$$

with λ being

$$\lambda = \frac{\mathrm{h}\cdot k_f^{1/2}}{4\cdot\pi\cdot\mathrm{k_B}\cdot T}\left(\frac{1}{\mu_{\mathrm{ZX}}^{1/2}}-\frac{1}{\mu_{\mathrm{ZY}}^{1/2}}\right). \tag{42}$$

k_f stands for the force constant of a bond, h is Planck's constant and $\mathrm{k_B}$ is the Boltzmann constant. μ stands for the respective reduced mass, being calculated for a molecule being composed of the elements Z and X as followed:

$$\mu_{\mathrm{ZX}} = \frac{M_{\mathrm{Z}}\cdot M_{\mathrm{X}}}{M_{\mathrm{Z}}+M_{\mathrm{X}}}. \tag{43}$$

M stands for the respective molar mass of each element.

In order to calculate the difference in the reaction rates the force constant is required. The force constant can be estimated by the use of the relation given in equation (44).

$$k_f = \mu\cdot(\tilde{\omega}\cdot 2\cdot\pi\cdot\mathrm{c})^2 \tag{44}$$

In this equation c stands for the speed of light and $\tilde{\omega}$ is the wave number of the regarded bond.

In order to be able to decide if a C-H bond cleavage is involved in the rds, theoretically expected values for the ratio of the rate constants for ODH with either C_2H_6 or C_2D_6 at different reaction temperatures need to be compared. By equations (41) to (43), the ratio of the rate constants of ODH with C_2H_6 and C_2D_6 as reactants is calculated.

The reduced masses are estimated via equation (43), whereby the molar mass of C is $12\,\mathrm{g\ mol^{-1}}$, the molar mass of D is $2\,\mathrm{g\ mol^{-1}}$ and the molar mass of H is 1 $\mathrm{g\ mol^{-1}}$, resulting in a reduced mass of $\mu_{CH} = 12/13\,\mathrm{g\ mol^{-1}}$ and a reduced mass of $\mu_{CD} = 24/14\,\mathrm{g\ mol^{-1}}$. Force constants are calculated by the use of equation (44) with the wave numbers being $\tilde{\omega}_{CH} = 3000\,\mathrm{cm^{-1}}$ and $\tilde{\omega}_{CD} = 2100\,\mathrm{cm^{-1}}$ [211]. Now, the following values can be obtained: $k_{f,CH} = 2,682\,\mathrm{E29\,N\ m^{-1}}$ and $k_{f,CD} = 2,948\,\mathrm{E29\,N\ m^{-1}}$. The average of these two force constants is calculated. By equations (42) and (41), the ratios of the rate constants at the different temperatures are calculated. The results are given in table 20 which contains the ratio of the respective rates.

Table 20.: Calculated rate constant ratios for an underying KIE in the case of C-H cleavage in ethane

T /°C	Calculated ratio k(C-H)/k(C-D) in the case of an underyling KIE
450	2.174
500	2.067
550	1.978
600	1.902
625	1.868
650	1.837

A.4.2. Combining steady state and transient operation mode: A steady state experiment with an abrupt stop of oxygen feed

A steady state experiment with an abrupt ending of oxygen feed was performed to check whether the oxygen pool showed in the transient step experiments is the same for the steady state experiments as well. Figure 53 shows the results of this experiment.

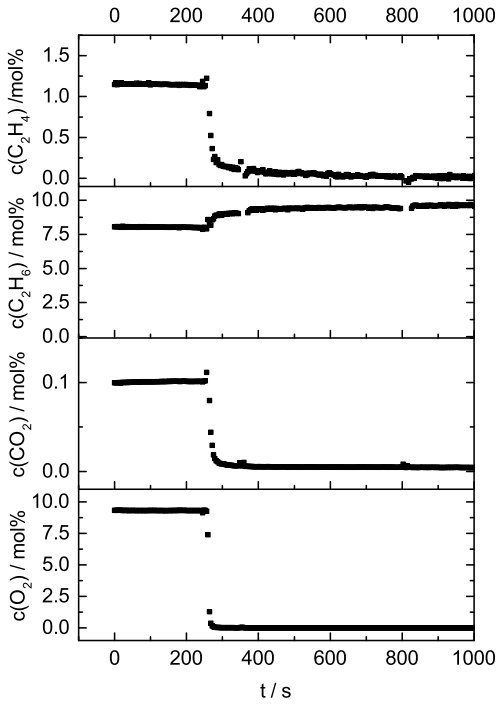

Figure 53.: Steady state experiment with abrupt stop of oxygen feeding ($LiKCl/MgO + Dy_2O_3$, T = 625°C)

After switching off oxygen, it could be shown that there is still a reservoir of oxygen intermediates stored in the melt, which is able to react with ethane to ethene. Notable ethene production prevails up to around 500 s after switching off the oxygen. By contrast, oxygen and CO_2 cannot be detected after less than 50 s any more. The reservoir stored in the melt after the steady state mode can be compared to the step experiments, where the reservoir is formed during the oxygen loading step. In this experiment, an amount of 36 μmol O is stored per gram catalyst, determined by integration of the formed ethene. This value is smaller compared to the step experiment under the same conditions (approximately 80 μmol O).

A.4.3. Supplementary material for Chapter 3

Table 21.: Kinetic measurements of ODH reaction and total combustion of ethane towards CO_2 (1)

T °C	Flow(He) $\mu mol\ min^{-1}$	$Flow(O_2)$ $\mu mol\ min^{-1}$	Flow(Ethane) $\mu mol\ min^{-1}$	r_{Ethene} $\mu mol\ min^{-1}\ g_{Cat.}^{-1}$	r_{CO_2} $\mu mol\ min^{-1}\ g_{Cat.}^{-1}$	$r_{CO)}$ $\mu mol\ min^{-1}\ g_{Cat.}^{-1}$
500	755.91	15.75	15.75	0.00	0.00	0.00
500	666.67	28.37	14.18	0.00	0.00	0.00
500	593.55	38.71	12.90	0.00	0.00	0.00
500	532.54	47.34	11.83	0.00	0.00	0.00
500	671.43	14.29	28.57	0.00	0.00	0.00
500	597.40	25.97	25.97	0.00	0.00	0.00
500	535.71	35.71	23.81	0.00	0.00	0.00
500	483.52	43.96	21.98	1.54	0.00	0.00
500	601.31	13.07	39.22	0.00	0.00	0.00
500	538.92	23.95	35.93	1.69	0.00	0.00
500	486.19	33.15	33.15	1.64	0.00	0.00
500	441.03	41.03	30.77	1.63	0.00	0.00
500	542.17	12.05	48.19	1.78	0.00	0.00
500	488.89	22.22	44.44	1.74	0.00	0.00
500	443.30	30.93	41.24	1.72	0.00	0.00
500	403.85	38.46	38.46	1.75	0.00	0.00
550	755.91	15.75	15.75	2.83	0.00	0.00
550	666.67	28.37	14.18	2.92	0.00	0.00
550	593.55	38.71	12.90	3.29	0.00	0.00
550	532.54	47.34	11.83	3.20	0.00	0.00
550	671.43	14.29	28.57	3.62	0.00	0.00
550	597.40	25.97	25.97	3.86	0.00	0.00
550	535.71	35.71	23.81	4.05	0.00	0.00
550	483.52	43.96	21.98	4.21	0.00	0.00
550	601.31	13.07	39.22	4.32	0.00	0.00
550	538.92	23.95	35.93	4.62	0.00	0.00
550	486.19	33.15	33.15	4.93	0.00	0.00
550	441.03	41.03	30.77	5.06	0.34	0.00
550	542.17	12.05	48.19	4.85	0.00	0.00
550	488.89	22.22	44.44	5.29	0.00	0.00
550	443.30	30.93	41.24	5.63	0.38	0.00
550	403.85	38.46	38.46	5.65	0.39	0.00
600	1511.81	31.50	31.50	10.08	0.00	0.00
600	1333.33	56.74	28.37	10.82	0.89	0.00
600	1187.10	77.42	25.81	11.09	1.17	0.00
600	1065.09	94.67	23.67	11.31	1.40	0.00
600	1342.86	28.57	57.14	13.91	1.54	0.00
600	1194.81	51.95	51.95	15.35	1.97	0.00
600	1071.43	71.43	47.62	15.96	2.43	0.00
600	967.03	87.91	43.96	16.33	2.65	0.00
600	1202.61	26.14	78.43	16.64	2.35	0.00
600	1077.84	47.90	71.86	18.65	2.95	0.00
600	972.38	66.30	66.30	19.85	3.43	0.00
600	882.05	82.05	61.54	20.14	3.81	0.00
600	1084.34	24.10	96.39	19.51	3.10	0.00
600	977.78	44.44	88.89	20.93	2.96	0.00
600	886.60	61.86	82.47	23.64	4.51	0.00
600	807.69	76.92	76.92	23.45	4.44	0.00

Table 22.: Kinetic measurements of ODH reaction and total combustion of ethane towards CO_2 (2)

T $^{\circ}C$	Flow(He) $\mu mol\ min^{-1}$	$Flow(O_2)$ $\mu mol\ min^{-1}$	Flow(Ethane) $\mu mol\ min^{-1}$	r_{Ethene} $\mu mol\ min^{-1}\ g_{Cat.}^{-1}$	r_{CO_2} $\mu mol\ min^{-1}\ g_{Cat.}^{-1}$	$r_{CO)}$ $\mu mol\ min^{-1}\ g_{Cat.}^{-1}$
625	1511.81	31.50	31.50	15.93	2.63	0.00
625	1333.33	56.74	28.37	15.91	3.54	0.00
625	1187.10	77.42	25.81	18.17	4.13	0.00
625	1065.09	94.67	23.67	18.80	4.87	0.00
625	1342.86	28.57	57.14	23.11	4.70	0.00
625	1194.81	51.95	51.95	23.92	6.15	0.00
625	1071.43	71.43	47.62	27.21	7.45	0.00
625	967.03	87.91	43.96	28.30	8.44	0.00
625	1202.61	26.14	78.43	28.20	6.65	0.00
625	1077.84	47.90	71.86	32.12	8.65	0.00
625	972.38	66.30	66.30	34.42	10.23	0.00
625	882.05	82.05	61.54	5.03	2.85	0.00
625	1084.34	24.10	96.39	6.17	0.76	0.00
625	977.78	44.44	88.89	36.77	9.83	0.00
625	886.60	61.86	82.47	39.37	11.94	0.00
625	807.69	76.92	76.92	40.70	13.22	0.00
650	1511.81	31.50	31.50	24.48	7.85	0.00
650	1333.33	56.74	28.37	26.13	11.17	0.00
650	1187.10	77.42	25.81	26.00	13.65	0.00
650	1065.09	94.67	23.67	25.65	14.98	0.00
650	1342.86	28.57	57.14	34.29	13.62	0.00
650	1194.81	51.95	51.95	38.89	18.72	0.00
650	1071.43	71.43	47.62	40.53	21.70	7.37
650	967.03	87.91	43.96	40.04	23.97	7.45
650	1202.61	26.14	78.43	41.09	16.95	0.00
650	1077.84	47.90	71.86	48.01	23.91	9.41
650	972.38	66.30	66.30	50.67	27.98	10.34
650	882.05	82.05	61.54	51.38	30.85	10.00
650	1084.34	24.10	96.39	44.99	19.40	8.10
650	977.78	44.44	88.89	54.47	27.85	10.82
650	886.60	61.86	82.47	58.36	32.94	11.66
650	807.69	76.92	76.92	60.07	36.60	12.30

Table 23.: Kinetic measurements of total combustion of ethene towards CO and CO_2 (1)

T °C	Flow(He) $\mu mol\ min^{-1}$	$Flow(O_2)$ $\mu mol\ min^{-1}$	Flow(Ethene) $\mu mol\ min^{-1}$	r_{CO_2} $\mu mol\ min^{-1}\ g_{Cat.}^{-1}$	r_{CO} $\mu mol\ min^{-1}\ g_{Cat.}^{-1}$
500	755.91	15.75	15.75	0.00	0.00
500	666.67	28.37	14.18	0.00	0.00
500	593.55	38.71	12.90	0.00	0.00
500	532.54	47.34	11.83	0.00	0.00
500	671.43	14.29	28.57	0.00	0.00
500	597.40	25.97	25.97	0.00	0.00
500	535.71	35.71	23.81	0.00	0.00
500	483.52	43.96	21.98	0.00	0.00
500	601.31	13.07	39.22	0.00	0.00
500	538.92	23.95	35.93	0.00	0.00
500	486.19	33.15	33.15	0.00	0.00
500	441.03	41.03	30.77	0.00	0.00
500	542.17	12.05	48.19	0.00	0.00
500	488.89	22.22	44.44	0.00	0.00
500	443.30	30.93	41.24	0.00	0.00
500	403.85	38.46	38.46	0.00	0.00
550	755.91	15.75	15.75	1.27	0.00
550	666.67	28.37	14.18	1.30	0.00
550	593.55	38.71	12.90	1.52	0.00
550	532.54	47.34	11.83	1.24	0.00
550	671.43	14.29	28.57	0.74	0.00
550	597.40	25.97	25.97	0.80	0.00
550	535.71	35.71	23.81	0.93	0.00
550	483.52	43.96	21.98	0.98	0.00
550	601.31	13.07	39.22	0.73	0.00
550	538.92	23.95	35.93	0.87	0.00
550	486.19	33.15	33.15	0.94	0.00
550	441.03	41.03	30.77	0.97	0.00
550	542.17	12.05	48.19	0.39	0.00
550	488.89	22.22	44.44	0.94	0.00
550	443.30	30.93	41.24	1.01	0.00
550	403.85	38.46	38.46	1.08	0.00

Table 24.: Kinetic measurements of total combustion of ethene towards CO and CO_2 (2)

T °C	Flow(He) $\mu mol\ min^{-1}$	$Flow(O_2)$ $\mu mol\ min^{-1}$	Flow(Ethene) $\mu mol\ min^{-1}$	r_{CO_2} $\mu mol\ min^{-1}\ g_{Cat.}^{-1}$	r_{CO} $\mu mol\ min^{-1}\ g_{Cat.}^{-1}$
600	755.91	15.75	15.75	1.36	0.00
600	666.67	28.37	14.18	1.56	0.00
600	593.55	38.71	12.90	1.73	0.00
600	532.54	47.34	11.83	1.79	0.00
600	671.43	14.29	28.57	1.33	0.00
600	597.40	25.97	25.97	1.73	0.00
600	535.71	35.71	23.81	2.24	0.00
600	483.52	43.96	21.98	2.62	0.00
600	601.31	13.07	39.22	2.19	0.00
600	538.92	23.95	35.93	2.71	0.00
600	486.19	33.15	33.15	3.03	0.00
600	441.03	41.03	30.77	3.22	0.00
600	542.17	12.05	48.19	2.46	0.00
600	488.89	22.22	44.44	3.09	0.00
600	443.30	30.93	41.24	0.84	0.00
600	403.85	38.46	38.46	3.53	0.00
625	755.91	15.75	15.75	2.16	0.00
625	666.67	28.37	14.18	2.67	0.00
625	593.55	38.71	12.90	3.07	0.00
625	532.54	47.34	11.83	3.28	0.00
625	671.43	14.29	28.57	0.92	0.00
625	597.40	25.97	25.97	4.20	0.00
625	535.71	35.71	23.81	4.84	3.88
625	483.52	43.96	21.98	5.42	4.71
625	601.31	13.07	39.22	4.37	4.13
625	538.92	23.95	35.93	5.73	5.62
625	486.19	33.15	33.15	6.68	6.41
625	441.03	41.03	30.77	7.53	6.99
625	542.17	12.05	48.19	5.50	6.01
625	488.89	22.22	44.44	7.33	7.82
625	443.30	30.93	41.24	8.69	8.88
625	403.85	38.46	38.46	9.58	9.22
650	755.91	15.75	15.75	5.33	0.00
650	666.67	28.37	14.18	6.78	5.38
650	593.55	38.71	12.90	7.91	6.27
650	532.54	47.34	11.83	8.93	6.67
650	671.43	14.29	28.57	7.89	7.81
650	597.40	25.97	25.97	10.64	9.45
650	535.71	35.71	23.81	12.50	10.13
650	483.52	43.96	21.98	14.05	10.71
650	601.31	13.07	39.22	10.23	10.33
650	538.92	23.95	35.93	13.97	12.73
650	486.19	33.15	33.15	16.45	13.42
650	441.03	41.03	30.77	18.33	13.58
650	542.17	12.05	48.19	12.01	12.03
650	488.89	22.22	44.44	16.70	14.58
650	443.30	30.93	41.24	19.86	15.73
650	403.85	38.46	38.46	21.90	15.77